THE RELATION OF TRANSPORT NOISE TO MEMBRANE KINETICS

by

MASAO YAFUSO

A dissertation submitted to the Graduate Faculty in Chemistry in partial fulfillment of the requirements for the degree of Doctor of Philosophy, The City University of New York.

1970

This manuscript has been read and accepted for the Graduate Faculty in Chemistry in satisfaction of the dissertation requirement for the degree of Doctor of Philosophy.

date — Chairman of Examining Committee

date — Executive Officer

Supervisory Committee

The City University of New York

ACKNOWLEDGEMENT

My investigations into the intricacies of fluctuation theory would not have been possible without the patient tutelage and guidance of my mentor, Professor Michael E. Green. His broad interests and wide technical competence encompassing a multitude of disciplines provided me with a constant atmosphere of imminent discovery and exciting progress.

I wish also to express my gratitude to Mr. Bernie Kline whose many ideas provided a great stimulus to my work.

Finally, my gratitude to my wife, Kiyo, who maintained a happy home for our three children and myself through many difficult years.

The Relation of Transport Noise to Membrane Kinetics

by Masao Yafuso — The City College of the
Mentor: Michael E. Green — City University of New York

ABSTRACT

The noise associated with ion transport across ion-exchange membranes was measured. Cation exchange and anion exchange membranes gave different results. Anion membrane noise was found to be independent of concentration polarization at the membrane surface and showed an ω^{-1} frequency dependence. Such an affect could be caused by a hyperbolic distribution of relaxation times. Similar behavior in semiconductors have been attributed to surface interactions with charge carriers.

Cation exchange membrane noise was observed only after the formation of a depletion layer at the membrane surface where water dissociation due to the electric field occurs. Analyses of the power spectra showed a behavior characteristic of a relaxation time.

Dilute HCl was studied extensively. The result showed an apparent relaxation time τ, that gave an empirical relation of $J = \chi f + \beta$ where J is the current density, f is $\frac{1}{2\pi\tau}$ and χ and β are empirical constants. Temperature

studies showed that log γ and log β were linear with reciprocal temperatures.

The empirical flux equation was combined with the equation for the relaxation time of a conductor, given by $\tau = \epsilon/\sigma$ where ϵ is the permittivity and σ is the conductivity, to obtain the relation $\gamma = 2\pi\epsilon E(x)$. This relation was combined with Onsager's equation for the dissociation of a weak electrolyte by an electric field K/Ko = F(b) where K and Ko are the dissociation constants as high field and zero field respectively, and F(b) is a function of the electric field, to give a relationship of f, the rate constant, to the electric field. Values of E(x) and F(b) ranged from 10^7 - 10^8 volts/meter and up to 100 respectively. It was now possible to find the change in log f with reciprocal temperatures at constant electric field to obtain the activation energy of the observed relaxation process. A value of 15.4 Kcal and 17.5 Kcal were obtained for 0.050M HCl and 0.025M HCl respectively.

TABLE OF CONTENTS

TABLES

Illustrations

Figure 1. Schematic of the noise, voltage measuring system.

Figure 2. The plexiglass cell used for noise measurements.

Figure 3. The Philbrick P85AH preamplifier hooked up as a follower with a gain of 100.

Figure 4. Schematic of the system for distance profiles of noise and membrane voltage.

Figure 5. Voltage and noise vs. current curves for 0.10M NaCl.

○ Membrane volts vs. current for MA 3148 anion exchange membrane.

● Membrane volts vs. current for MC 3235 cation exchange membrane.

□ Total noise vs. current for MA 3148 anion exchange membrane.

■ Total noise vs. current for MC 3235 cation exchange membrane.

Figure 6. Noise-time oscilloscope display, 5 sec/div.

Top: MC 3142, 0.033M HCl, 44 ma/cm^2.

Bottom: MA 3148, 0.050M Nacl, 16 ma/cm^2.

Figure 7. Voltage-time oscilloscope display for MC 3235 at different HCl concentrations and current densities.

a) 0.10M HCl, 5 sec./div., 0.225 volts/div. From top to bottom: J in ma/cm^2: 167, 125, 100, 83.

b) 0.050M HCl, 5 sec./div., 0.225 volts/div. From top to bottom: J in ma/cm^2: 67, 60, 42, 37.5, 33.

c) 0.010M HCl, 2 sec./div., 0.75 volts/div. From top to bottom: J in ma/cm^2: 67, 50, 33, 17, 12.

Figure 8. Change of resistance, $\frac{V}{J}$, with J for HCl solutions and MC 3235.

1. 0.010M HCl
2. 0.025M HCl
3. 0.050M HCl
4. 0.10M HCl

Figure 9. Voltage-time oscilloscope display for 0.025M HCl with two different cation exchange membranes.

a) MC 3142, 5 sec./div. From top to bottom: J in ma/cm^2: 11, 16.5, 22, 33, 44, 55.

b) MC 3235, 10 sec./div., 0.67 volts/div. From top to bottom: J in ma/cm^2: 13, 17, 25, 33, 50, 67. Note: Electrometer output was inverted.

Figure 10. Voltage-time curves at various distances, x from membrane, MC 3142, 0.025M HCl, 44 ma/cm^2, 2 sec./div., 0.2 volts/div. From top to bottom: x in 10^{-4}cm: 0, 40, 200, 800, 200.

Figure 11. Voltage-time curve with micro-electrode touching and possibly penetrating the membrane. MC 3142, 0.025M HCl, 1 sec./div., 0.05 volts/div. From top to bottom: J in ma/cm^2: 33, 33, 44, 55. Note: The first run at 33 ma/cm^2 triggered after the sweep was initiated

Figure 12. Voltage-time curves for Na_2HPO_4 with MC 3235 and NaCl with MA 3148.

a) 0.056M Na_2HPO_4, MC 3235, 5 sec./div., 0.334 volts/div. From top to bottom: J in ma/cm^2: 33, 42, 50, 67, 83.

b) 0.10M NaCl, MA 3148, 5 sec./div., 0.835 volts/div. From top to bottom: J in ma/cm^2: 11, 22, 33, 44
Note: Electrometer output has been inverted.

Figure 13. Membrane volts and noise vs. distance, MC 3235, 0.025M HCl, 83 ma/cm^2.

Figure 14. Proposed equivalent circuit to explain the noise distance curve of figure 13.

Figure 15. Band-pass spectra of 0.10M Na_2SO_4 with MA 3148 at three different currents. From top to bottom: ma/cm^2: 44, 22, 11.

Figure 16. Band-pass spectra of cupric and sodium ions:

0.10M $CuSO_4$, MC 3235, 44 ma/cm^2

0.10M $CuSO_4$, MC 3142, 44 ma/cm^2

0.056N Na_2HPO_4, MC 3235, 44 ma/cm^2

Figure 17. Band-pass spectra of 0.10M $CuSO_4$ with MC 3235 using copper and platinum electrodes at 44 ma/cm^2.

. . . Platinum

o o o Copper

Figure 18. Band-pass spectra of 0.10M $CuSO_4$ with MC 3235 at various current densities. From top to bottom in ma/cm^2: 54, 43, 33, 22, background.

Figure 19. Band-pass spectra of 0.050M $CaCl_2$ with MC 3235 at various current densities. From top to bottom in ma/cm^2: 33, 19, 16.

Figure 20. Band-pass spectra of 0.033M CsCl and 0.033M HCl with MC3142. From top to bottom: CsCl at 43 ma/cm^2, HCl at 43 ma/cm^2, CsCl at 22 and 18 ma/cm^2, background.

Figure 21. Band-pass spectra of 0.10M tetramethyl ammonium chloride with MC3235. From top to bottom in ma/cm^2: 43, 22, 14, 11. Membrane area is 0.092 cm^2.

Figure 22. Band-pass spectra of 0.10M tetramethyl ammonium chloride with MC3142. From top to bottom in ma/cm^2: 31, 25, 22, 19. Membrane area was 0.16 cm^2.

Figure 23. Higher resolution spectra of 0.050M HCl and MC3235 taken with the 3L5 spectrum analyzer at 30°C. From top to bottom in ma/cm^2: 75.5, 59, 50, 45, 36, 31.

Figure 24. Plot of break frequency, $f = \frac{1}{2\pi\tau}$, against current density where τ is a relaxation time.

Figure 25. Change of critical current density with time for 0.050M HCl and MC3235.

a) Double tape with "No-Stix" on the inside, Mystik tape on the outside.

b) Friction tape only.

Figure 26. Plot of break frequency f, with total noise and membrane voltage for 0.050M HCl, MC 3235, 30°C.

1. Membrane volts.
2. Total noise $x10^{-4}$ in rms volts.

Figure 27. Diffusion noise from 0.10M $CuSO_4$ passing through a hole 0.6mm in diameter and 3.3mm long.

a) Power spectrum.

b) IR drop vs. current density.

Figure 28. Plot of $\log \chi$ vs $\frac{1}{T}$

○ 0.025M HCl, MC 3235

⊖ 0.050M HCl, MC 3235

Figure 29. Plot of $\log \beta$ vs $\frac{1}{T}$

○ 0.050M HCl, MC 3235

⊖ 0.025M HCl, MC 3235

Figure 30. Corrected curves for: $J = \chi f + \beta$

A. 0.050M HCl

B. 0.025M HCl

1. 19°C, 2. 30°C, 3. 40°C, 4. 49°C.

Figure 31. Plot of $F(b)E(x)^2$ vs. $E(x)$. From 1 to 4: 49°C, 40°C, 30°C, 19°C.

A. 0.050M HCl

B. 0.025M HCl

Figure 32. Plot of F(b) vs. E(x). From 1 to 4: 49°C, 40°C, 30°C, 19°C.

A. 0.050M HCl

B. 0.025M HCl

Figure 33. $f = \frac{1}{2\pi\tau}$ vs. E(x). From 1 to 4: 49°C, 40°C, 30°C, 19°C.

A. 0.050M HCl

B. 0.025M HCl

Figure 34. Log f vs. $\frac{1}{T}$ at $E(x) = 3.16 \times 10^7$ volts/meter.

△ 0.050M HCl Ea = 15.4 Kcal

○ 0.025M HCl Ea = 17.5 Kcal

Figure 35. Equivalent circuit for filtered noise.

Figure 36. Power spectrum with a relaxation time of 10^{-3} seconds unfiltered (1) and filtered through a low-pass filter (2).

Figure 37. Proposed qualitative concentration profiles at various time intervals after current is applied.

Co = Bulk concentration.

O = Membrane surface.

Ci = Residual concentration in depletion layer.

tss = Time for the formation of a steady state concentration profile.

Figure 38. The super-position of f^{-2} noise source with a noise source with a relaxation time of 10^{-4} seconds.

Figure 39. Comparison of power spectra of NaCl and Na_2HPO_4 with MC 3235 at 43 ma/cm^2.

1. 0.056M Na_2HPO_4
2. 0.10M NaCl

Figure 40. Proposed qualitative profile of specific resistance with distance from membrane.

Rd = Specific resistance of region of thickness, a, where water dissociation occurs.

Ro = Specific resistance of the bulk solution.

Figure 41. Current source noise with HCl spectra to show unmodified white noise. Broken line represents the external white noise level supplied by the 1390-B random noise generator. The initial slope is a HCl spectrum at 31 ma/cm^2 with MC 3235.

Introduction

The intricate chemical balance necessary for life would not be possible but for the selective control of material fluxes by membranes. Although membranes had been long recognized as vital physiological entities, the characterization of their chemical composition and electrophysiological properties are recent developments and still subjects of active investigation.[1]

The biological systems demonstrate the potential uses of synthetic membranes which at present have not been realized. Even as scientific interest intensifies, social developments suggest use of synthetic membranes as a solution of a critical problem. As the technological capacity of industrial man increases he is faced with an increasing pollution problem that threatens otherwise stable ecological systems. For this problem alone, artificial membranes offer a tremendous potential.

The facet of fundamental importance that has thus far eluded investigators is the mode and energetics of membrane transport. Success in this phase of the inquiry would constitute a new breakthrough in biological science.

While electrophysiologists devote intensive efforts to the very complex problems of biological membrane transport, the energetics of ion transport of the relatively

simple commercial membranes still remain only rudimentarily defined. It is on this problem that we have decided to focus our investigation with a tool as yet essentially untried in membrane studies: the analysis of fluctuations associated with transport.

Our system is made up of two ionic solutions separated by an ion exchange membrane. An electrode in each compartment connected to a dry cell battery provides the energy for the transport of ions across the membrane. The movement of the ions through the solution and the membrane is a random process which imparts a fluctuating component to the direct current supplied by the battery. This fluctuating component, commonly referred to as noise, is amplified and resolved by frequency to give information about the transport process.

The remainder of the introduction is devoted to the development of ion-exchange and noise theories which were applied to this study.

I. Different Approaches to Membrane Transport

Current treatments of membrane kinetics may be grouped into three categories based on the nature of the flux equation used in the formulations.[2] The first group uses the Nernst-Planck equation as the basic flux equation:

$$(1) \qquad J_i = J_{i(d)} + J_{i(e)} = -D_i C_i \frac{d \ln a_i}{ds} - u_i z_i C_i E_{(s)}$$

$J_{i(d)}$ = flux of species i due to diffusion.

$J_{i(e)}$ = flux due to migration in an electric field.

D_i = diffusion coefficient.

a_i = activity.

u_i = mobility.

C_i = concentration.

$E_{(s)}$ = electric field.

z_i = number of charges on the ion.

The second group uses the theorems of Irreversible Thermodynamics to evaluate the fluxes. The fundamental theorem gives the expression for entropy production:[3]

$$(2) \qquad T \frac{dS}{dT} = \sum_i J_i X_i$$

where the J_i's are the fluxes and the X_i's are the conjugate forces corresponding to the gradients of the intensive properties. The fluxes are related to the phenomenol-

ogical coefficents, L_{ik}, by:

(3) $$J_i = \sum_k L_{ik} X_k$$

The Onsager reciprocal relations require that $L_{ik} = L_{ki}$ such that the phenomenological coefficients form a symmetric, square matrix:

(4) $$\vec{J} = [L_{ik}] \vec{X}$$

The third category utilizes the theory of rate processes, and requires knowledge of the potential energy profile within the membrane. This approach is still in a rudimentary state of development because the system is too complex for rigorous theoretical treatment and a detailed picture of the internal kinetics of membrane transport has not been accessible to conventional experimental techniques.

However, electrical noise analyses has been used successfully to study transport kinetics in semoconductors and the theory of fluctuations and the experimental applications have been sufficiently developed to make applications feasible in membrane transport. Since noise is directly related to the microscopic interactions of the systems, kinetic information should be obtained directly from the observed fluctuations.

II. Equilibria and Permselectivity

Ion exchange membranes have fixed ionic groups on the membrane matrix.[6] When immersed in an ionic solution the presence of fixed ionic groups ($-SO_3^-$, $-CO_3^-$ etc. in cation exchange membranes, and $-NH_3^+$, $>NH_2^+$ etc. in anion exchanges) causes exclusion of colons by electrostatic repulsion. This is a result of the membrane equilibria and the consequent membrane potential, the relations of which was derived by F. G. Donnan[5] and bears his name. By equating the chemical potential of solvents, and the diffusable ions in the two phases, two equations for the osmotic pressures are obtained.[2, 6, 7]

(5) a) $U_s^I = U_s^\circ + PV_s + kT \ln a^I = U_s^{II}$

b) $P^I - P^{II} = \frac{kT}{V_s} \ln \frac{a_s^{II}}{a_s^I}$

c) $U_+^I + U_-^I = U_+^{II} + U_-^{II}$

d) $P^I - P^{II} = \frac{kT}{V_+ + V_-} \ln \frac{a_+^{II} a_-^{II}}{a_+^I a_-^I}$

P = vapor pressure of the solvent.

U_s = chemical potential of solvent.

U_+, U_- = chemical potential of − and + ion.

V = partial molar volume.

k, T, a = Boltzman's constant, temperature, activity.

Subscripts denote solvent or charged species, superscripts I and II denotes the phase with the nondiffusible ion and the phase with unrestricted mobility respectively.

On eliminating $\frac{P^I - P^{II}}{RT}$, the equilibrium law is obtained:

(6) $$\frac{a_+^{II} a_-^{II}}{a_+^{I} a_-^{I}} = \left(\frac{a_s^{II}}{a_s^{I}}\right)^{\frac{\nu_+ + \nu_-}{\nu_s}}$$

The electrical potential across the interface is given by:

(7) $$V = \frac{RT}{z'C} \ln \frac{a_s^{II}}{a_s^{I}}$$

Permselectivity of ion exchange membranes develops when the counterion activity in the bathing solution is less than in the membrane phase. The difference in activity causes the counterion to diffuse into the region of lower potential. A similar migration of coion into the membrane (region of lower potential for the coion) occurs. The net result is the formation of an electrostatic potential at the membrane interface called the Donnan Potential.[6] The Donnan equilibrium is established when the electrostatic potential balances the chemical potential at the state of minimum electrochemical free energy. A stable electrostatic potential develops across the interface, which acts as an electrostatic barrier to coions (Donnan exclusion) the macroscopic manifestation of which is the permselectivity observed in ion exchange membranes. It follows that the permselectivity of a membrane decreases with increasing solution electrolyte concentration. Permselectivity no longer exists when the activity of the counterion in the solution equals or exceeds the activity in the membrane phase.

III Membrane Transport

It is convenient to evaluate transport in terms of flux which is the flow of the quantity of interest per unit area per unit time. The driving forces for fluxes are the gradients of the intensive variables of the system.[2, 3] A chemical potential gradient results in diffusion and osmosis. An electric field (gradient of the electrical potential) is responsible for drift (migration or conduction) and electroosmosis which is the flow of solvent through a semipermeable membrane due to an electric field. Temperature and pressure gradients give rise to heat conduction, thermoosmosis and hydraulic permeability (reverse osmosis). The interactions are such that a chemical potential gradient can cause an electrostatic potential difference (membrane potential) such as the Donnan potential. Similarly, a temperature gradient can result in a chemical potential gradient (Soret effect) and an electrostatic potential gradient can result in the thermal diffusion potential. As previously stated the products of the forces and the Onsager coefficients form elements of the flux vector and these form a square symmetric matrix.[8]

Membrane effects when observed under the conditions of constant bulk concentration and temperature with pressure and electrical potential as variables are called electrokinetic effects.[3]

When the fluxes result from differences in electrical and chemical potentials only, the Nernst-Planck equation and Fick's diffusion laws can be applied.[2] Most electrode processes and electrolyte conductivity studies fall into this category.

The effect of an ion-exchange membrane on an electrolyte in the presence of an electric field is to increase the transport number of the counter-ion in the membrane. When Donnan exclusion is complete the transport number of the counter-ion in the membrane will be one. The membrane charge carriers may not be the same as the solution charge carriers for this reason since the solution current will be carried by both charged carriers.

An effect of the Donnan exclusion can be seen when the current density is increased gradually. Due to the difference in the counter-ion transport numbers, the counter-ion transport through the membrane is faster than through the solution. This causes an electrolyte depletion at the membrane surface. The difference in the transport number must be made up for by diffusion and convection. With increasing current density a critical current density is reached when the additional flux from diffusion and convection can no longer bridge the gap. The concentration at the membrane surface drops and the electric field becomes suffi-

ciently large to dissociate water. Any further increase in the flux will come from the dissociation products of water. A voltage-current plot would show a vertical rise in the voltage drop across the membrane at the critical current density.[9] Gregor and Miller[10] concluded that a field of 10^3 volts/cm was sufficient to significantly affect water dissociation at the membrane surface. Their results were based on the knowledge of a Nernst layer thickness, δ, the transport number, t_{w}, of protons from water dissociation and an assumed discontinuity of the dissociation constant at the membrane surface. The Nernst layer, the layer on the membrane surface that is not disturbed by stirring, was calculated from diffusion studies based on the Nernst-Planck equation.

IV Noise Theory

In a generalized sense, noise is the fluctuation of a random variable.[11] The observed parameter α is the deviation of the thermodynamic extensive variables, a, from an equilibrium value, a_{eq}, or from some steady state value a_{ss}.

$$\alpha = a - a_{eq} \tag{8}$$

$$\alpha = a - a_{ss}$$

The force, X_i, conjugate to α_i can be expressed in

terms of the fundamental thermodynamic potential, entropy, S:[4]

$$X_i = \frac{\partial S}{\partial \alpha_i} \tag{9}$$

The total noise can be analyzed into its various Fourier components by means of a filter. The output then is the power spectrum. The Wiener-Khintchin theorem[12, 13] shows that this power spectrum is the Fourier cosine transform of the correlation function:

$$G(f) = 4\,\mathrm{Re}\int C(\tau)\, e^{-i\omega t}\, dt = 4\int C(\tau)\cos\omega t\, dt \tag{10}$$

Where f is the frequency $2\pi\omega$ and t is time.

It follows that knowledge of the correlation function completely specifies the power spectrum by use of the Fourier integral theorem:[13]

$$f(x) = \frac{1}{2\pi}\int du \int F(t)\, e^{[iu(t-x)]}\, dt \tag{11}$$

The correlation function is given by:

$$C(\tau) = \int G(f)\cos\omega t\, df \tag{12}$$

Kinetic information is contained in the correlation function, which is defined as the time average of the product of $\alpha(t)$ and $\alpha(t+\tau)$:

$$C(\tau) = \langle \alpha(t)\alpha(t'-t)\rangle = \langle \alpha(0)\alpha(\tau)\rangle \qquad \tau = t'-t \tag{13}$$

A few limitations have been imposed on the system in the above expression for $C(\tau)$.

(1) The system is Markoffian such that knowledge of the value of α at time, t, determines the value of this variable at all later times which makes any knowledge of α prior to t obsolete.

(2) The system is stationary, i.e., at equilibrium or at a nonequilibrium steady state such that

$$\langle \alpha(t)\,\alpha(t+\tau)\rangle = \langle \alpha(0)\,\alpha(\tau)\rangle$$

(3) The time average of $\langle\alpha\rangle$ is zero, i.e., $\bar{\alpha} = \langle\alpha\rangle = 0$

Since the correlation function is the second moment of the distribution function of the Markoff variable, the power spectrum can be calculated from the distribution function. A distribution function is completely specified by all its moments. However, for equilibrium fluctuations the second moments can be obtained exactly starting from Boltzmann's statement relating entropy S to probability W :

$$S(\alpha) = k \ln W(\alpha) \tag{14}$$

$$\alpha = \sum \alpha_i$$

The second moments calculated from this distribution were shown to be exact.[14]

$$W(\alpha) = N \exp\left(-\tfrac{1}{2}\,\frac{\vec{\alpha}\cdot S\cdot\vec{\alpha}}{k}\right) \tag{15}$$

For the nonequilibrium fluctuations, a linear system defined as a system with linear responses to the forces,[11] gives rise to a Gaussian distribution, $W(\alpha)$. The same treatment can be applied to quasi-linear systems of sufficiently small fluctuations or where the deviation from linearity is not appreciable. Assuming that α is a Markoffian random variable, α is completely specified by the conditional probability $P[\alpha(\omega)|\alpha,t]$. This conditional probability must obey the Smoluchowski consistency condition.[4, 15]

$$(16) \qquad P[\alpha(\omega)|\alpha(t)] = \int d\alpha' \, P[\alpha(\omega)|\alpha(t)] \, W[\alpha'|\alpha,\Delta t]$$

where $W[\alpha'|\alpha,\Delta t]$ is the transition probability from α' to α in time Δt which is assumed known from prior investigations into statistical mechanics.

The ensemble average of $\alpha(t)$ subject to initial conditions can be obtained from the conditional probability:

$$(17) \qquad \langle \alpha(t+\Delta t) \rangle_{\alpha_0} = \int \alpha \, P[\alpha_0|\alpha,t+\Delta t] \, d\alpha$$
$$= \int d\alpha' \, P[\alpha_0|\alpha',t] \int d\alpha \, \alpha \, W[\alpha'|\alpha\Delta t]$$

The condition of linearity gives a linear expression for the last integral of the form:

$$(18) \qquad \int d\alpha \, \alpha \, W(\alpha|\alpha,\Delta t) = \alpha' - \Lambda\alpha\Delta t$$

Then:

$$\langle \alpha(t+\tau) \rangle = \langle \alpha(t) \rangle - \Lambda \langle \alpha(t) \rangle \Delta t \tag{19}$$

To give:

$$\frac{d\langle \alpha(t) \rangle}{dt} = -\Lambda \langle \alpha(t) \rangle \tag{20}$$

$$\langle \alpha(t) \rangle = \alpha_0 \exp -(\Lambda t) \tag{21}$$

The correlation function is then given as:

$$\langle \alpha(t) \alpha_0 \rangle = \langle \alpha \alpha \rangle \exp -(\Lambda t) \tag{22}$$

where Λ is the relaxation matrix containing the relaxation times.

When the behavior of the system can be characterized by a single relaxation time the correlation function can be set immediately as:

$$C(\tau) = \langle \alpha \alpha \rangle \exp -\left(\frac{t}{\tau}\right) \tag{23}$$

where τ is relaxation time. In this situation all the thermodynamic variables follow the same regression law determined by the characteristic relaxation time.[16]

For a linear system the microscopic regression obeys the macroscopic laws of motion, the difference between a fluctuation and a macroscopic displacement being one of size,[4] thus the power spectrum arising from the fluctuations can be obtained from the phenomenological equations describing

the macroscopic system[14,15]. Then noise from transport phenomena can be calculated from the Green's function $g(x,t;x|t')$ of the transport equation[15,18]. For the case of transport due to drift and diffusion, the Green's function of Fick's second law is appropriate.[13]

$$(24) \qquad \frac{\partial g(x,t;x',t')}{\partial t} = D\frac{\partial^2 g(x,t;x',t')}{\partial x^2} + u\varepsilon\frac{\partial g(x,t;x',t')}{\partial x} + \delta(t)\delta(x-x')$$

The Green's function gives the value of g at x at time t due to a concentration disturbance by a unit impulse at x' at time t'. The power spectrum is obtained by integrating the Fourier transform of $g(x,t;x',t')$ over x and x'.

For the case of a chemical reaction, the phenomenological equation of motion is the decay to equilibrium of a displacement contained in the rate laws.[17]

$$(25) \qquad \frac{d\vec{\alpha}}{dt} = -M\vec{\alpha}$$

$$\vec{\alpha} = \Sigma\alpha_i$$

$$\alpha_i = a_i - \bar{a}_i$$

M is the symmetric relaxation matrix, analogous to Λ containing the chemical relaxation times. The α_i's are the principle axes of the chemical system and are obtained from the true concentration variables by an affine coordinate transformation. The true concentration variable $\beta = b - \bar{b}$ is related to α by:

$$(26) \qquad \beta_i = \Sigma r_{ik}\alpha_k$$

The value B is the displacement of the concentration b from the equilibrium concentration $\bar{b}$.

For a simple reaction involving an equilibrium of a dissociating species:

(27) $$AB \underset{k_2}{\overset{k_1}{\rightleftharpoons}} A^{+} + B^{-}$$

The time behavior of a fluctuation is characterized by a single relaxation time τ, which is given by:

(28) $$\tau = \frac{1}{k_1 + k_2(c_a + c_b)}$$

$$\alpha = \alpha_0 e^{-t/\tau}$$

The correlation function is:

(29) $$C(\tau) = \langle \alpha_0^2 \rangle e^{-t/\tau}$$

The power spectrum is given by:

(30) $$G(f) = \frac{4\langle \alpha_0^2 \rangle \tau}{1 + \omega^2 \tau^2}$$

A graph of the Log P vs. Log f shows that the spectrum is flat (white) up to the neighborhood where ω is equal to $\frac{1}{\tau}$ after which point the power spectrum decays by ω^{-2}. Johnson noise, the noise characteristic of all resistances has been explained in this form but by a microscopic derivation of the Nyquist theorem. (This theorem was first derived by Nyquist using the lossless transmission line model.) The

microscopic derivation gives a relaxation time of the order of the jump time of electron. This makes the Nyquist noise white up to 10^{12} Hertz which is inaccessible to experimental verification.[12]

The methods described have been used successfully to explain shot noise, drift noise, generation-recombination noise and noise of mixed origins.[15, 20]

One previous attempt to use noise measurements to study transport kinetics across a biological membrane found only 1/f noise attributed to passive potassium transport.[21] (The term "1/f noise" is used to describe noise sources whose power dissipation is inversely proportional to the frequency. The phenomenom is observed commonly in semiconductors but analyses have not resulted in any firm conclusions as to cause. A theoretical model[22, 23] based on a distribution of energy states indicates that 1/f noise or modified forms of it could be descriptive of potential energy profiles within a membrane.)

V Relation of Noise to Membrane Transport

Previous experimental studies of membrane kinetics have dealt with measurements of diffusion coefficients and electrokinetic effects. The kinetic measurements within the membrane by such conventional methods are seriously hindered by the fact that ion exchange is usually not the rate determining step.[2, 6]

Theoretical treatments are hampered by the usual difficulties in the study of strong electrolytes. The lower activities observed with polyelectrolyte solutions have been explained in terms of ion-binding of counterions to the polyelectrolyte backbone.[24]

Such binding would lead to a potential energy topography consisting of a sequence of potential energy barriers to ion transport. Theoretical investigations have been made based on hypothetical potential energy profiles[2] but it would be helpful to obtain some kinetic data for the ion-binding mechanism itself.

The similarity of the ion-binding process to the generation-recombination mechanism of semiconductors is worth noting. The dissociation of an ion at a site on the polyelectrolyte resembles the excitation of an electron in a semiconductor from the valence band to the conduction band.[25]

The analogy of ion-exchange membranes to semiconductors cannot be extended much farther than this. The energy gap between bands can be calculated from principles of quantum mechanics and verified from spectroscopic as well as conductivity studies. In addition, other intermediate energy levels can be introduced by impurities or crystal defects. These levels act as trapping sites of the charge carriers such that the conductivity is lowered.

On the other hand, the ion-binding force of polyelectrolyte salts is expected to be purely electrostatic and localized. As such, solvation effects, steric effects, and space charge effects from neighboring sites become important. The conductivity is also dependent on pore sizes due to frictional effects on the migrating ion and the tortuosity factor which affects diffusivity by lengthening the diffusion path.[26] In addition, electrokinetic effects must be considered.

Whereas in semiconductors only two species of charge carriers exist, electrons and holes, membrane charge carriers can vary with respect to charge, mass and volume.

The basic considerations indicate that membrane processes will be more complex than solid state processes. However the larger variability of the membrane parameters may serve to increase the understanding of random processes itself.

The attractive feature of noise analysis is the possibility of observing relaxation times associated with processes other than the rate determining step. The noise expected from a particular sequence of steps can be obtained from the solution of the continuity equation under appropriate boundary conditions. In this way it is possible that the energetics of the ion-binding processes will reveal itself in the power spectrum of the generated noise.

EXPERIMENTAL

I General Scheme

Measurement of electrical fluctuations across the membrane calls for two compartments separated by a membrane. A noise-free constant current dc field supplied by two outer electrodes causes the ions to migrate across the membrane. The fluctuations caused by the transport processes are picked up by another pair of electrodes placed opposite each other on either side of the membrane which feeds into a low noise preamplifier. This noise is fed to a spectrum analyzer to obtain the power spectrum. In the early phases of the investigation, a Khronhite model 3100 band-pass filter with a band width of the order of the center frequency was used. Later a Tektronix 3L5 spectrum analyzer with variable resolution down to 10Hz became available. The noise cell dc current circuit and the preamplifier were placed in an aluminum box lined with magnetic shielding to minimize pickup.

The cell current was supplied by a 90 volt carbon-zinc battery. A 100K potentiometer was connected in series with the cell served as a swamping resistor and a current control device. A milliammeter was connected in series in the circuit for current measurement, then removed during spectrum analysis (Figure 1).

Figure 1. Schematic of the noise, voltage measuring system.

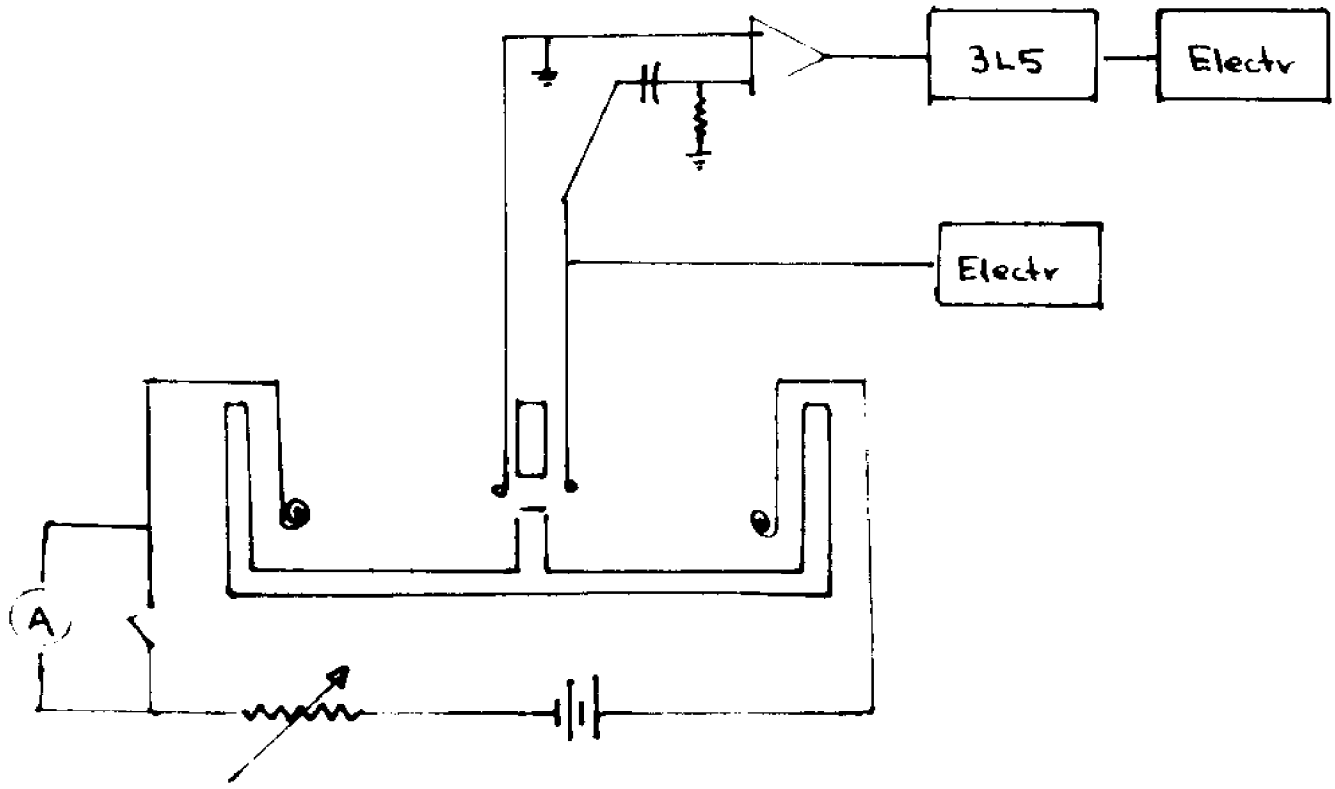

II. Noise Cells

Two types of cells were constructed to serve this function. Both were fitted for temperature control from an external reservoir. The first consisted of two cylindrical compartments each having a 2 ml. volume. The compartments were separated by a membrane taped onto a rubber gasket. The tape, which was impermeable to water, was provided with a hole 3.5 mm. in diameter. Brass bolts, passed through the four corners of flanges attached to the outer ends of the compartments, served to hold the assembly together. There were three holes in the top of each compartment. Two outer holes held the field electrodes which provided the current. The inner holes, positioned as close as possible on either side of the membrane, held the probe electrodes. The center holes were used to change solutions.

A plexiglass box with inner dimensions of 4.0cm. by 10.9cm. by 3.0cm. divided into two compartments by a middle divider with a hole served as a second cell. The cover for this cell had five holes on each half. Two holes on each side held the electrodes. Two more holes were used for circulating heating oil through glass tubing that extended into the solution. The last hole was used to change solutions. (Figure 2)

Figure 2. The plexiglass cell used for noise measurements.

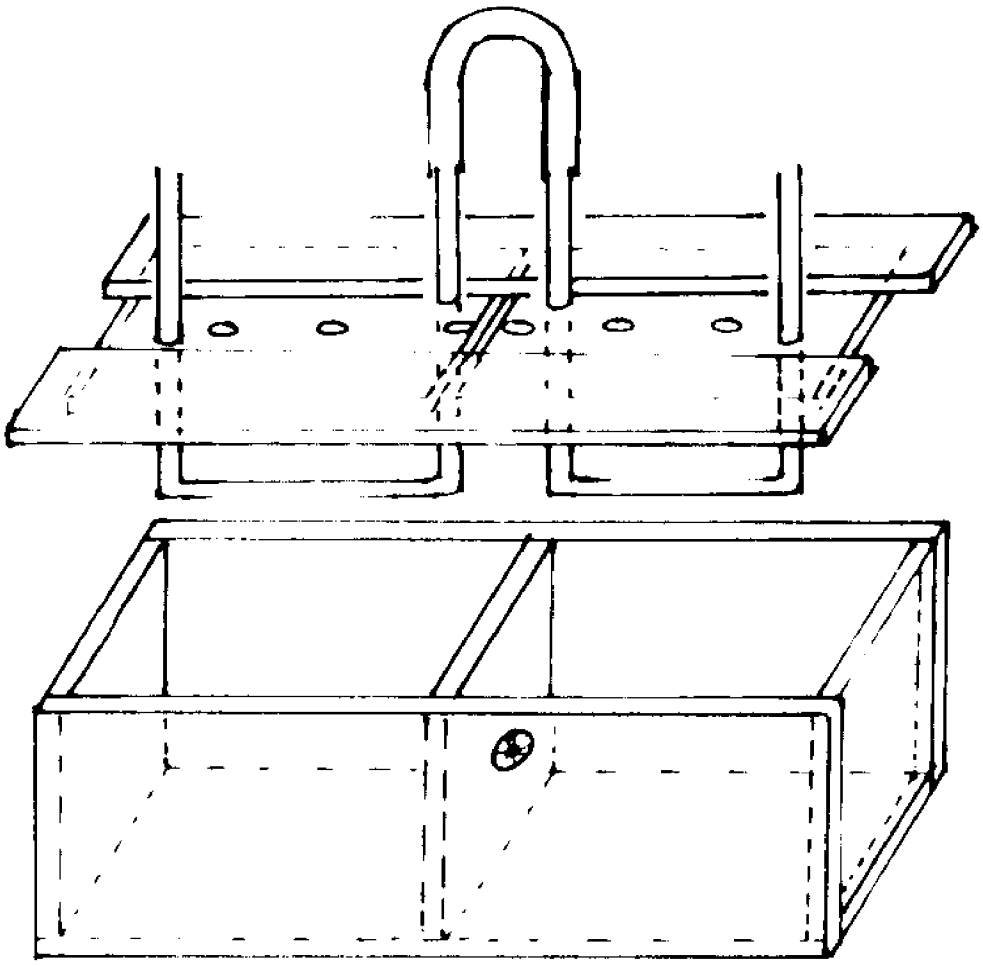

III Material

The membranes were obtained in 9x12 inch sheets from the Ionac Chemical Company. They consisted of crosslinked sulfonated polystyrene for the cation membranes, MC-3142 and MC-3235 and crosslinked aminated polystyrene for anion membranes MA-3148 and MA-3236. The general properties supplied by the manufacturer for MC-3142, MC-3235, MA-3148 and MA-3236 respectively were: ac electrical resistance in 0.1 N NaCl, in ohm-cm^2: 9.1, 18, 10.1 and 35; membrane thickness, in mils: 6, 12, 7 and 12; approximate density, in $gm\text{-}cm^{-2}$: 196, 358, 196 and 358; capacity in mequiv cm^{-2}: 0.021, 0.045, 0.019 and 0.027.

Circular pieces of membrane were cut out with cork borers of 11 mm. diameter. The membrane was taped onto the rubber gasket in the case of the cylindrical cell and to the center piece on the larger cell with a rectangular piece of Mystik tape. Friction tape was used above room temperature because Mystik tape deteriorated. The membrane area exposed to transport was determined by the diameter of a hole previously cut into the tape. Holes with three different diameters were used on the tape: 3.5 mm., 3.2 mm. and 2.75 mm.

Platinum electrodes were used for most of the measurements. The platinum was cleaned periodically by heating in the oxidizing part of the bunsen burner flame. The platinum

electrode is adequate for noise (ac) measurements but is not a reversible electrode. Comparison of a reversible electrode with platinum electrodes was made by using copper wire with copper sulfate solutions and silver-silver chloride electrodes with chloride salts.

IV General Procedures

The membranes were soaked in distilled water a minimum of 24 hours before use. The membrane was positioned into place with tape as described earlier. To convert the membrane to the counterion salt of interest, the cell was filled with the salt solution and a current of 1 ma was passed through the membrane for 5 to 10 minutes. The solution was changed before measurements were taken. No effects attributed to a possible lack of equilibration were observed in any of the results.

The desired current was set by adjusting the swamping potentiometer with a milliameter. The cover was placed on the chassis and the total noise was recorded. In the case of the band-pass filter, measurements were taken at three equidistant points on the log of Hz scale per decade (10Hz, 20Hz, 50Hz, etc.). To plot as a power spectrum a conversion had to be made.

Power is proportional to V^2, $P = \frac{V^2}{R}$, and the power spectrum is a function of frequency. However, the measured

rms voltage represents a band width, Δf. Therefore as measured:

$$(31) \qquad G(f) = \frac{V^2(f)}{R \Delta f}$$

The data were generally plotted in terms of decibels vs. log of frequency.

$$(32) \qquad db = 10 \log \frac{P}{Po}$$

$$= 10 \log \frac{V^2}{Vo^2} - \log R - \log f$$

Since log R was a constant, it only served to shift the curve up or down and it was ignored. This gave a final form of db = 20 log V - log f. Decibels could be read directly on the meter and Δf was equal to f for the Khronhite model 3100 filter.

Higher resolution was made possible when a Tektronix 3L5 spectrum analyzer was obtained. This instrument displayed the noise spectrum on the oscilloscope in frequency ranges of 100Hz, 200Hz, 500Hz, 1KHz, 2KHz, 5KHz, 10KHz, 100KHz, 1MHz, with resolutions of 10, 20, 50, 100, 200, 500, 1KHz, 10KHz and 100KHz. Sweep rates of 1 microsec./div. to 15 sec./div. were available including a manual sweep.

V The 3L5 on an Automatic Sweep

It had been hoped that the 3L5 would give useful spectra either on the CRT which could be photographed or on a suitable recorder which could be connected to the 3L5 output. This method would then give a continuous spectrum in an efficient and uniform manner.

However, several complications made this method impractical. By the nature of a power spectrum it was more significant to obtain noise power as a function of the log of frequency. Since the spectrum analyzer was designed to sweep linearly with respect to frequency it was necessary to replot whatever data was obtained from the 3L5. There was also a finite time within which a complete measurement had to be made since the concentration changed with time due to the transport of ion and the electrode reactions. Therefore it was desirable to sweep the lower frequencies which necessarily required higher resolutions and thus longer averaging time at a lower rate and to increase the resolution and sweep rate at higher frequencies. The spectrum analyzer was not designed for these requirements.

An attempt was still made to use the automatic sweep. Photographs taken at various sweep rates and resolutions when replotted could not be made continuous from one picture to the next. Several difficulties became immediately obvious.

The apparent amplitude on the photograph was a function of the trace intensity and exposure time in addition to the resolution and attenuation setting. The oscillscope intensity could be set at one position for as long as necessary. However, the exposure time was determined by the sweep rate which could not be compensated for very easily. Then it was found that the resolution was not independent of dispersion and center frequency settings. As a result photographs of overlapping portions of the spectrum did not overlap when replotted.

To circumvent these artificial parameters injected by the varying intensity on the photograph the oscilloscope output was fed to a recorder. This method still did not remove the difficulty of the varying band width of the various 3L5 settings. However, the main setback was still the lack of efficiency in terms of time and precision of a sweep that was linear with frequency.

It became obvious that a manual sweep was the most advantageous mode of operation. A manual sweep allowed as much time averaging as was desired and it permitted observation of only the points of interest. Precise calibration in terms of frequency was easier and it removed the intermediate step of extracting data from a photograph or recorder chart paper. The difficulty of the varying band width was avoided by using a single resolution throughout

the measurement. Since the 3L5 freed the RMS voltmeter, it was now possible to monitor membrane voltage and total noise throughout the period of spectrum analysis. This last method required from 7 to 15 minutes to obtain 6 points per decade for a spectrum.

For current noise and current-voltage measurements it would have been convenient to have external control of the swamping resistor and a built-in visible ammeter. Whether this can be done without excessive pickup must be investigated. As arranged these measurements had to be done by first putting an ammeter into the circuit to measure the current, remove the ammeter, replace the chassis cover and take a noise reading. As many points as necessary were taken in this manner. The same procedure was repeated for voltage measurements, which did not require shielding. An additional output BNC plug on the chassis for simultaneous voltage readings was a later modification.

Noise-time measurements required an external control to switch on the current with minimum pickup. This was accomplished by installing a mercury switch into the circuit. A flat piece of plastic with a loop to hold the mercury switch was slipped between the cover and base of the chassis. The current was set at the desired value, and the output connected to the 3L5 fitted with a camera. The camera. The camera was set on time exposure and the cell and

oscilloscope sweep activated together.

VI The AC Amplifier Circuit

The main requirements of a preamplifier for this investigation were a high input impedance, wide range frequency response, up to 100KHz, low noise and high gain. A Philbrick P85AH operational amplifier used as a follower with a gain of 100 served these purposes (Figure 3).

An additional gain of 100 was obtained when necessary with a 466A Hewlett-Packard operational amplifier with maximum output of 1.5VRMS. Amplifier noise was a function of the input impedance which was determined by the resistor which grounded the input capacitor. When this resistor was 1 megohm the total amplifier noise was 5.7 μV, referred to input.

Another low noise self-contained amplifier, LA260V from Applied Cybernetics was used. This amplifier had a total noise level of 1.4 μV. In both cases an input capacitance of .5μf was put in series with the input to block out the dc signal. This made it necessary to lower the input resistance of the amplifier so that large fluctuations would not block the ac response. Such blocking could be observed on the oscilloscope display as a cutting-off of the signal. This was progressively diminished as the input resistance was lowered. However, too small a time constant decreased the low frequency response, the cut-off frequency follow-

Figure 3. The Philbrick P85AH preamplifier hooked up as a follower with a gain of 100.

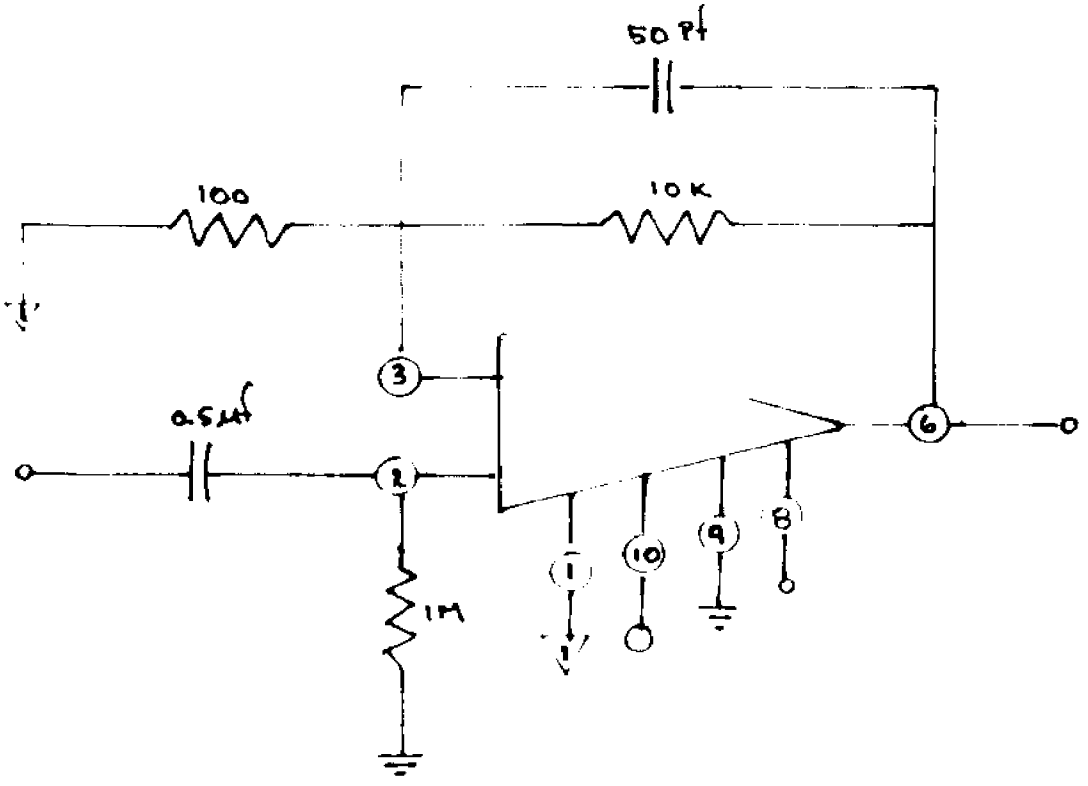

ing the relation of a high pass filter: $f = \frac{1}{2\pi RC}$

The final workable instrumental sequence for the 3L5 will now be discussed. The schematic can be seen in Figure 3. The amplified noise from the amplifier was passed through the Krohnhite Model 3100 filter set as a high pass filter. (it was found to be necessary to cut off frequencies below that being measured in order to prevent overloading the spectrum analyzer which was found to have approximately a 30 db dynamic range.)

The 3L5 was set for the frequency range and resolution of interest and the frequency desired set manually. The amplitude was measured by feeding the oscillscope output to a Keithley electrometer. Some damping was necessary to facilitate meter reading and this was accomplished by connecting a 1000 μF capacitor across the oscilloscope output.

Use of the manual sweep produced some unexpected complications. The 3L5 was fitted with a potentiometer voltage output to be fed into the time base set for external input. The oscilloscope required only 1v for a full-scale horizontal deflection. However, the 3L5 manual sweep generated 10 volts full-scale. Since it was desirable to have a visible signal for calibration purposes the manual sweep was attenuated with a simple voltage divider to make the manual sweep coincide with the oscilloscope display.

The size of the manual sweep signal fed into the time base affects the calibration of the 3L5. To obtain maximum accuracy the 3L5 calibration procedure set in the manual should be followed for each value of the input to the time base. However, even with the most careful calibration it was found that the dispersion was not linear with the horizontal displacement of the oscilloscope trace. This made necessary a calibration graph of the frequency dispersion (Hz/div) with respect to the horizontal displacement by means of a sine-wave generator. This sine wave generator was in turn calibrated with a General Radio Type 1150-B digital frequency meter.

VII Response Check

A background power spectrum was taken periodically. The total background noise was 5.7 μV for a 1M input resistor. To check the frequency response of the amplifier system, white noise from a General Radio 1390-B White Noise Generator was fed into the preamp input and the amplifier response recorded through the spectrum analyzer. This check primarily gave an indication of the frequency response of the amplifier and the distributed capacitances that cause power losses.

The dynamic power range of the amplifier was tested by first passing the white noise through a high pass and double high pass filter. The resulting power spectra should have

slopes of ω^{-2} and ω^{-4} respectively. It was found that the 3L5 had a dynamic range of 30db beyond which it stopped responding. This necessitated the interjection of a high pass filter between amplifier and 3L5 in order to cut off the low frequency power. By continually reducing the signal in this manner the proper response was obtained.

Any hidden response functions that may be moderating the signal under experimental conditions were checked by converting the 1390-B Noise Generator output to a current source. This was done by inserting a 1M resistor to the output of the White Noise Generator in series with the cell. This check showed that the instrument response to external signals under experimental conditions remained unaffected.

VIII Membrane Voltage Measurements

The membrane voltage (IR drop) was measured with the Keithley electrometer through the input electrodes. Additional leads were connected from the input electrodes to a BNC type male connector placed on the chassis. In this manner the noise and the voltage could be measured simultaneously for each current setting. The absolute voltage was unreliable due to the irreversibility of the platinum electrode. The irreversibility caused a hysteresis effect on the current-voltage plot. Nevertheless, the effect of the depletion layer could be graphically examined as a sharp

unambiguous decrease in conductance at the critical current density.

IX Temperature Studies

Most of the controlled temperature studies were carried out with the large cell. Silicone oil from a Messgerate-Werk Lauda Ultra K2 Thermostat was circulated via tygon tubes that passed through holes on the chassis. The tygon tubes were connected to the glass tubing which passedthrough the cell cover into the solution studied. Temperatures from 10-50°C were obtained in this manner. Silicone oil was necessary because lower molecular weight polar solvents introduced large 60Hz pickup which could be seen on the oscilloscope display.

X Voltage/Time/Distance

Voltage vs. distance from membrane and noise vs. distance measurements were made by using a tapered microelectrode which was attached to a S.S. White Industrial Miniprobe Model 356-8245Y. This miniprobe had a 3.5mm. maximum movement corresponding to a 180° turn of an Allen wrench attachment. By attaching a stationary protractor on the movement and a pointer on the Allen wrench it was possible to divide the 3.5mm. total displacement into 180 parts or to 1.94×10^{-3} cm/deg.

The microelectrode was prepared by passivating 10 mil tungsten wire in saturated potassium nitrate solutions.[27] The tapered wire was coated except for the very tip with

nail polish (wax and dissolved plexiglass were unsatisfactory) and slipped into a hyperdermic needle which acted as a holder. A coating material that adhered properly to the tungsten wire was not found but nail polish was found to be barely adequate. The size of the exposed electrode tip was measured under a microscope with calibrations on the eyepiece and found to be in the range of about 2×10^{-3}cm.

The microelectrode was connected to an electrometer (Keithley 610B) for voltage measurement and to a P85AH Philbrick preamplifier for total noise measurements. In this way total noise and membrane voltage were monitored simultaneously. The ground was attached to another tungsten wire at the opposite side of the membrane surface. The electrometer output was fed into a Tektronix Type 3A72 dual trace amplifier plug-in with a Type 564 storage oscilloscope. The voltage-time behavior was photographed with the C-27 oscilloscope camera. A family of voltage-time curves for various current densities was put on a single photograph by using a triggered sweep (Figure 7). The pulse caused by the switch that closed the circuit was used as the trigger. To minimize pickup the first stage including the electrometer was put on the first shelf of a bus-boy's cart and covered on three sides with aluminum foil.

A magnifying glass was perched directly over the membrane but it was not possible to observe when the electrode made contact with the surface. Positive proof of contact was obtained by detecting the bending of the microelectrode by eye. A schematic diagram is provided in Figure 4.

Figure 4. Schematic of the system for distance profiles of noise and membrane voltage.

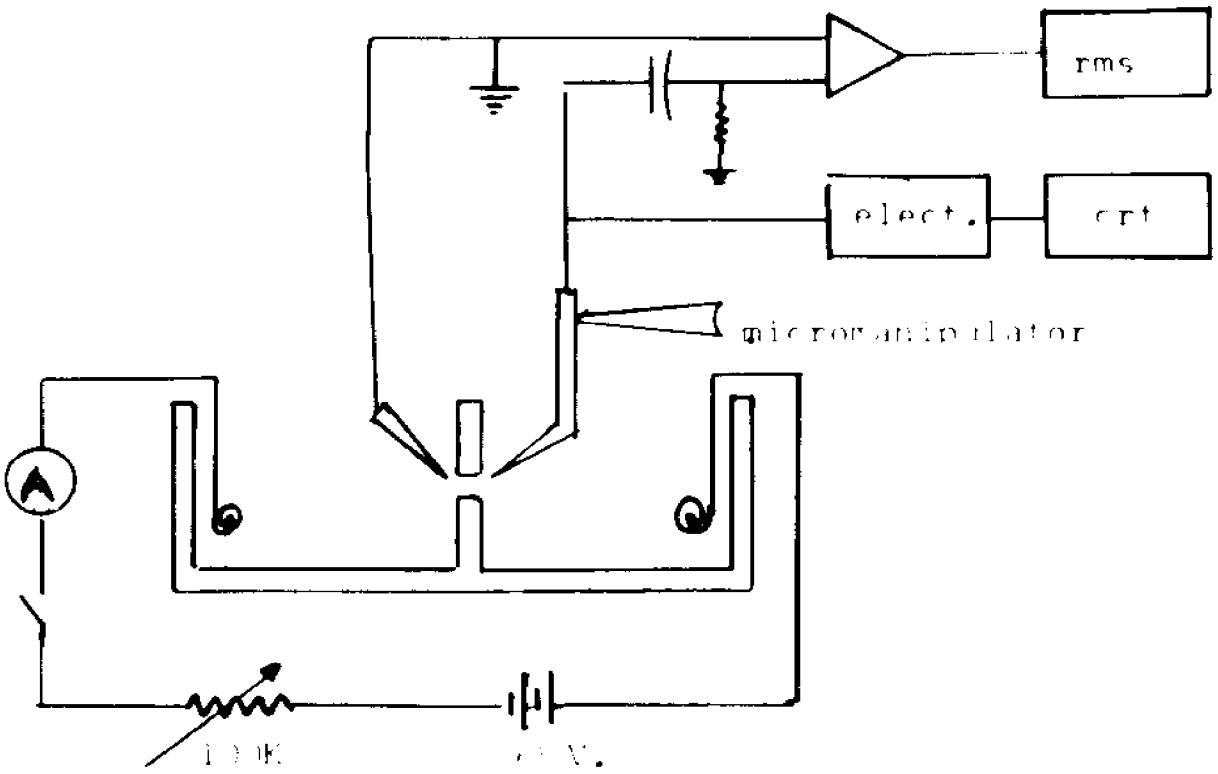

RESULTS

I General Electrical Properties

Cation membranes gave results that were different from those of anion membranes. The cation noise was not detected below a critical current density. At the critical current density, the noise level rose sharply over a short range of current, after which it increased slowly. The noise from anion membranes did not show such a relationship between noise and critical current density. In the current-voltage plot the critical current density can be observed as a sharp departure from ohmic behavior. These features can be seen in Figure 5.

The critical current densities determined from current-voltage plots for various salts and membranes and the currents at which noise was detected are listed in Table 1. The critical current density increased with salt concentration and increasing counter-ion mobility.

The time lag for the appearance of noise on the cation membrane was displayed on an oscilloscope and photographed. The lag is associated with the time required for the formation of a depletion layer. As such, lower current densities, higher concentrations, and ions of higher mobility have longer time lags. No time lag was observed for anion membrane noise. This is consistent with the observed independence of anion noise from critical current density. These features can be seen in Figure 6.

Figure 5. Voltage and noise vs. current curves for 0.10M NaCl.

- ○ Membrane volts vs. current for MA 3148 anion exchange membrane.
- ● Membrane volts vs. current for MC 3235 cation exchange membrane.
- □ Total noise vs. current for MA 3148 anion exchange membrane.
- ■ Total noise vs. current for MC 3235 cation exchange membrane.

Figure 5

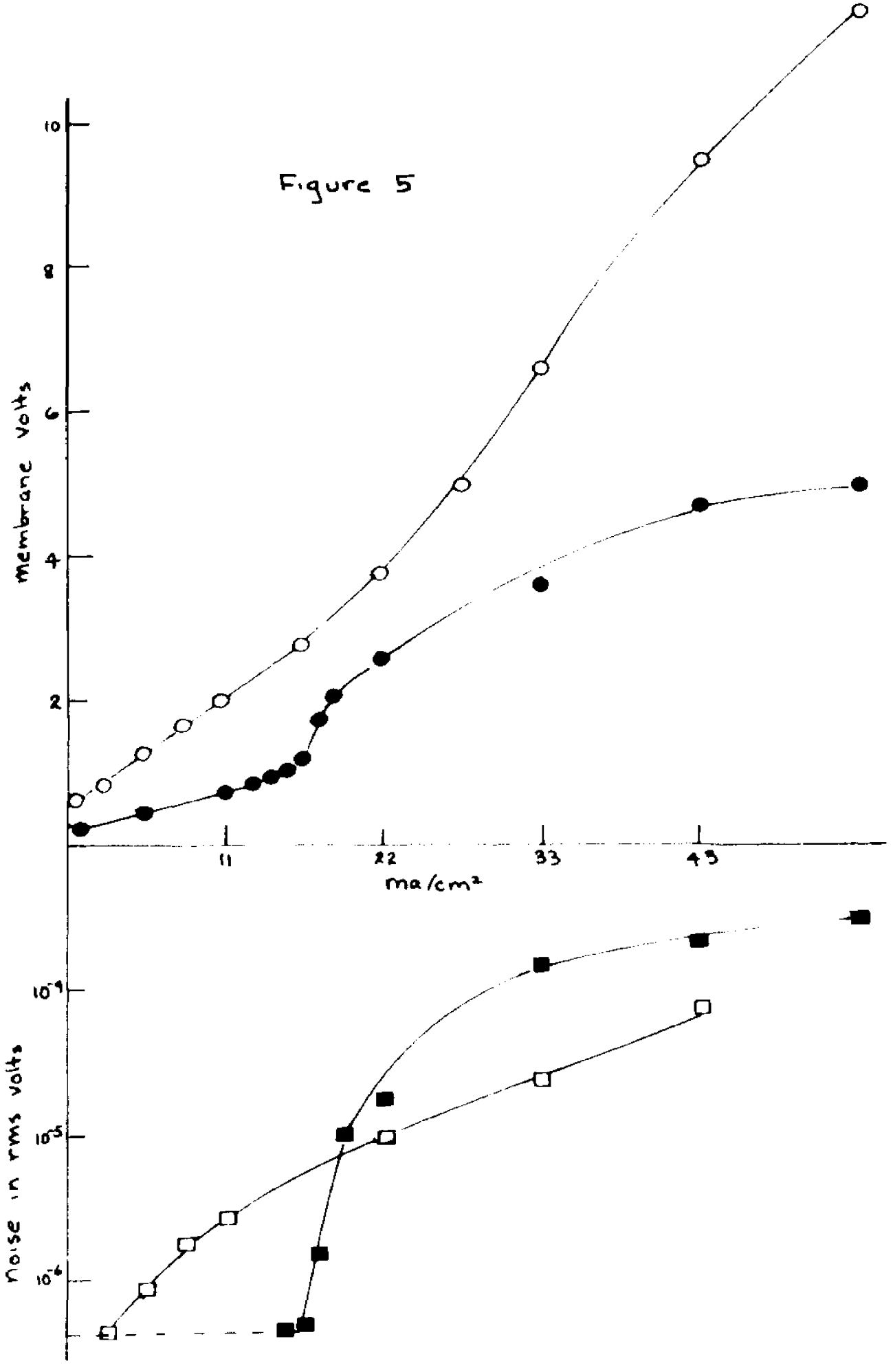
membrane volts
10
8
6
4
2
11
22
33
44
ma/cm²
noise in rms volts
10⁻⁴
10⁻⁵
10⁻⁶

Figure 6. Noise-time oscilloscope display, 5 sec/div.

Top: MC3142, 0.033M HCl, 44 ma/cm^2.

Bottom: MA3148, 0.050M NaCl, 16 ma/cm^2.

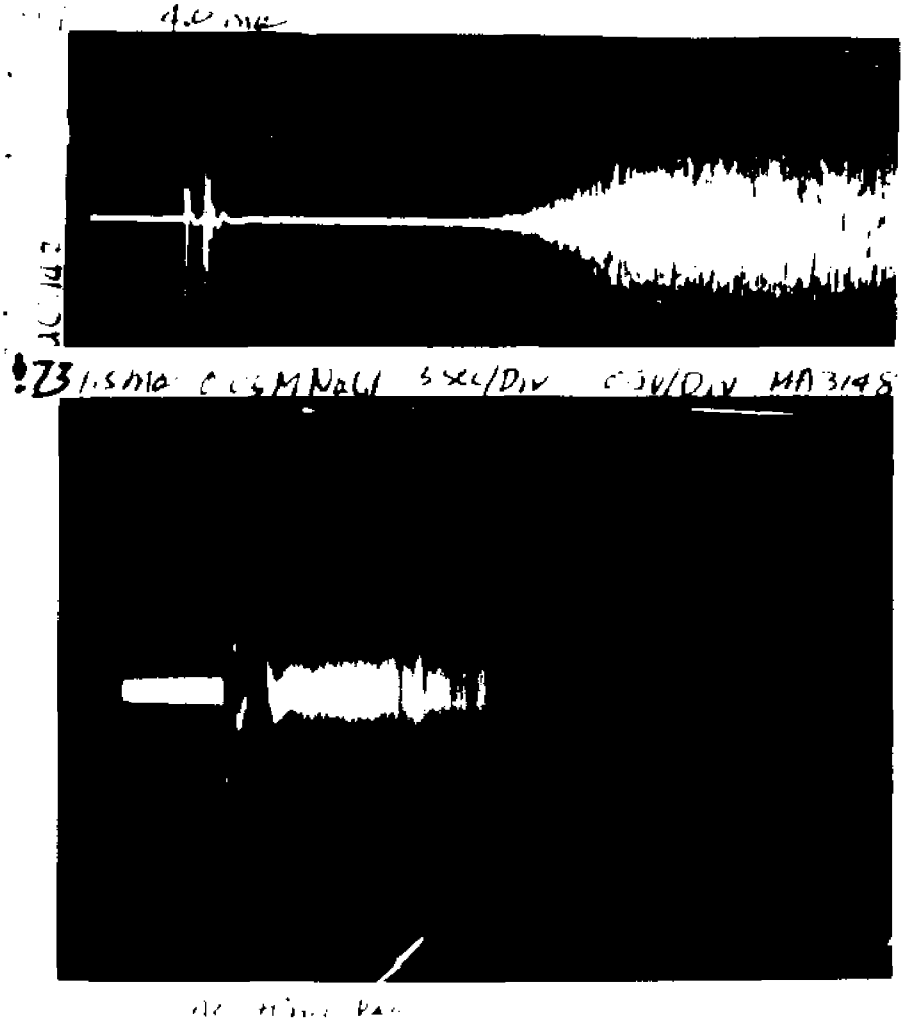

Photographs of the time lag for the membrane voltage buildup showed the time lag increasing with decreasing current densities and increasing concentrations (Figure 7,9). This is the expected trend for a voltage drop associated with the formation of a depletion layer. The time dependence is similar to that observed for electrode polarization in polarography. The time behavior should be obtainable from diffusion equations with the appropriate boundary conditions.

A plot of steady state membrane voltage vs. current for a constant distance between the electrodes shows an apparent decrease in the ohmic resistance with current. A constant resistance corresponding to a stationary concentration profile would show a constant slope on the voltage-current curve. Figure 8 shows the apparent drop of the resistance with the current. The voltage time curves for MC 3142 and MC 3235 are qualitatively alike as can be seen by comparing Figure 9a with Figure 9b. The voltage drop increases slowly until depletion is complete at which point the voltage increases sharply. The V-t curves for lower concentrations (Figure 7C, 0.01OM) and higher current densities suggests voltage contributions with different kinds of time behavior. This is easily seen on curves for 42 - 67 ma/cm^2 of Figure 7B and 17.0 - 67.0 ma/cm^2 of Figure 7C. The first part of the curve appears to be an accelerated and amplified version of curves at lower current and higher concentrations which is

Figure 7. Voltage-time curves for HCl and MC3235, 5 sec/div, 0.225 volts/div.

a) 0.10M HCl. From top to bottom in ma/cm^2: 167, 125, 100, 83.

b) 0.050M HCl. From top to bottom in ma/cm^2: 67, 60, 42, 37.5, 33.

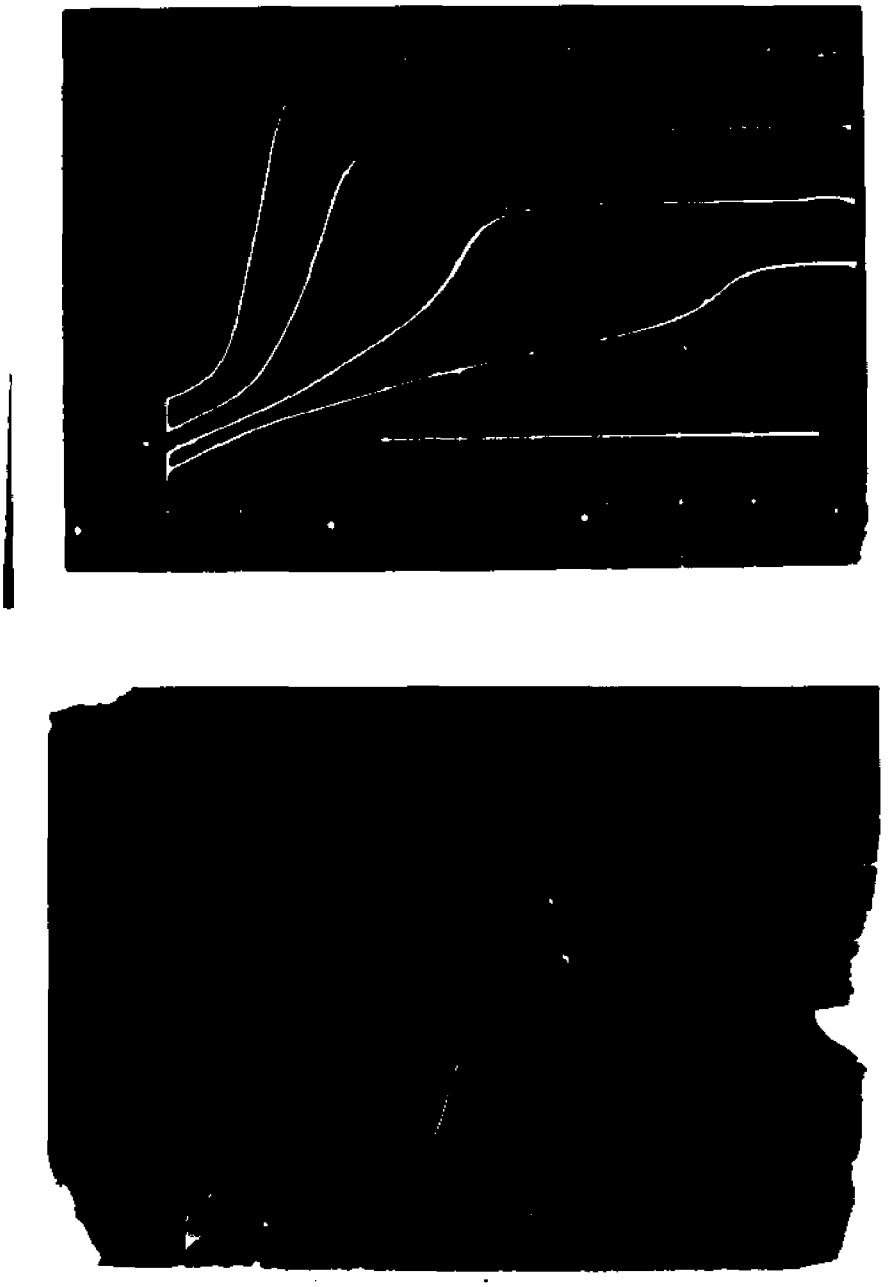

Figure 7. Voltage-time curves for HCl and MC3235, 2 sec./div., 0.75 volts/div.

c) 0.010M HCl. From top to bottom in ma/cm^2: 67, 50, 33, 17, 12.

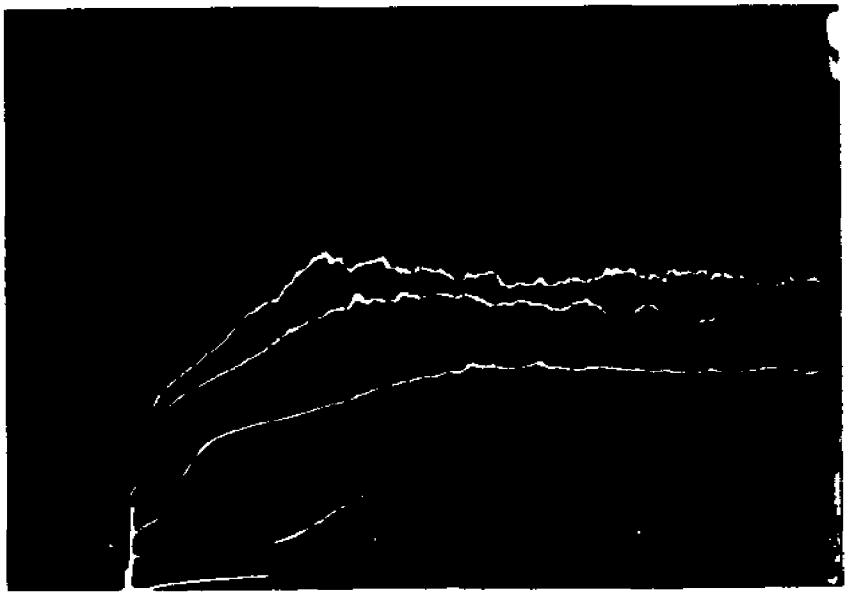

Figure 8. Change of resistance, $\frac{V}{J}$, with J for HCl solutions and MC 3235.

1. 0.010M HCl
2. 0.025M HCl
3. 0.050M HCl
4. 0.10M HCl

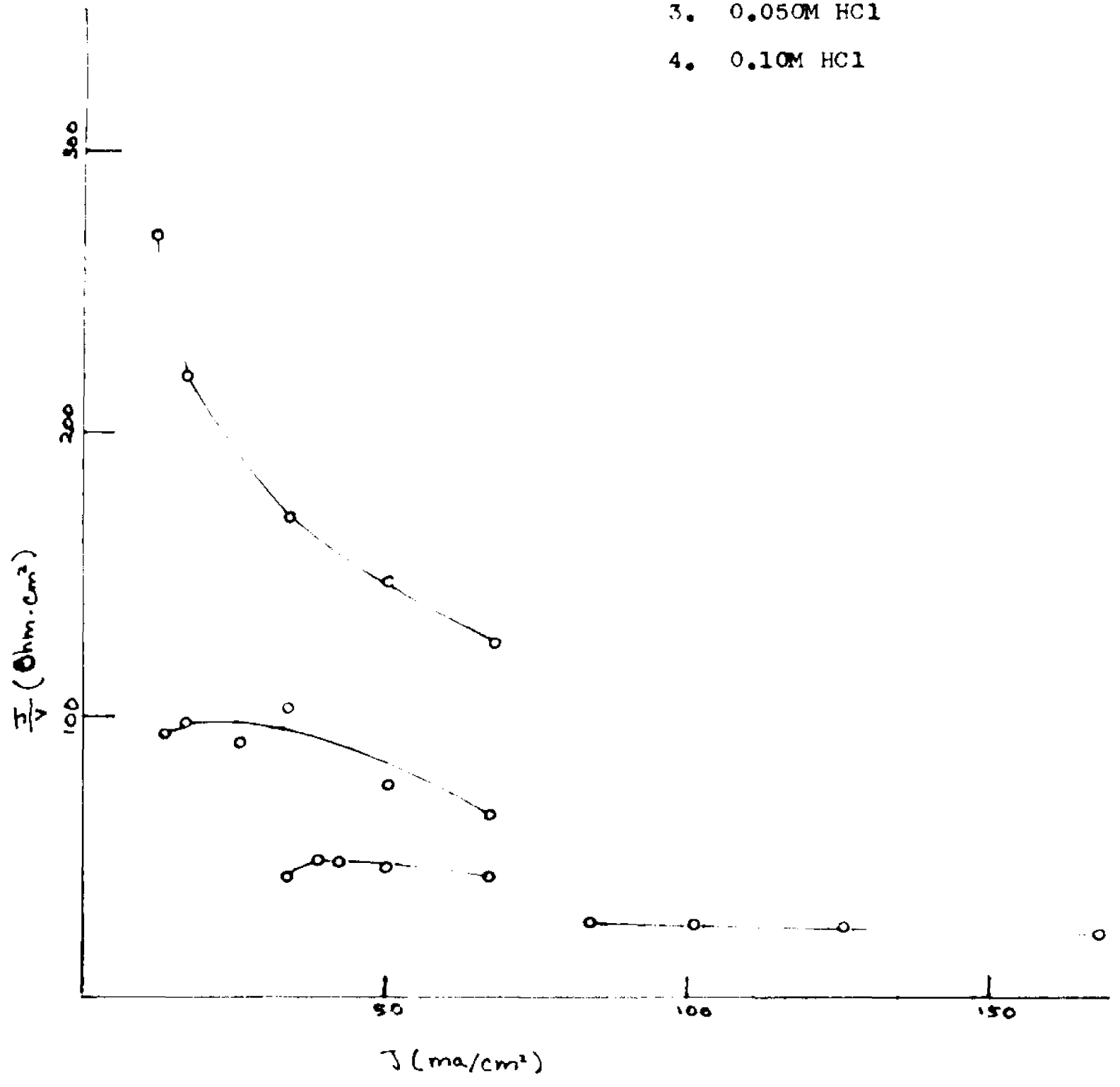

Figure 9. Voltage-time curves for 0.025M HCl with two different cation exchange membranes.

a) MC3142, 5 sec/div. From top to bottom in ma/cm^2: 11, 16.5, 22, 33, 44, 55.

b) MC3235, 10 sec/div., 0.67 volts/div. From top to bottom in ma/cm^2: 13, 17, 25, 33, 50, 67. Note: Electrometer output was inverted.

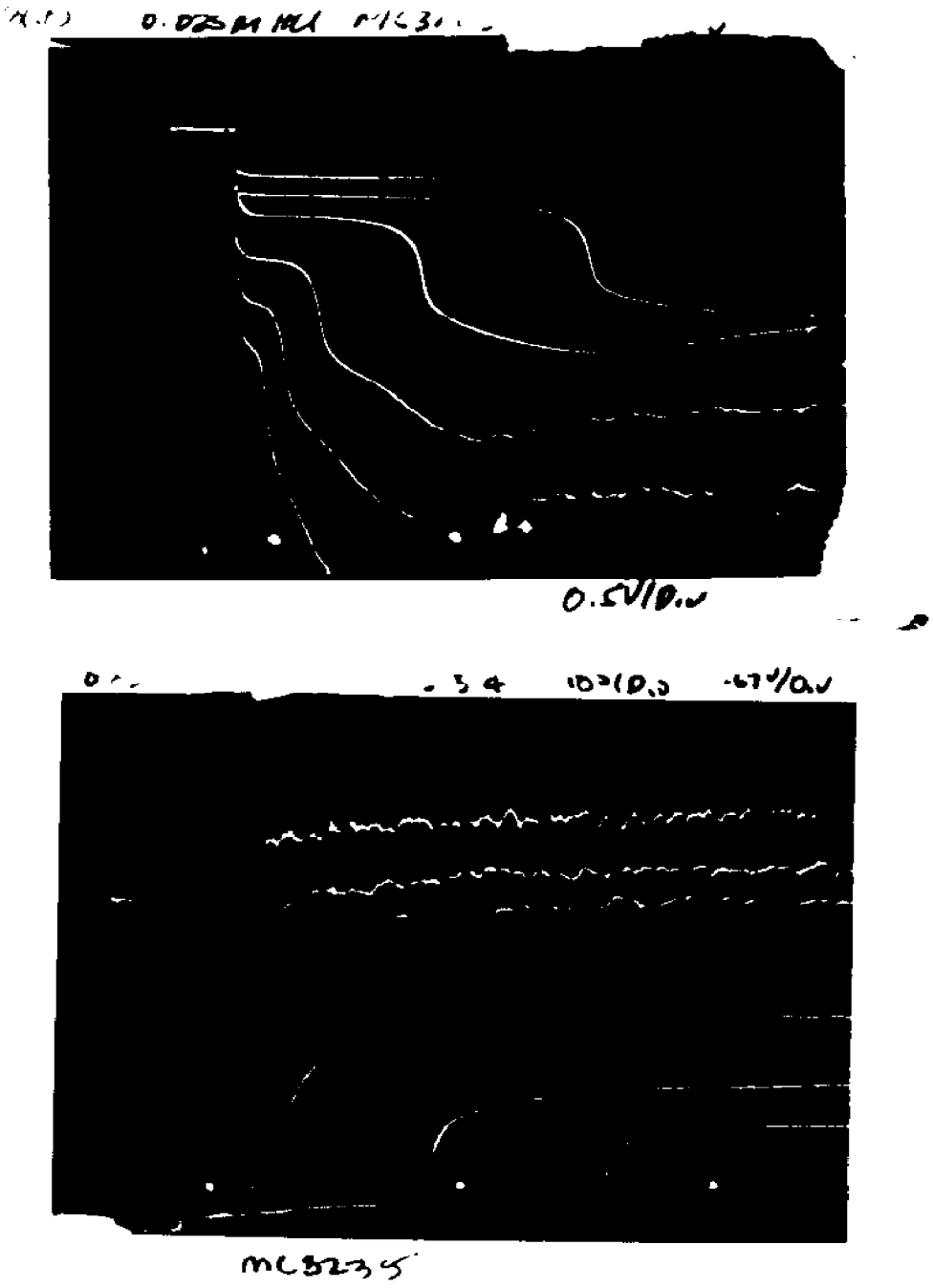

the pattern associated with the formation of a depletion layer. The subsequent voltage change appears to be linear with time and occurs in a region 40μM out from the membrane surface. This can be seen by Figure 10. In this photograph the voltage change at increasing distance, x, from the membrane can be seen. At about 40μM the second phase of the curve has been cut off. This is an indication that the second phase is due to the formation of a steady state concentration profile after the development of the depletion layer. It also suggests that the depletion layer is within a distance of 40μM = 400,000 A^{o}. The initial drop may even occur in the membrane as can be seen in Figure 11. Figure 11 is a voltage-time curve with the electrode touching and possibly penetrating the membrane. Total voltage drop was only 0.20V at 67 ma/cm^2 at this point.

A qualitative difference can be seen between the V-t curve of sodium salts (Figure 12) and HCl. The time required for depletion is shorter for Na^{+} (lower critical current density) and the voltage change at depletion is sharper for hydrogen (Figure 7, 9). The anion voltage-time curve resembles the Na^{+} curve (Figure 12).

A voltage-distance (from membrane) dependence was measured concurrently with a noise vs. distance dependence for HCl with MC 3235. The result shows that the voltage

Figure 10. Voltage-time curves at various distances, x from membrane, MC3142, 0.025M HCl, 44 ma/cm^2, 2 sec./div., 0.2 volts/div. From top to bottom: x in 10^{-4}cm: 0, 40, 200, 800, 200.

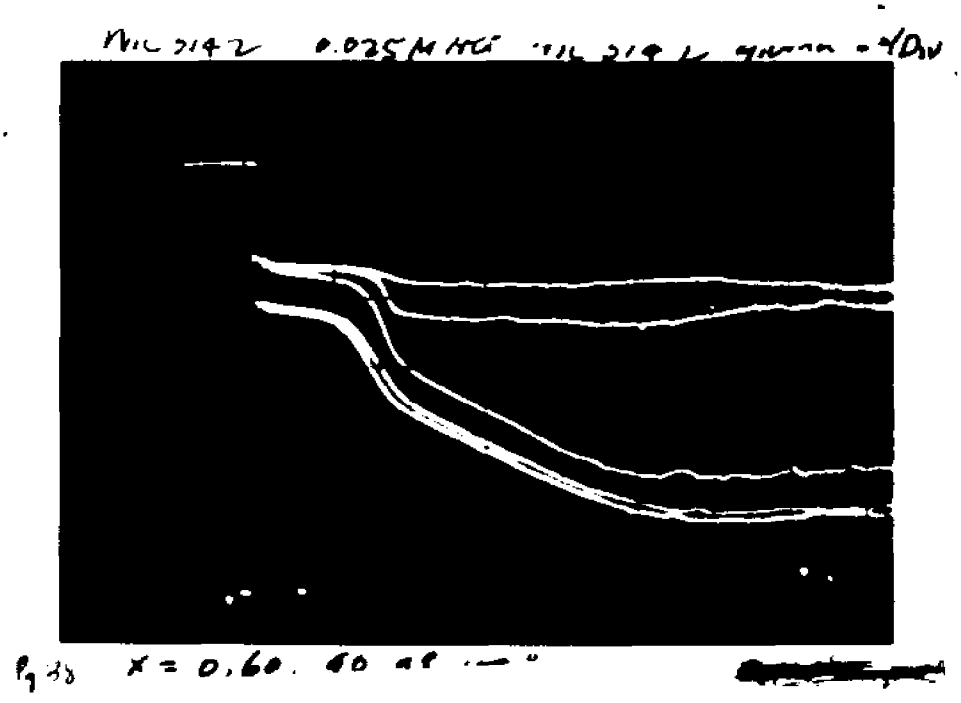

Figure 11. Voltage-time curve with micro-electrode touching and possibly penetrating the membrane. MC3142, 0.025M HCl, 1 sec./div., 0.05 volts/div. From top to bottom: J in ma/cm^2: 33, 33, 44, 55. Note: the first run at 33 ma/cm^2 triggered after the sweep was initiated should be ignored.

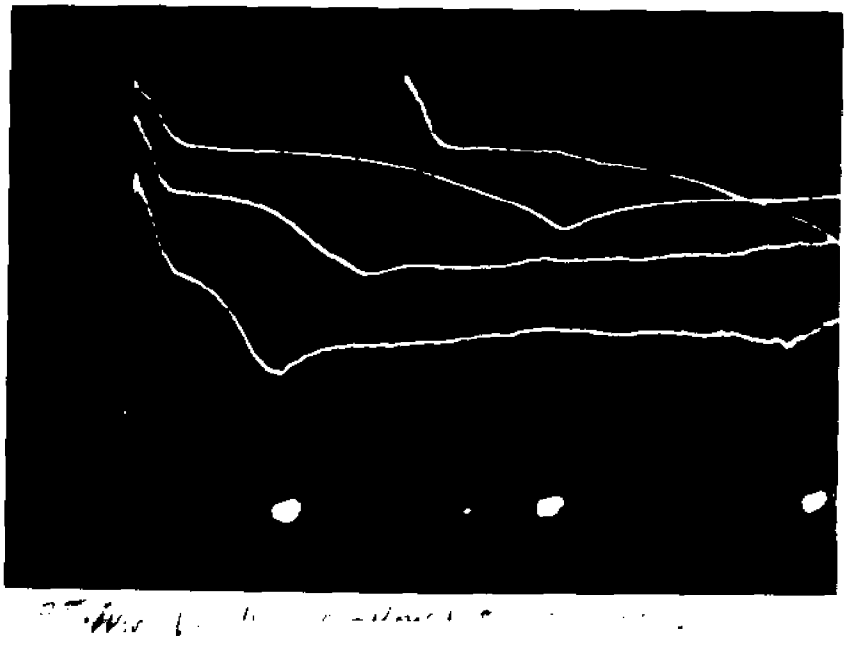

Figure 12a. Voltage-time curve for Na_2HPO_4 with MC3235. 0.056M, 5 sec./div., 0.334 volts/div. From top to bottom in ma/cm^2: 33, 42, 50, 67, 83.

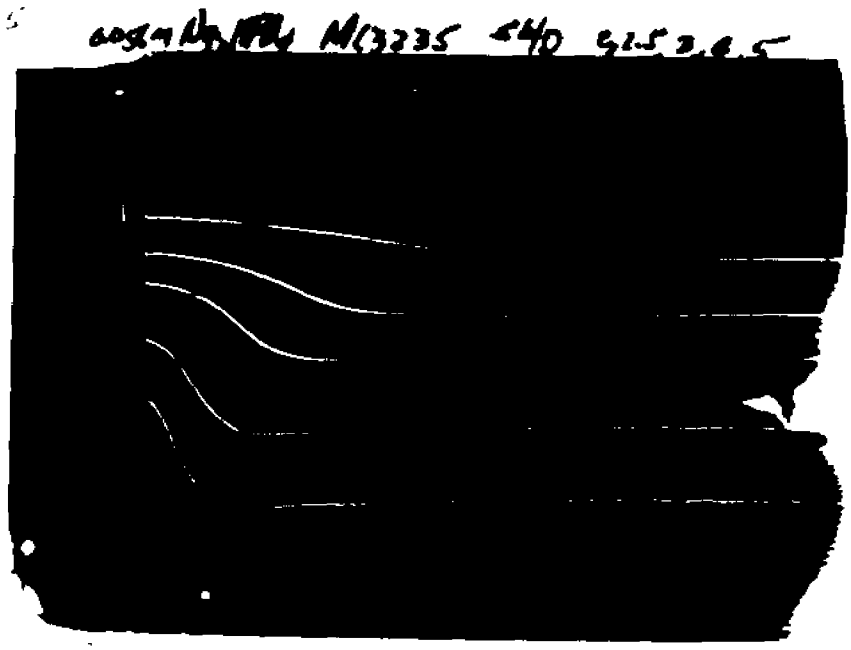

Figure 12b. Voltage-time curve for NaCl with MA3148. 0.10M, 5 sec./div., 0.835 volts/div. From top to bottom in ma/cm^2: 11, 22, 33, 44. Note: Electrometer output was inverted.

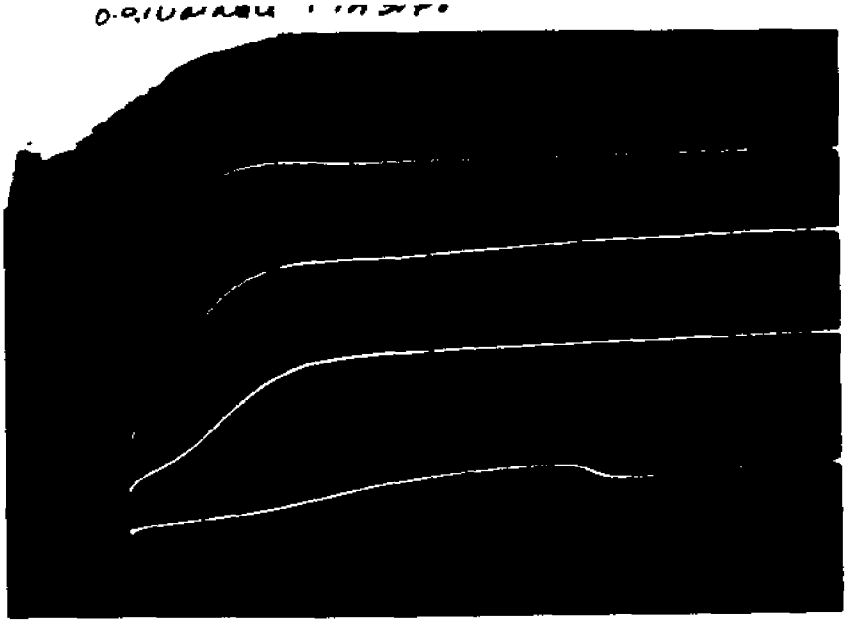

becomes negative after a sharp decline at the membrane surface (Figure 13). The accompanying noise increases sharply reaching its peak at the negative voltage drop. Similar behavior was observed for NaH_2PO_4 with a cation membrane and for NaCl with an anion membrane except that a negative voltage was not observed in these cases. However, this lack of inversion of voltage may have been due to a failure of the electrode to penetrate the membrane surface, or due to an improperly insulated electrode. The voltage inversion with HCl has been established by sufficient trials and indicates the presence of a measurable double layer. The derivative of this curve should give the electric field at each point. This field should be inversely affected by the concentration.

The noise-distance curve cannot be explained directly. An ac signal such as noise cannot be eliminated by a nonconducting insulator and therefore the effective probe is not located at the exposed tip of the electrode. Nevertheless the noise-distance profile shows that the noise increases as the noise source is approached. One possible explanation is that an internal resistance in series with the noise source accounts for considerable signal loss, and this resistance extends less than 40μM out from the membrane. One possible equivalent circuit is given in Figure 14. Another possibility is that the contact of the electrode with

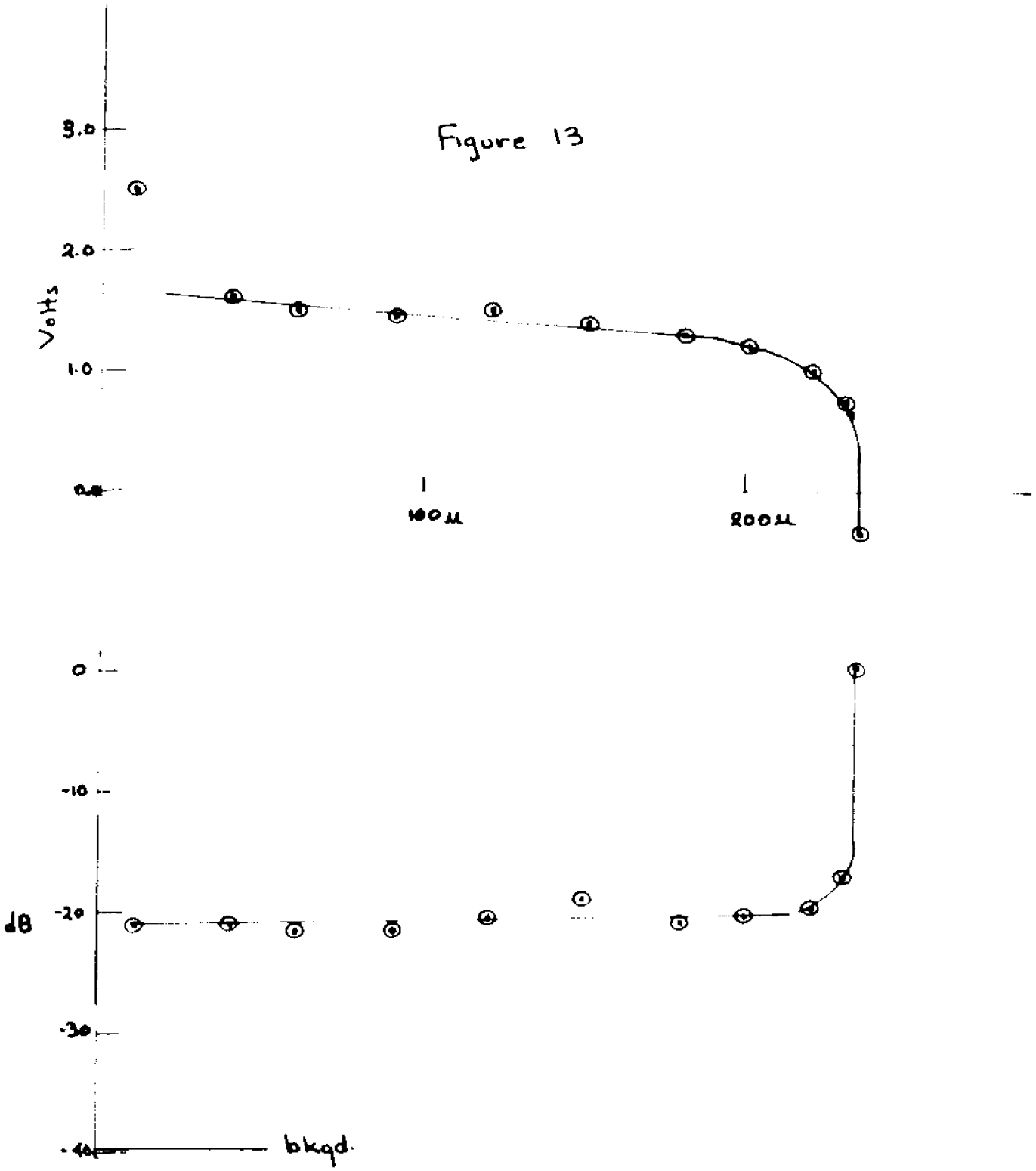

Figure 13. Membrane volts and noise vs. distance, MC 3235, 0.025M HCl, 83 ma/cm^2.

Figure 14. Proposed equivalent circuit to explain the noise distance curve of Figure 13.

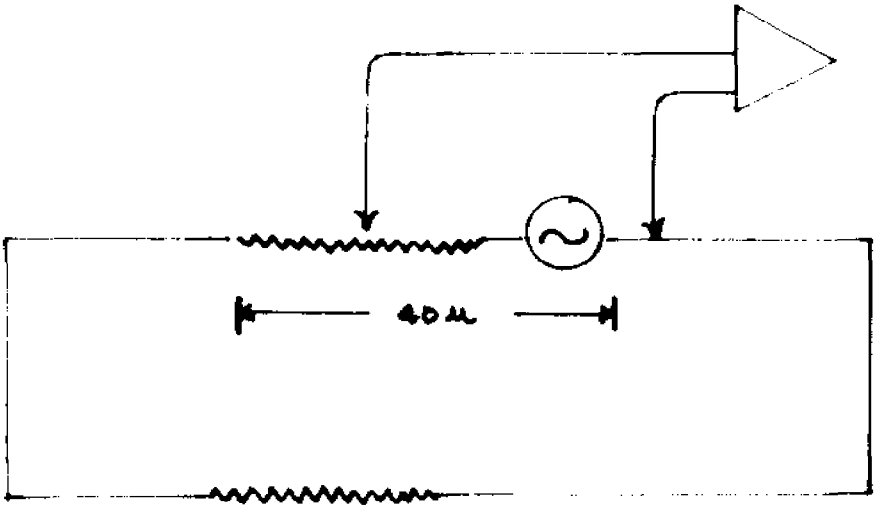

the membrane produces contact noise.

II Power Spectra

Three anions, Cl^{-1}, HPO_4^{-2}, SO_4^{-2}, gave similar results. The curves are parallel straight lines on a decibels vs. log (frequency) plot, with the noise level proportional to the square of the current and inversely proportional to the concentration. The power spectrum showed an ω^{-1} to ω^{-2} dependence. Figure 15 illustrates the case for sodium sulphate and membrane MA 3148. Table 2 gives the exponential dependence on ω of the power spectra for cation and anion membranes.

Cation membranes generally gave more interesting spectra. Sodium acid phosphate and copper sulphate gave initial slopes of ω^{-2} and apparent relaxation times at about 10 KHz (Figure 16).

The effects of reversible copper electrodes was compared with spectra obtained with platinum electrodes. The results can be seen in Figure 17.

The change of the copper sulfate spectra with current density is shown in Figure 18. The trend of increasing negative slope with increasing current density is a general feature of cation noise. The large difference in noise level between 22 ma/cm^2 and 33 ma/cm^2 corresponds to the sharp

Figure 15. Band-pass spectra of 0.10M Na_2SO_4 with MA 3148 at three different currents. From top to bottom: ma/cm^2: 44, 22, 11.

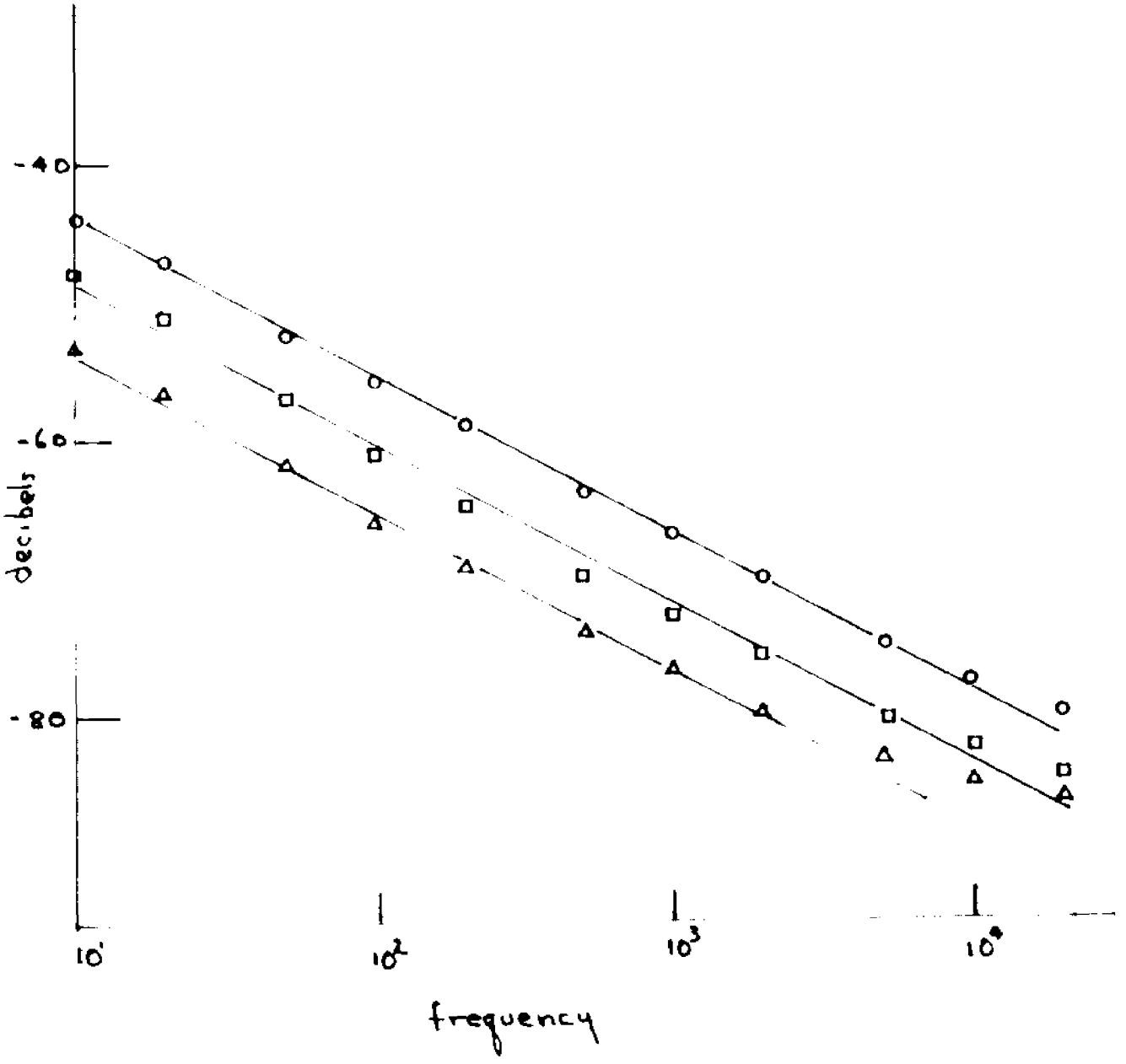

Figure 16. Band-pass spectra of cupric and sodium ions:

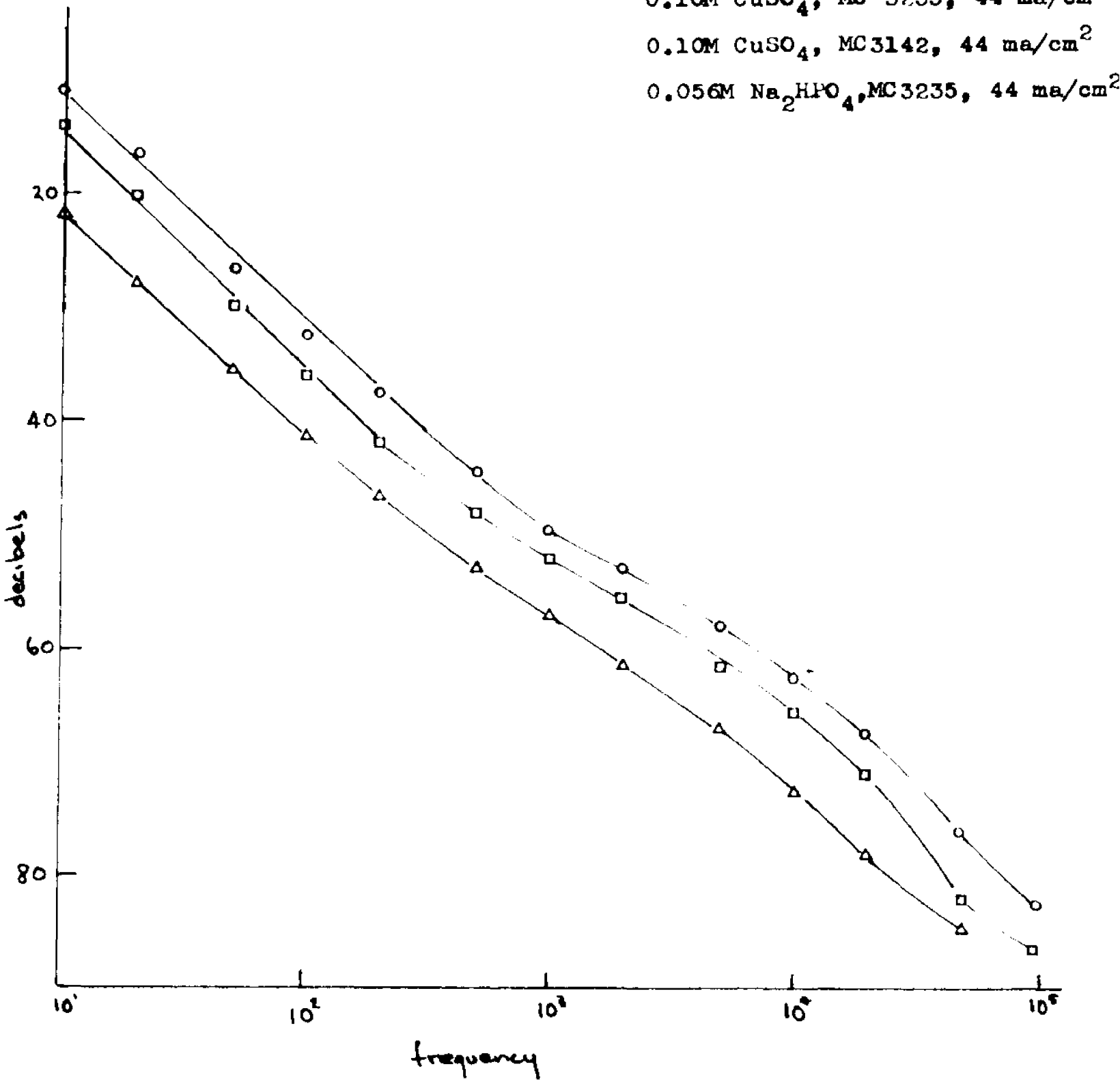

Figure 17. Band-pass spectra of 0.10M $CuSO_4$ with MC3235 using copper and platinum electrodes at 44 ma/cm^2.

. . . Platinum

o o o Copper

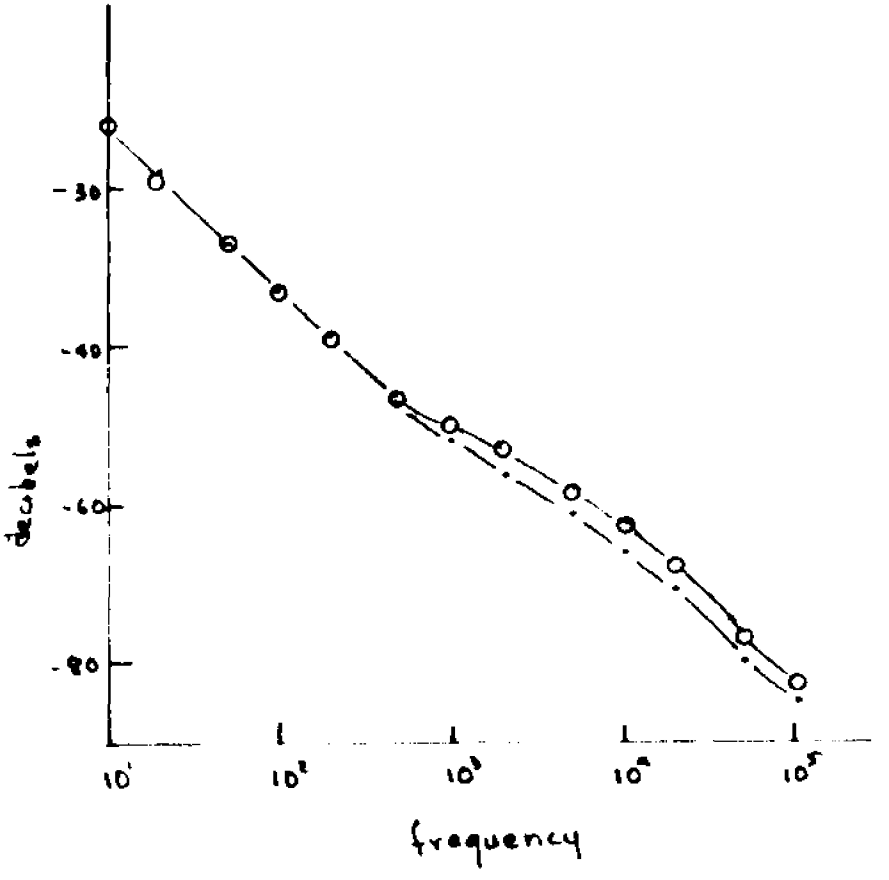

Figure 18. Band-pass spectra of 0.10M $CuSO_4$ with MC3235 at various current densities. From top to bottom in ma/cm^2: 54, 43, 33, 22, background.

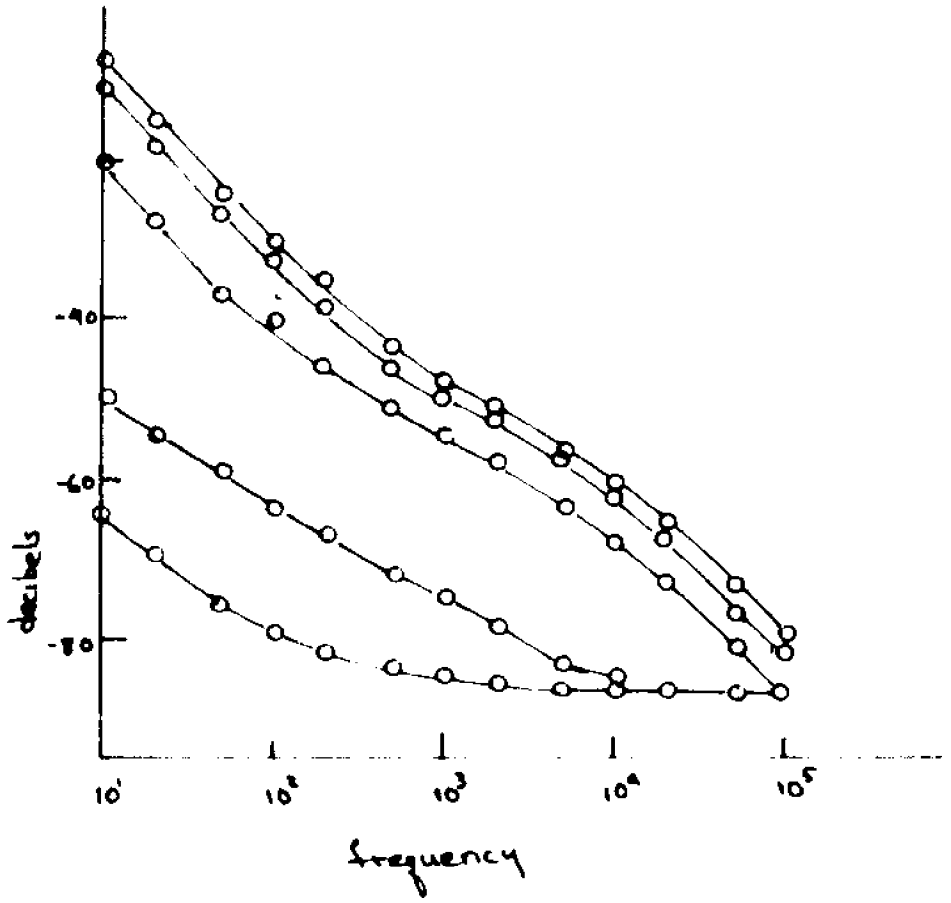

Figure 19. Band-pass spectra of 0.050M $CaCl_2$ with MC3235 at various current densities. From top to bottom in ma/cm^2: 33, 19, 16.

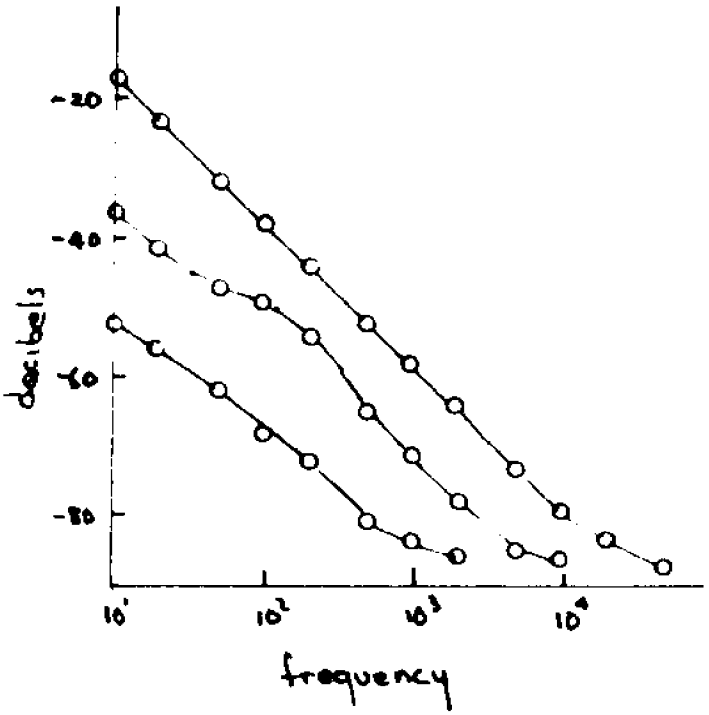

Figure 20. Band-pass spectra of 0.033M CsCl and 0.033M HCl with MC3142. From top to bottom: CsCl at 43 ma/cm^2, HCl at 43 ma/cm^2, CsCl at 2[illegible] and 18 ma/cm^2, background.

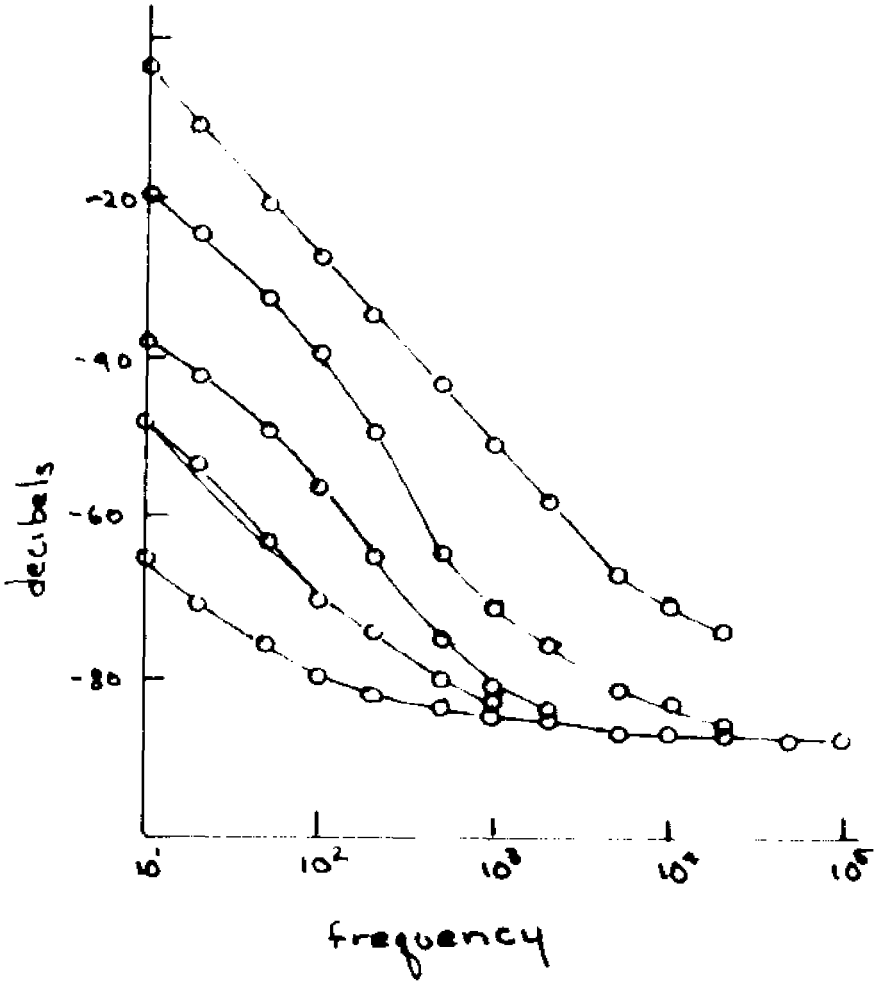

Figure 21. Band-pass spectra of 0.10M tetramethyl ammonium chloride with MC3235. From top to bottom in ma/cm^2: 43, 22, 14, 11. Membrane area is $0.092cm^2$.

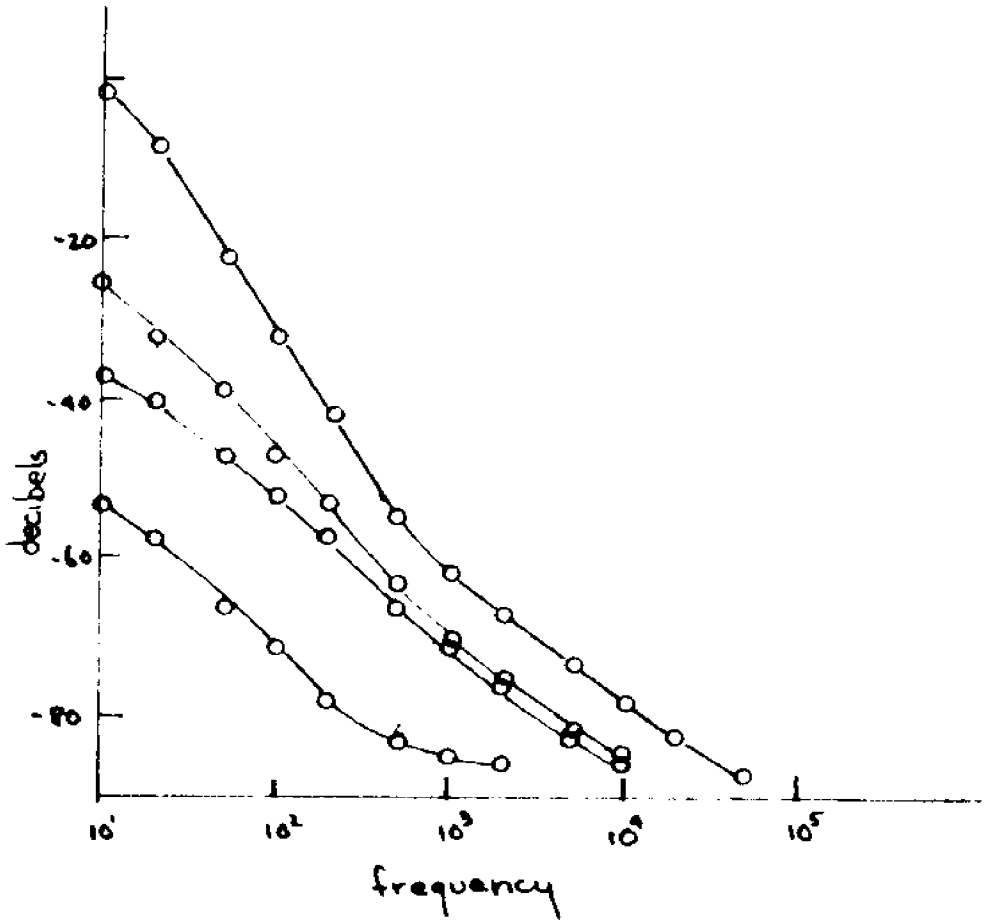

Figure 22. Band-pass spectra of 0.10M tetramethyl ammonium chloride with MC3142. Membrane area was 0.16cm^2. From top to bottom in ma/cm^2: 31, 25, 22, 19.

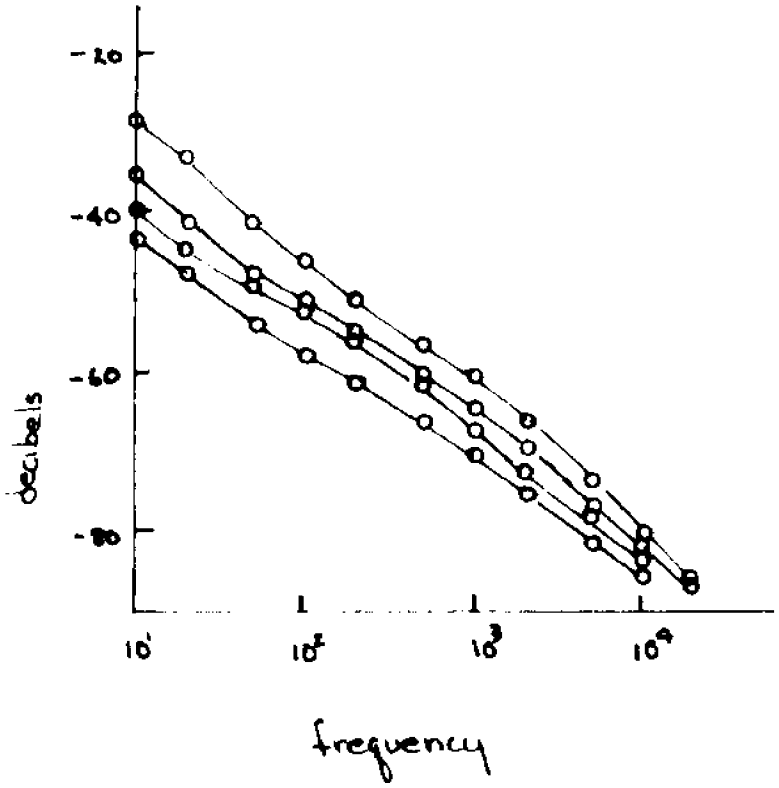

rise in noise in the vicinity of the critical current density. The semblance of a relaxation time is sharpest at a small range of current densities. This is encountered with other salts of which $CaCl_2$ is another example(Figure 1?). The apparent relaxation time can be seen at 19 ma/cm^2 for a 0.050M solution. This feature is lost below and above this current density. Such behavior suggests the presence of many noise sources, the relative importance of which can be controlled to a degree with the proper choice of the current density and concentration.

The NH_4^+ ion responded like the Na^+ ion except that the curvature expected at the relaxation time was very small, rising only a few decibels above the ω^{-2} line at about 10 KHz. The Cs^+ ion and the tetramethyl ammonium ions were studied cursorily. The Cs^+ ion behaved similarly to the H^+ ion except at the high current region. Comparisons can be made in Figure 20.

The spectra for tetramethyl ammonium chloride is shown in Figure 21 and 22. The power spectrum has a slope of $\omega^{-1.4}$ at 43 ma/cm^2. Such a loss rate, which is even more severe with HCl as will be seen later, is difficult to explain. A filtering effect by the instrumentation was ruled out for reasons explained in the instrumentation section. It can be seen that this type of noise dominates only at higher current densities. This was true also for Ca^{2+} and H^+ ions.

Dilute hydrochloric acid was studied extensively. The spectrum obtained with a band pass filter is shown in Figure 20. The higher resolution available on the 3L5 spectrum analyzer gave the unexpected structure seen in Figure 23.

A similar collection of curves were obtained for 20°C, 40°C, 49°C, and for 0.025M HCl at the same temperatures. The characteristic features for all the curves were the intersecting straight lines with slopes of -2 for the lower frequencies and -4.5:1 for the higher end. The intersection of the two lines, labeled f for convenience, was found to have a linear relationship to the current density. This can be seen in Figure 24. The slopes are given in Table 3. A logarithmic relationship was found to exist between f and total noise and membrane voltage. This can be seen in Figure 26. The functional relationship is listed in Table 4.

The determination of the critical current densities and its expected relationship to increased mobility with higher temperatures met with some difficulties. To keep concentration effectively invariant and to keep overall battery consumption to a reasonable level it was necessary to limit the membrane area exposed, thus limiting total ion transport. With the smaller surface area determined by the hole in the tape as described earlier, the critical current density was found to change with time at higher temperatures.

Figure 23. Higher resolution spectra of 0.050M HCl and MC3235 taken with the 3L5 spectrum analyzer at 30°C. From top to bottom in ma cm^2: 75.5, 59, 50, 45, 35, 31.

Figure 23

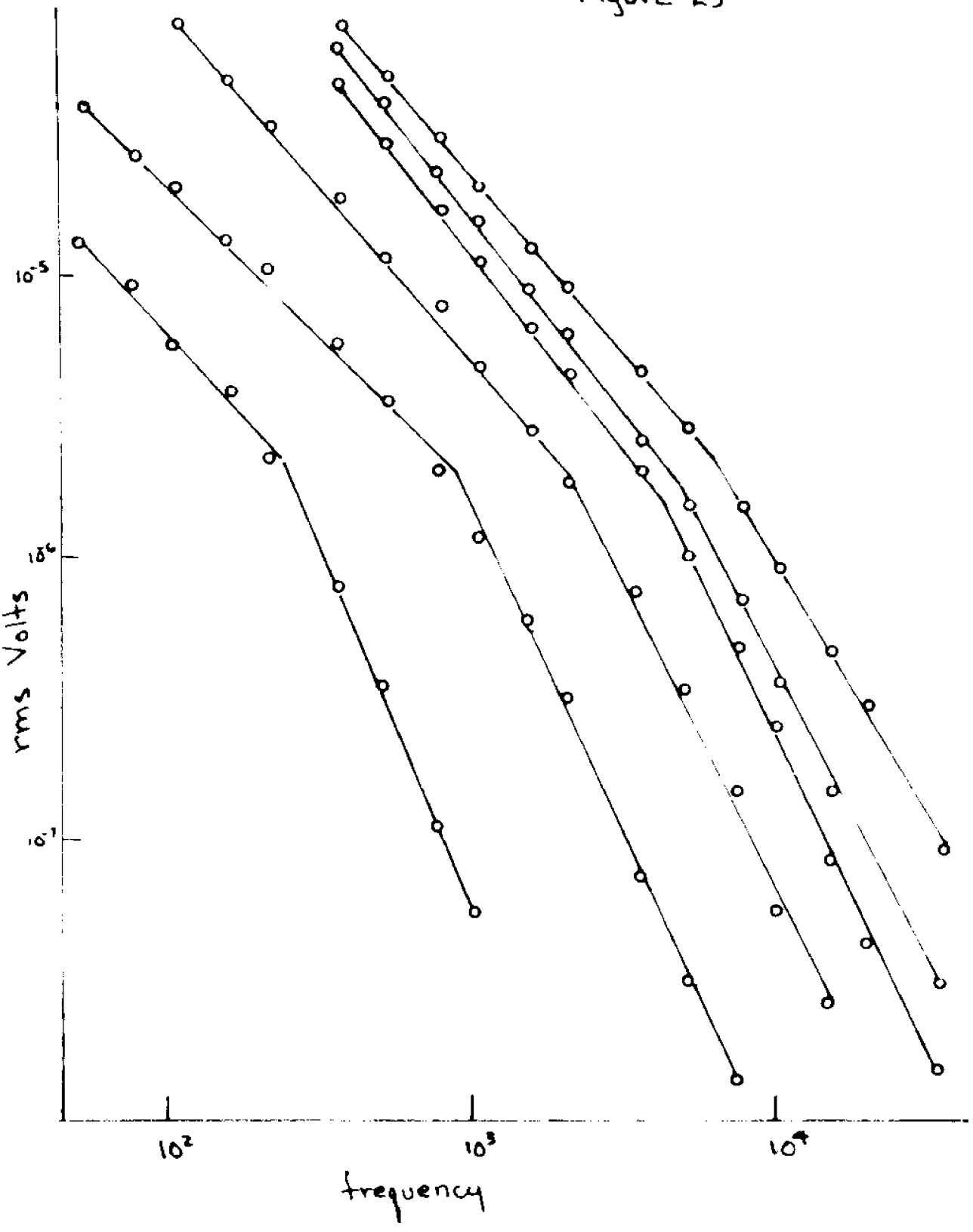

Figure 24a to Figure 24h.

Plot of break frequency, $f = \frac{1}{2\pi\tau}$, against current density where τ is a relaxation time.

a. 0.050M HCl, 19°C

b. 0.050M HCl, 30°C

c. 0.050M HCl, 40°C

d. 0.050M HCl, 50°C

e. 0.025M HCl, 19°C

f. 0.025M HCl, 30°C

g. 0.025M HCl, 40°C

h. 0.025M HCl, 50°C

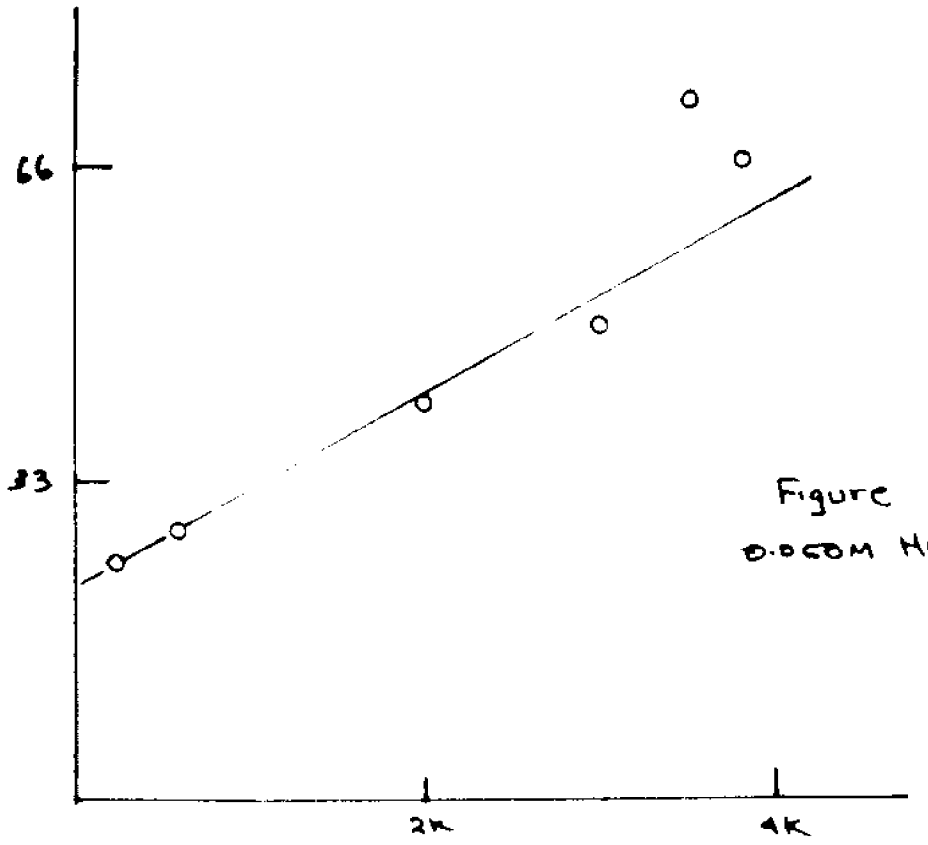

Figure 24a
0.050M HCl 19°C

$f = \frac{1}{2\pi C}$

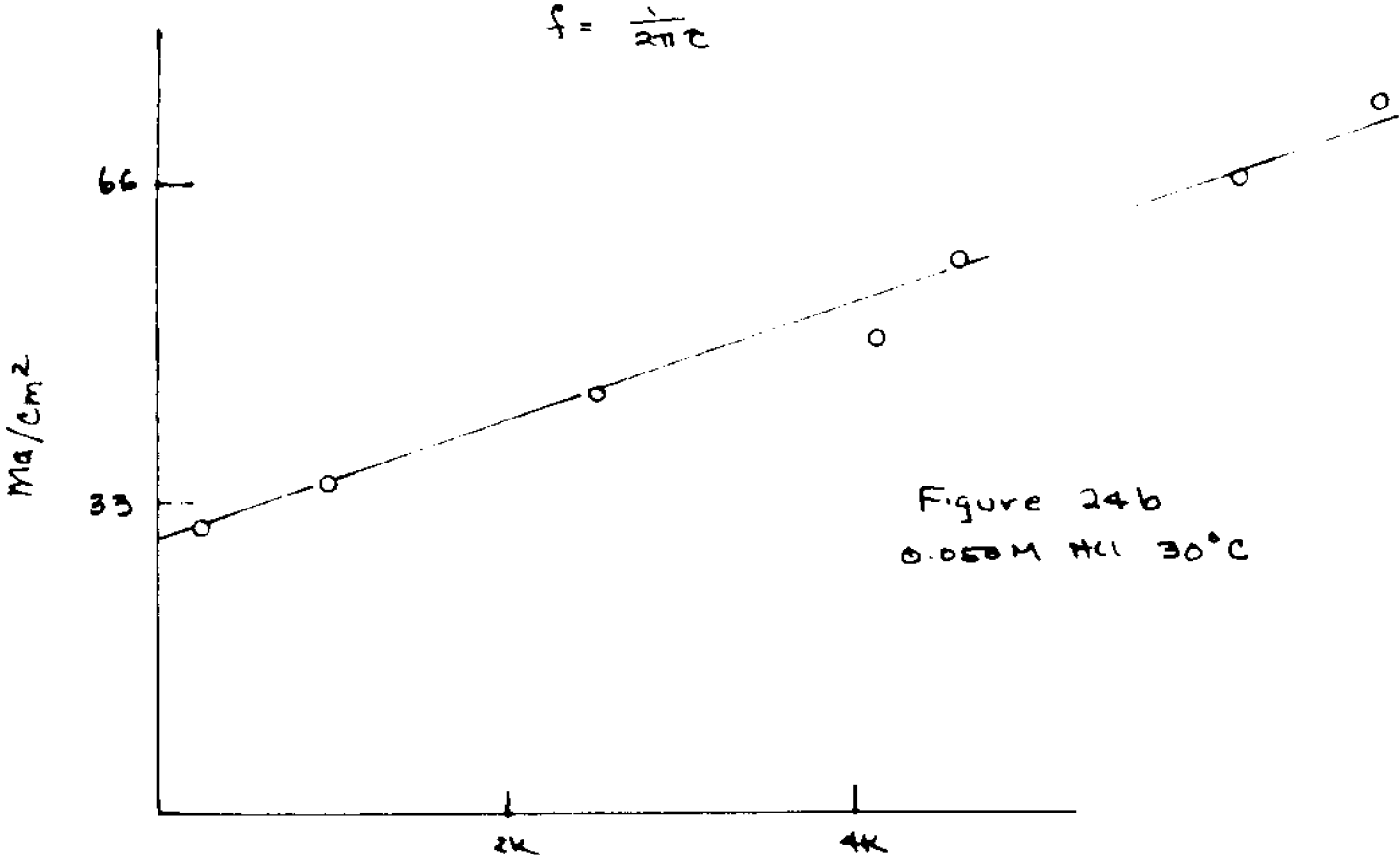

Figure 24b
0.050M HCl 30°C

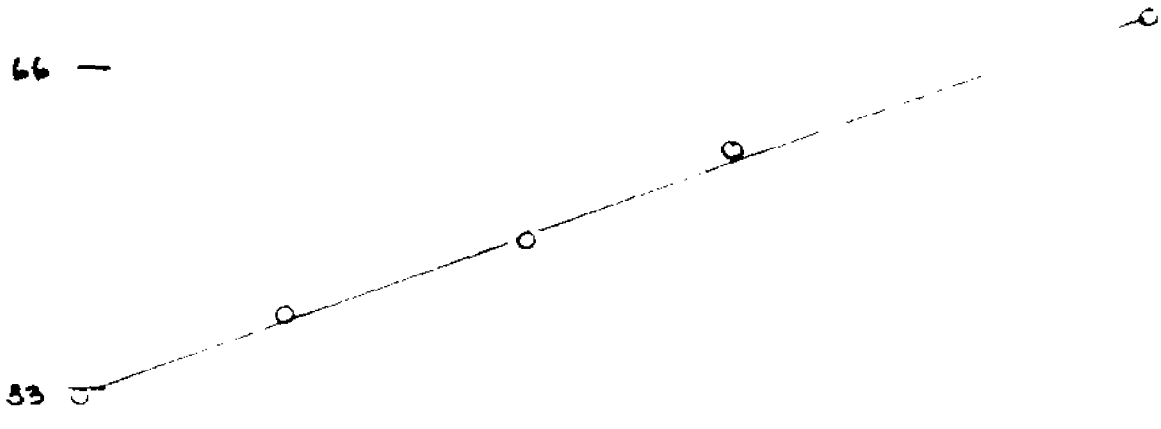

Figure 24c
0.050 M HCl 40°C

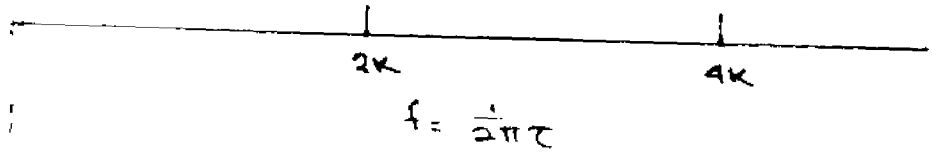

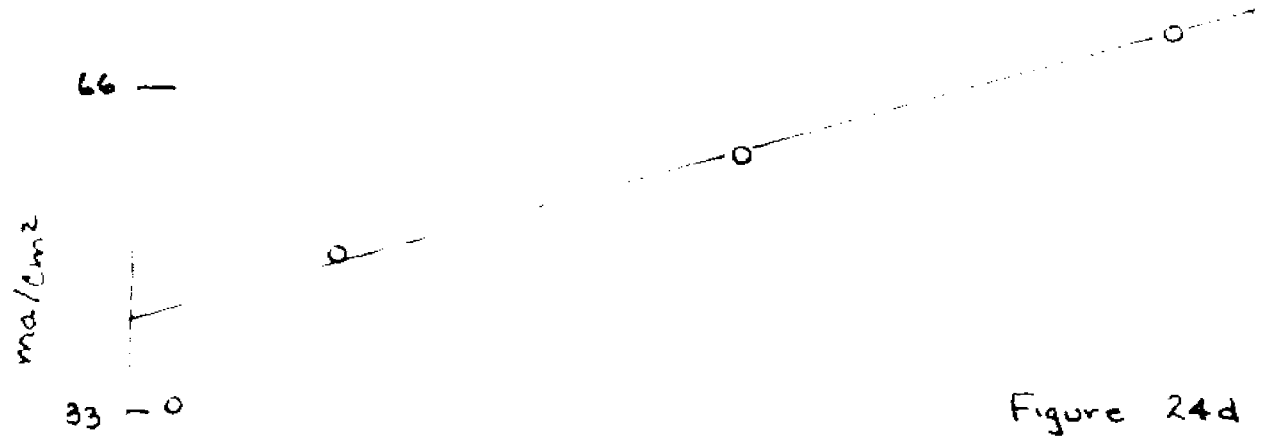

Figure 24d
0.050 M HCl 50°C

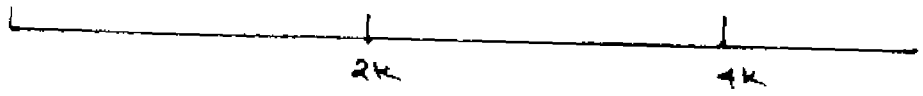

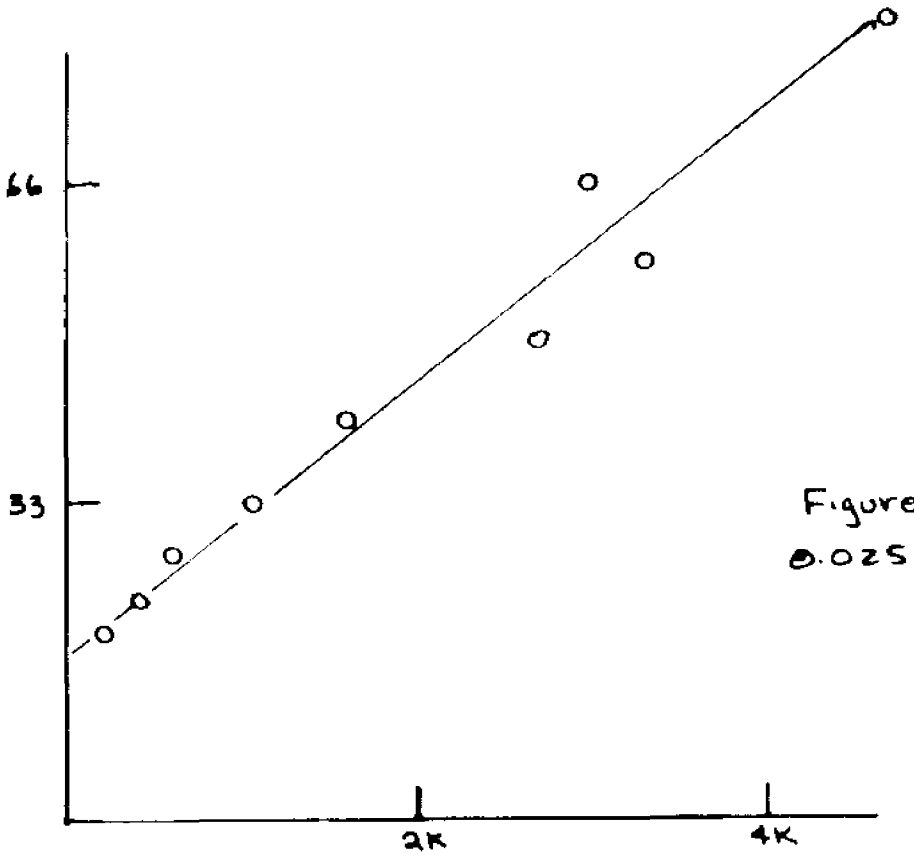

Figure 24e
0.025M HCl 19°C

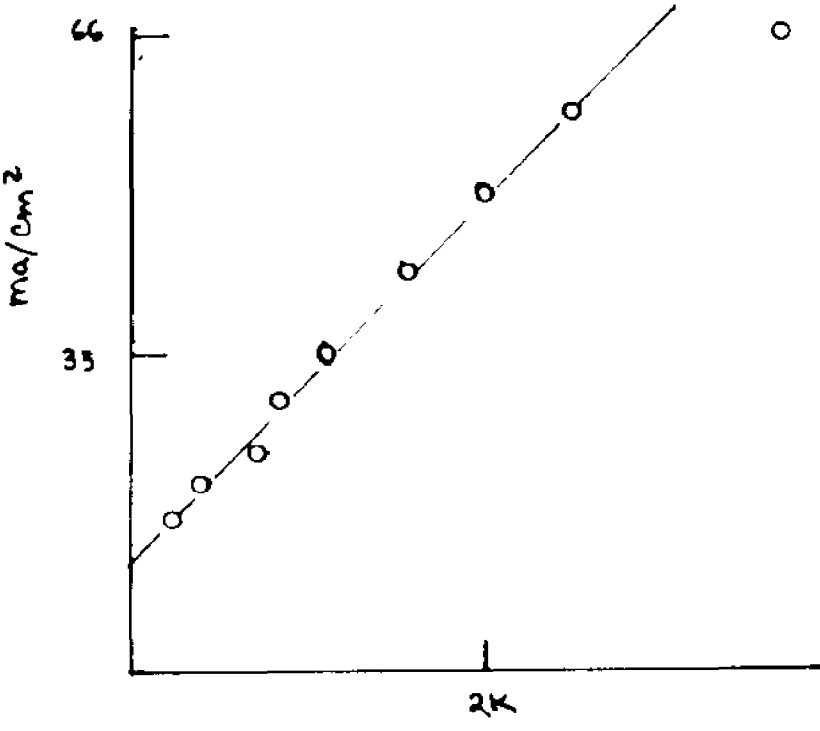

Figure 24f
0.025M HCl 30°C

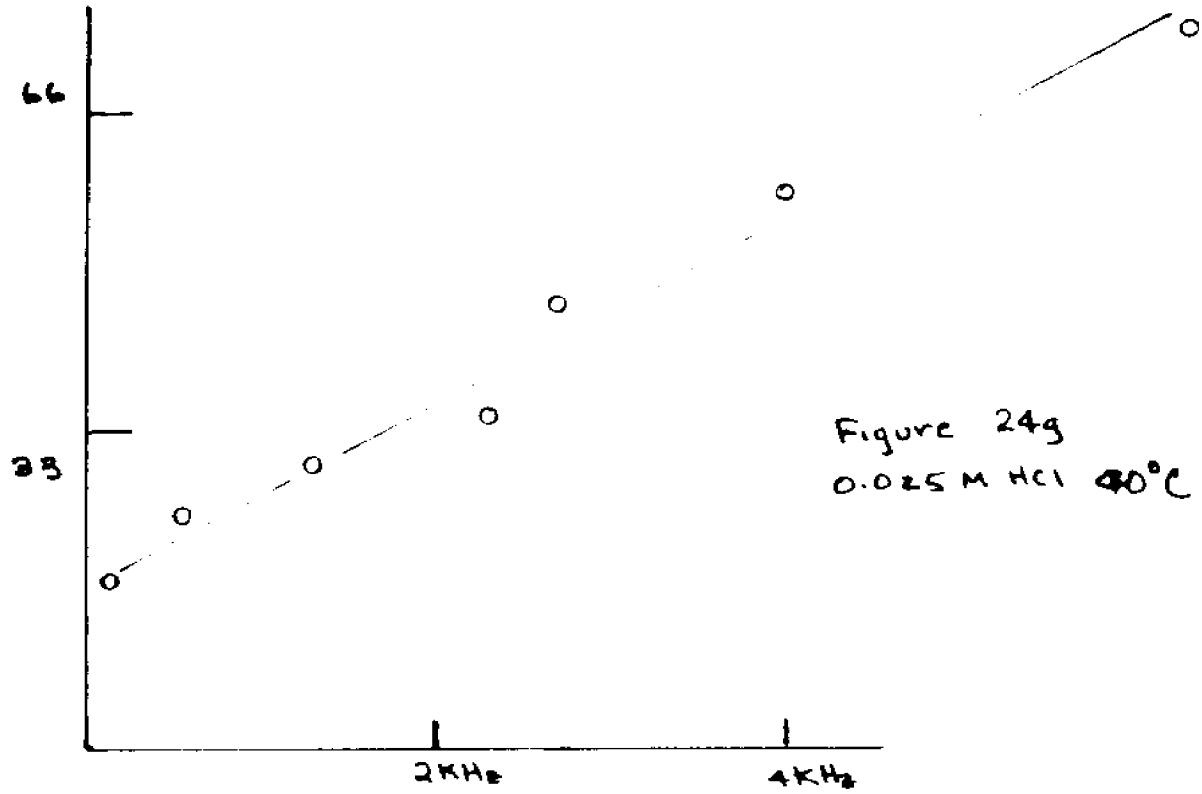

Figure 24g
0.025 M HCl 40°C

$f = \frac{1}{2\pi C}$

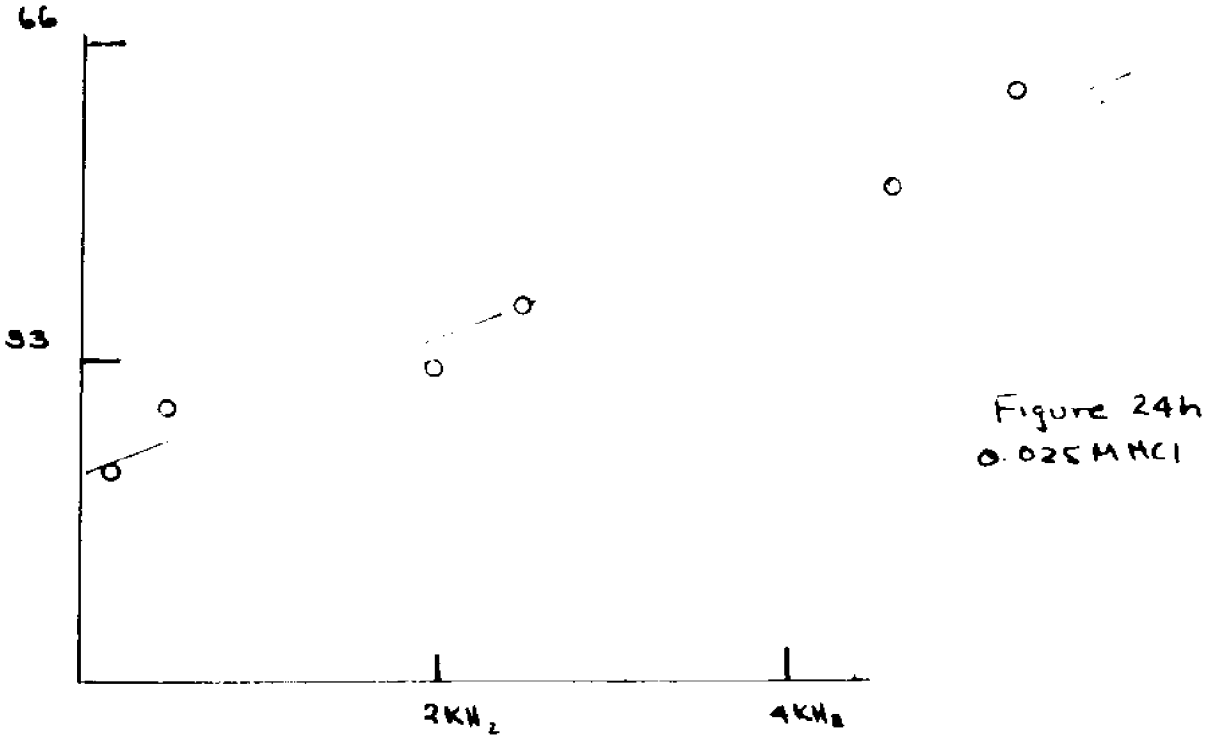

Figure 24h
0.025 M HCl 50°C

These effects were attributed to leaks when the critical current density increased and to the swelling of the tapes and membrane when the critical current density decreased with temperature. Some tape deterioration was detected causing leakage after a day of use. It was found that black friction tape with a plastic backing minimized these effects. However, friction tape did not adhere strongly to the membrane. Whether this caused some leakage was uncertain.

Leaks were determined by putting a strip of friction tape over the hole on the tape, and then checking the conductance. When no current was detectable the system was assumed to be leakproof. However, this method eliminated leaks between the plexiglass divider and the tape but not between the tape and the membrane. A method to check for leakage between the tape and the membrane could not be found.

The leakage through the interstices between membrane and tape probably was not important. At the concentrations employed (0.050M to 0.025M), and under the conditions of electrolyte depletion, the conductivity of the membrane should exceed that of the solution by an order of magnitude. Also the tortuous leakage path and the small area available between tape and membrane increases the resistance to leakage flux. The change of CCD with time is shown in Figure 25.

Figure 26. Plot of break frequency f, with total noise and membrane voltage for 0.050M HCl, MC3235, 30°C. 1. Membrane volts. 2. Total noise.

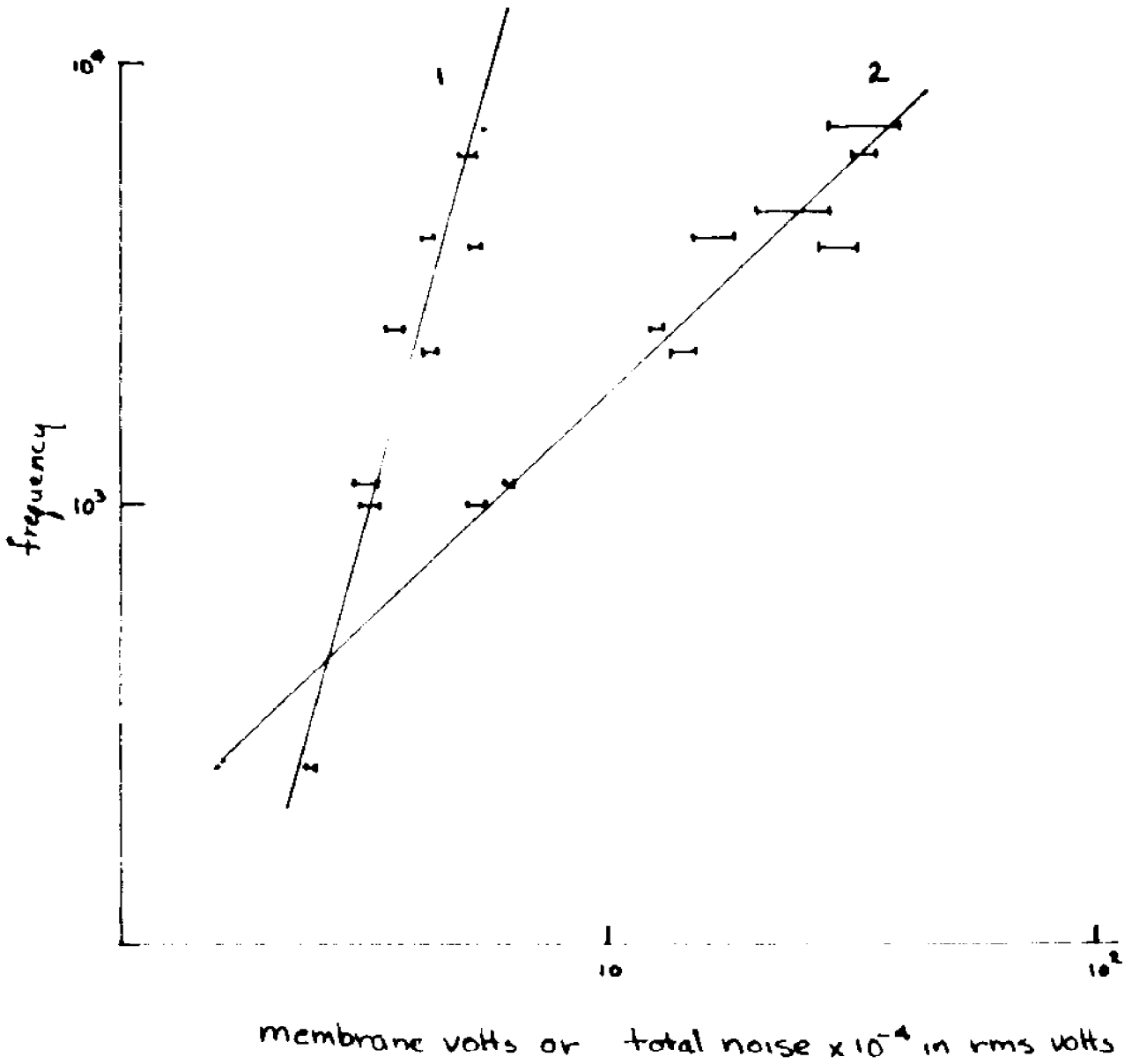

Figure 25. Change of critical current density with time for 0.050M HCl and MC3235.

a) Double tape with "No-Stix" on the inside, Mystik tape on the outside.

b) Friction tape only.

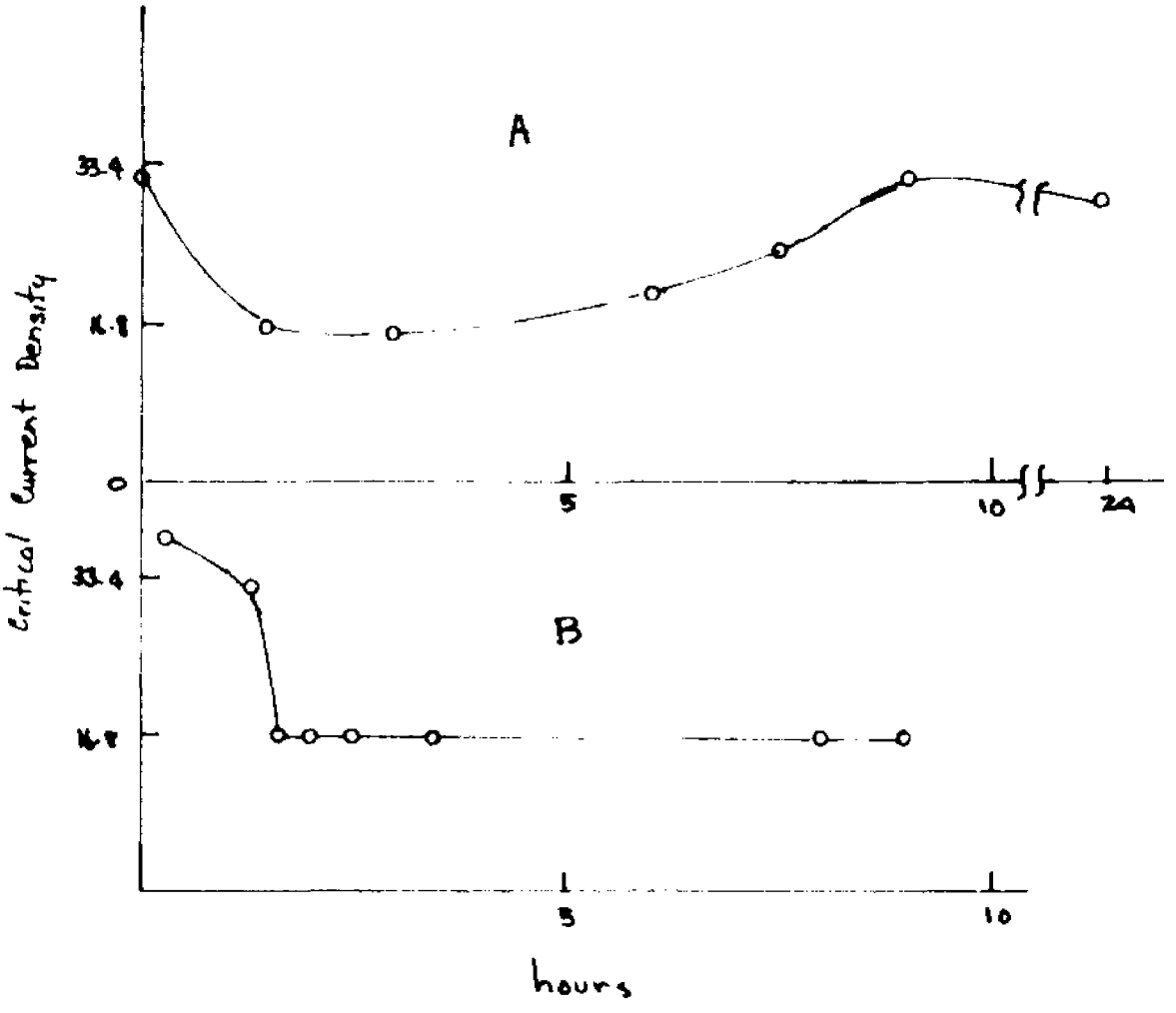

Finally the power spectrum of drift and diffusion noise is shown in Figure 27. This spectrum was obtained by running a $CuSO_4$ current through a hole 0.7 mm. in diameter. Copper electrodes were used. In consonance with theoretical calculations,[19] this spectrum had an $\omega^{-3/2}$ dependence.

Figure 27. Diffusion noise from 0.10M $CuSO_4$ passing through a hole 0.6mm in diameter and 3.3mm long.

a) Power spectrum.

b) IR drop vs. current density.

Figure 27

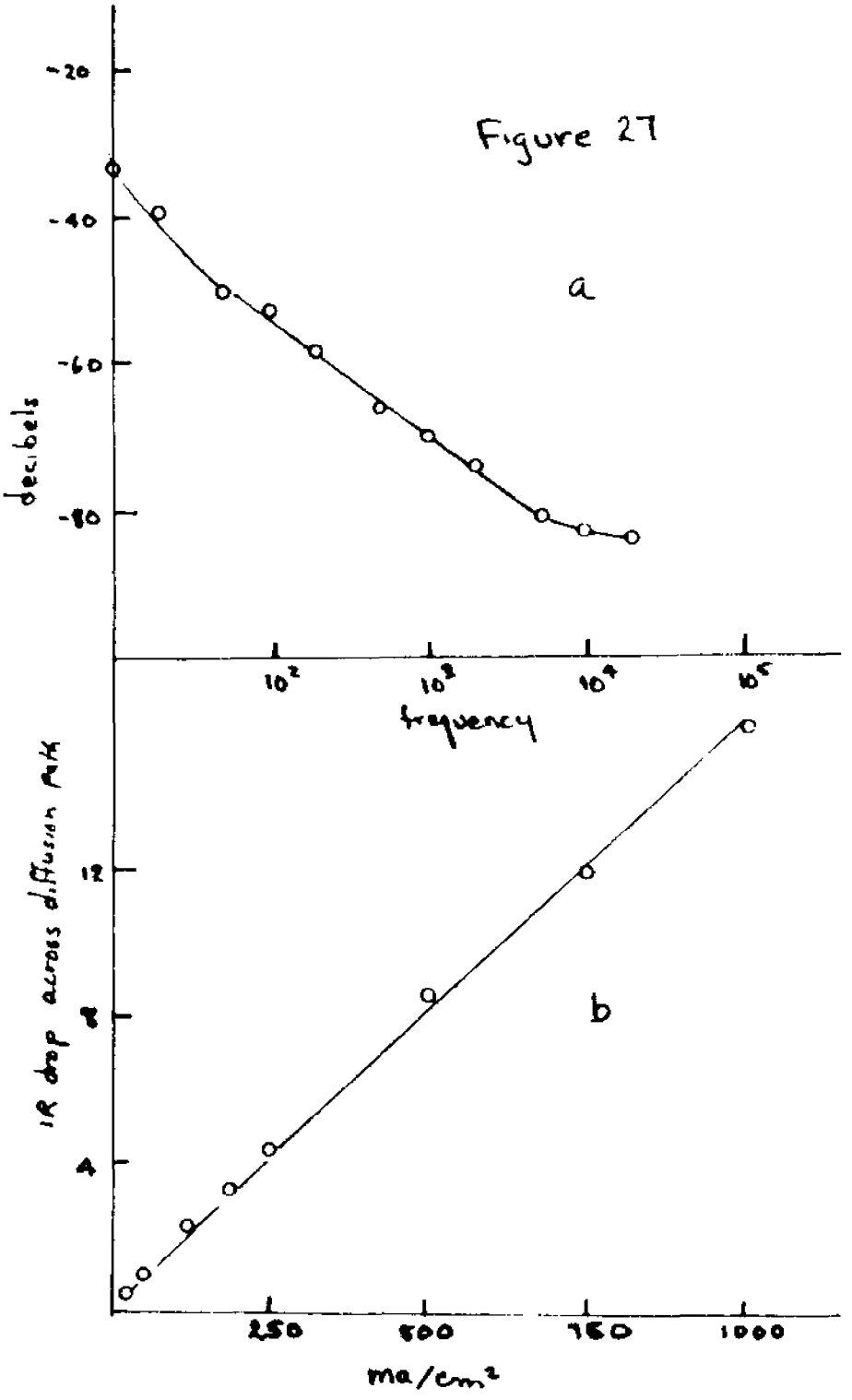
-20
-40
-60
-80
decibels
a
10^2
10^3
10^4
10^5
frequency
IR drop across diffusion path
12
8
4
b
250
500
750
1000
ma/cm²

DISCUSSION

I General Considerations

The interpretation of the data depends on the answers to several questions:

(1) Where is the location of the noise source?

(2) What causes the steep slopes?

(3) Are the two intersecting lines of the HCl spectrum a result of a relaxation time?

The subsequent analysis strives to answer these questions and then some tentative projections are made to put this work in the context of related physical-chemical phenomena.

The relationships of voltage and noise to current (Figure 5), voltage to time (Figures 7, 9, 12), voltage and noise to distance from membrane (Figures 10, 13) and the noise to time (Figure 6) were useful in determining the location of the noise source. The data showed that cation exchange membranes differed from anion exchange membranes. This difference resulted in a different mechanism for noise production which will be discussed later when the power spectra are analyzed.

II Noise Sources

The anion noise appeared immediately after current was passed through the membrane (Figure 6) and was detectable

at currents far below the critical current density (Figure 5). This indicated that anion membrane noise occurred in the membrane or at the membrane surface.

Noise from cation exchange membranes appeared abruptly at the critical current density and increased sharply with the voltage (Figure 5). In addition, there was a time lapse after the current was turned on before the noise appeared (Figure 6). This suggests that the noise is generated by ion transport across a region of high electric field. This field results from the high ohmic drop in the region depleted of ions. The time lag corresponds to the time required to form a depletion layer after turning on the current. This same time lag should be observed in the voltage. This was the experimental observation (Figures 7,9,10).

III Voltage-Time and Voltage-Distance Relations
(Cation Membrane)

Examination of the voltage-time curves show some secondary features that can be explained. At high current densities an initial sharp rise in voltage at the point of depletion is followed by a more gradual voltage change before a steady state condition was reached (Figures 7,9,10).

The first large change in voltage is the result of the formation of a high field layer in which water dissociation occurs. The subsequent voltage change is caused by the for-

mation of a steady state concentration gradient which provides the diffusional flux to the depleted region. A measurement of the change of the voltage drop with distance from the membrane served to clarify this behavior (Figure 10). The secondary voltage changes were eliminated as the electrodes were brought closer to the membrane. This measurement and a point by point voltage versus distance plot, located the high field depletion layer in a region of thickness of less than 40 microns (Figure 13). The secondary changes occurred in a region outside this layer. The spatial resolution of this measurement was limited by the diameter (20 microns) of the tungsten electrode and by the resolution (40μM) of the miniprobe which moved the electrode.

It was hoped that a concentration profile of ions outside the membrane could be obtained with the miniprobe electrode combination. With sufficient care in preparation, the tungsten electrode can be made reversible to the hydrogen ion;[27] the voltage reading will be equal to However, the total voltage measured would include the large contribution from the electrical free energy of the ions:

$$\Delta G_{el} = q_0 V \qquad (33)$$

where q_0 is the electronic charge and V the difference in electrical potential between the two electrodes. The separation of the two effects was not possible with the present

system.

As a first approximation, Ohm's law can be used to relate voltage to concentration:

$$(34) \qquad V = IR = \frac{I}{FC(\mu_1 + \mu_2)}$$

where F is Faraday's constant, V is the dc voltage, I is the current, C the salt concentration and μ_1 and μ_2 the individual ionic mobilities.

IV Noise-Distance Curves

The noise-distance curve (Figure 13) shows that the noise is invariant in magnitude above 40 microns. Then, a drastic increase in noise occurs within the 40 microns and at the point of contact with the membrane. The increase could be caused by a large contribution from contact noise which commonly occurs at the junction point of two conductors that are not bonded securely. This would predict a step function type noise-distance curve for Figure 13. (To check this a micromanipulator with a more precise movement would be necessary.) If however, the noise-distance curve is not discontinuous the explanation might be found in the depletion layer. The noise may be dissipated in the region in which a concentration gradient connects the bulk concentration to the depleted region. Such an effect is similar to the effect of the internal resistance of a galvanic cell

on its measured voltage. Outside the depletion layer the conductivity is too high to cause a measurable loss in power and would correspond to the flat portion of the noise-distance curve. In the region where the concentration gradient exists the conductance drops severely causing a significant ohmic loss of the signal. The magnitude of the loss would be inversely affected by the conductivity, and therefore by the concentration, as can be expected from the relation:

(35) $$\sigma = F \sum C_i \mu_i$$

where σ is the conductivity, F is Faraday's constant, C_i and μ_i are the concentrations and the mobilities of the i^{th} ionic species respectively. The noise-distance curve predicted by this model would be a flat curve outside the depletion layer. Within this layer, there would be a sharp continuous increase in noise during passage through the concentration gradient, the slope being inversely proportional to the concentration gradient. The maximum slope should be approached when the totally depleted region is reached. An equivalent circuit is given in Figure 14.

V Summary of Potential, Noise Data

The data considered so far have been reconstructed qualitatively in Figure 37. The curves represent the instantaneous concentration profiles with increasing time from t_1 to

t_{ss} when a steady state profile has been formed. The initial sharp drop occurs at t_3 . At this point, the electric field rises high enough to dissociate water and can rise no further. Secondary changes occur outside the depletion layer from t_4 to t_{ss} . The lack of secondary changes at higher concentrations and at lower current densities can be easily explained in terms of the required diffusional flux:

$$J = -FD\frac{\partial C}{\partial x} \tag{36}$$

where J is the flux and D is the coefficient of diffusion related to mobility by:

$$\mu = \frac{DF}{RT} \tag{37}$$

$\frac{\partial C}{\partial x}$ is the concentration gradient. The surface across which diffusion occurs is an approximate hemisphere located outside the membrane surface. The magnitude of the diffusional flow is a function of this surface area as well as of the concentration gradient. For low current densities and/or high concentrations a small surface area is sufficient. At high current densities and/or low concentrations the diffusion flux must be increased by a larger surface area provided by a larger hemisphere. This requires further changes in the concentration profile.

The second model for the noise-distance curve requiring a dissipative region requires a specific resistance vs. distance curve represented in Figure 40. Noise is generated in the region x = o to x = a and noise should be a maximum for an electrode in this region. From a to b there is still a considerable contribution to the overall resistance without a noticeable contribution to noise. This results in a dissipative loss in noise power. Outside b, the contribution to the total resistance is negligible and therefore the effect on the observed noise is negligible. No ac signal loss can be expected in the region from zero to a since ac signals do not require reversible electrodes.

The above considerations strongly suggest that the noise is generated in a high field depletion layer of thickness less than 40 microns where water dissociation occurs. A more detailed description will become possible when the power spectra are analyzed.

To complete this phase of the analysis other features of the voltage behavior must be discussed. The change in sign observed when the electrode penetrated the depleted layer and possibly the membrane surface seems to indicate the presence of an electrical double layer (Figure 13). Such a layer is required for a Donnan equilibrium. A study of this double layer would be interesting. Unfortunately, a phenomenom of this type requires reversible elec-

trodes for quantitative study and at this point it is not certain that a true voltage inversion has been observed.

The voltage-time curves measured by pressing the electrode against the membrane and possibly penetrating the membrane (Figure 11) show that the voltage change with time is smaller within the membrane. This is an indication of concentration changes within. A possible explanation for this is the depletion of the small concentration of coions that is in the membrane.

The differences in the voltage-time curves of different ions is shown in Figure 12. The curve for the anion membrane MA 3148 serves to show that a depletion layer was formed with the anion membrane, thus fortifying the conclusion that anion membrane noise is independent of the depletion layer. The differences in the behavior of hydrogen ion and sodium ion with the cation exchange membrane lie primarily in the sharper voltage change with time for the hydrogen ion. A larger $\frac{dV}{dt}$ results from a high field depletion layer forming faster than the formation of a steady state concentration gradient. Such a situation occurs with ions of high mobility where the ionic velocity given by $v = \mu E_{(x)}$, where v is the velocity and $E_{(x)}$ the electric field, can far exceed the particle velocity due to diffusion. With a lower mobility the velocity at the same field is lower and closer to the diffusional velocity.

VI Temperature Effects

The diffusional flux can be used to explain the increase of the critical current density with increasing coefficient of diffusion (Table 1) and with increasing concentration. The current density must exceed the maximum diffusional flux before the critical current density can be reached. The diffusional flux is proportional to the diffusion coefficient and the concentration gradient. The coefficient of diffusion increases with temperature and the concentration gradient increases with concentration.

VII Power Spectra

The descriptive features of a power spectrum when plotted in terms of the log (power) vs. log (frequency), are the slope(s) and relaxation time(s). For a system with a single relaxation time, the correlation-function $C(\tau)$ is given by $\langle C_0^2 \rangle e^{-t/\tau}$. The power spectrum, which is the real part at the Fourier transform of $C(\tau)$, is given by $4\langle C_0^2 \rangle \frac{\tau}{1+\omega^2\tau^2}$. The spectrum is white at low frequencies when $\omega^2\tau^2$ is much smaller than unity. At high frequencies when $\omega^2\tau^2$ exceeds unity the log P vs. log ω plot will have a slope of -2. The curve is reconstructed in Figure 36(1). Figure 36(2) shows the effect of passing this noise through a low pass filter with a time constant, RC, that is less than τ.

For transport noise, the transport equation can be used to find the power spectrum.[14,15] Thus diffusion noise is found to give a power spectrum with an $\omega^{-3/2}$ dependence and noise due to pure drift is found to give an ω^{-2} dependence.[15] For a transport equation derived from the Nernst-Planck equation where diffusion and drift occur together the calculations show that the noise again has an $\omega^{-3/2}$ dependence.[19] Experimentally the drift and diffusion noise was measured by passing a current through two copper sulfate solutions separated by a hole 0.7 mm. in diameter. The predicted $\omega^{-3/2}$ dependence can be seen in Figure 27.

Power spectra with slopes of -1 were observed with anion membranes only (Figure 15). The slopes of -1 obtained at moderate currents changed gradually to -3/2 with larger currents for certain ions (Table 2).

Noise with $1/\omega$ dependence have been discussed repeatedly in the literature[22,28,29] but firm conclusions are lacking. The $1/\omega$ behavior was found to persist at frequencies below 6×10^{-5} sec.$^{-1}$ for carbon resistors and germanium filaments.[30] The magnitude of the power for $1/\omega$ noise for carbon resistors was found to change by a factor of ten from 4.2°K to 290°K.[31] The persistence of the slope at low frequencies requires very long relaxation times, which is difficult to explain.

A $1/\omega$ dependence can be obtained by an ad-hoc assumption of a $1/\tau$ distribution of states, $g(\tau)$, between τ_1 and τ_2.[22]

A $\frac{k}{\tau}$ distribution for $g(\tau)$ where k is a constant could result from a uniform distribution of barrier heights such that:

$$\tau = a e^{qE/kT} \tag{38}$$

where E is the barrier height. The number of states with τ_x between τ_x and $\tau_x + d\tau$ is given by:

$$dn = \frac{dn}{dE}\frac{dE}{d\tau}d\tau = \frac{kT}{q\tau}\frac{dn}{dE}d\tau \tag{39}$$

$$g(\tau) = \frac{dn}{d\tau} = \left(\frac{kT}{q}\frac{dn}{dE}\right)\frac{1}{\tau} = \frac{k}{\tau} \tag{40}$$

The sensitivity of $1/\omega$ noise in semiconductors to ambient conditions such as the composition of the atmosphere indicate[32] that $1/\omega$ noise is a surface phenomenon. This is probably because in a homogeneous semiconductor a continuous uniform surface.

The relationship of the above properties of $1/\omega$ noise to anion membranes is speculative. It is known that anion membranes are easily and irreversibly contaminated by surface adsorption of anionic impurities present in water unless special precautions are observed.[33] This effect may alter

the membrane properties drastically and even affect the permselectivity. Under such conditions unusual distributions of activation energies may arise to account for the $1/\omega$ noise. On the other hand the required distribution may already exist in the membrane. The assortment of configurational strains and steric effects of a randomly crosslinked matrix may not be expected to result in a uniformly varying potential energy topography. A distribution of energy barrier heights is expected.

In light of these arguments answers to two questions, not available at present, must be found before more insight can be obtained: Is $1/\omega$ anion noise the result of absorbed impurities? Is the $1/\omega$ noise a result of a natural hyperbolic distribution of states?

Cation exchange noise from solutions of several kinds of salts were studied cursorily to determine general trends. Based onthis survey the HCl spectrum was chosen for detailed study with the higher resolution available with the 3L5 spectrum analyzer.

The cation spectra had the common characteristic of a -2 initial slope observed in anion exchange membranes only at higher current densities. The additional feature of interest was the occurrence of a curvature inthe spectra (figures 16-20); this is indicative of a relaxation spectrum

superimposed on a noise source with a-2 slope. The expected shape of such an interaction is shown in figure 38. This curvature moves from lower frequency to higher frequency with increasing current density to indicate a field dependence of the proposed relaxation time (figure 18).

It is of interest that copper sulfate and disodium acid phosphate gave similar spectra (figure 16). The reason for this similarity cannot be explained at the moment. Any relation of spectra to the reversibility of the electrodes was eliminated by using copper electrodes with copper sulfate solutions for comparison with the spectra obtained with platinum electrodes (figure 17). Some measure of the effect of the coion (anion in this case) was obtained by comparing the disodium acid phosphate spectrum with a sodium chloride spectrum (figure 39). Apparently the difference lies only in the magnitude of the curvature, it being smaller for sodium chloride. The lack of sufficient information makes further discussion speculative.

Calcium chloride showed an apparent relaxation time that could be observed only at a specific current density (figure 19). Only at intermediate currents and low concentrations (0.050M or less) was a curvature observable. This feature disappeared at lower current densities and seemed to be masked by another noise source at higher current densities. A similar situation was observed for copper sulfate in the same region.

Information for a proper interpretation is lacking.

The low resolution spectrum of dilute hydrochloric acid in comparison with a cesium chloride spectrum can be seen in (figure 20). A comparison was made with the hydrated size and the ionic mobilities in mind. The hydrogen ion has the highest mobility. The cesium ion was the ion of next highest mobility that was available. For the effects of low mobilities quarternary ammonium ions were sought. However, only the tetramethyl ammonium ion was used (figure 22). These three ions have in common a sharp change in slope. This feature was the focus of a detailed study which will now be discussed. Hydrochloric acid was selected because of its availability and the extensive information that exists on its aqueous properties.

VIII THE HCl SPECTRA

The spectra for 0.050M HCl with MC3235 at 30°C obtained with the higher resolution of the 3L5 spectrum analyzer can be seen in figure 23. A similar family of curves were obtained at 19°C, 40°C and 50°C and for 0.025M HCl at the same temperatures. Of prime interest were the intersecting straight lines with slopes of approximately -2 and -4 respectively. Except for an excess of two, this behavior was exactly that expected from a relaxation time.If

point of intersection was taken as the point where the product $\omega\tau$ became unity, an empirical relation was obtained of the form:

$$(41) \qquad J = \chi f + \beta$$

where $\omega = 2\pi f$ was the frequency at the point of intersection and χ and β were empirical constants. The experimental plots of J vs f can be seen in figure 24. If the flux equation has any analogy to other electrochemical rate expressions it is expected that f would be a function of the rate constants and χ would be a concentration term. The equivalent equation of electrochemistry is given by[34]:

$$(42) \qquad i = zF\upsilon = \left\{ k_o \frac{kT}{h} \exp - \frac{\Delta\bar{G}_o}{RT} \right\} zF(C_R)_s(1-\theta)$$

where zF is the number of coulombs involved in the charge-transfer step of rate υ. The rate constant in terms of absolute rate theory is given by the terms in the bracket where ko is the transmission coefficient, r, R, h and T have their usual significance and $\Delta\bar{G}o$ is the electrical free energy of activation. The surface concentration of reactants is given by $(C_R)_s$ and the adsorbed surface area by $(1-\theta)$. Then χ should have a Boltzman type exponential relation to temperature such that $d\ln\chi/d\frac{1}{T}$ would be a straight line. This plot can be seen in figure 28. It was assumed that the best straight line was a reasonable interpretation of the data.

β should be the critical current density. Then it should obey the diffusion equation:

(36) $$J_i = -FD\partial c/\partial x$$

If it is assumed that the concentration gradient is invariant of temperature, then β would be expected to have the form:

(43) $$\beta = \beta_0 \exp - E_a/RT$$

where E_a is the activation energy of diffusion and β_0 is a constant. The plot of $\ln\beta$ vs. $1/T$ is shown in figure 29. From the plot, E_a is found to be 4.0 Kcal and 4.9 Kcal for 0.050M HCl and 0.025M HCl respectively. The literature value for the diffusional activation energy of the hydrogen ion and chloride ion are 3.23 Kcal and 4.22 Kcal respectively.[35] For the diffusion of hydrochloric acid the higher activation energy of the chloride ion should prevail.

IX Interpretation of the Observed Relaxation Time:

The empirical flux equation:

(41) $$J = Kf + \beta$$

may be rewritten in another form if β is assumed to be the critical current density:

(44) $$J_{Total} = J_{diff} + J_{mig}$$

The observed flux is $J_{observed}$ and J_{HCl} is the critical density which is the contribution to the flux by the residual HCl in the depleted region. J_{diss} is the additional flux made possible by water dissociation. If the relaxation time for a conductor [36]:

$$\tau = \frac{\epsilon}{\sigma} \tag{45}$$

is substituted for the relaxation frequency:

$$f = \frac{1}{2\pi\tau} \tag{46}$$

equation 44 has the new form:

$$J = \frac{\chi\sigma}{2\pi\epsilon} + B \tag{47}$$

where ϵ is the permittivity and σ the conductivity.
The flux can also be expressed in the form:

$$J = \sigma E_{(x)} = (\sigma_{diss} + \sigma_{HCl}) E_{(x)} \tag{48}$$

where σ_{HCl} is the conductivity due to the residual HCl and σ_{diss} is the contribution from water dissociation. Comparison of equation 47 and 48 results in the relation:

$$\chi = 2\pi\epsilon E_{(x)} \tag{49}$$

This relation can be used with the field dissociation equation for weak electrolytes.

The problem of the effect of the electric field on the

dissociation of a weak electrolyte was investigated by Onsager.[37] The relation obtained was:

(50) $K = K_o F(b)$

where Ko is the dissociation constant at zero field and K is the dissociation constant at a field $E(x) = dV/dt$. F(b) is a Bessel function and is given by:

(51) $F(b) = 1 + b + b^2/3 + b^3/18 + b^4/180 + \ldots$

At high values of b, F(b) can be used in the form:

(52) $$F(b) = \frac{\left(\frac{2}{\pi}\right)^{1/2} e^{(8b)^{1/2}}}{(8b)^{3/4}}\left[1 - \frac{3}{8(8b)^{1/2}} - \frac{15}{128(8b)} - \frac{105}{1024(8b)^{3/2}} \ldots\right]$$

The field dependent term b is given by:

(53) $$b = \frac{9.636 \times 10^{-12} E_{(x)} \epsilon_o}{\epsilon T^2}$$

The ratio ϵ/ϵ_o is the dielectric constant for the medium. By the use of equation 49, can be eliminated. Using in addition the permittivity of free space, 8.85×10^{-12} farad/meter, b is converted to the form:

(54) $$b = \frac{5.358 \times 10^{-12} E_{(x)}^2}{\lambda T^2}$$

Another expression for F(b) can be obtained in terms of empirical parameters starting from:

(55) $$K = C_{H^+} C_{OH^-} = (C_{OH^-} + C_{A^-}) C_{OH^-}$$

The concentration of the hydrogen ion can be equated to the sum of the anions by the electroneutrality condition.

The ionic concentration of the hydroxyl and chloride ions can be obtained in terms of β and χf:

(56) $$\beta = E_{(x)} \sigma_{HCl} = F C_{Cl^-} U_{HCl} E_{(x)}$$

(57) $$\chi f = E_{(x)} \sigma_{diss} = F C_{OH^-} U_{NaOH} E_{(x)}$$

(58) $$U_{NaOH} = \mu_{Na^+} + \mu_{OH^-}$$

The μ's are the ionic mobilities at infinite dilution. From 56 and 57 the concentration of the hydroxide and chloride ions can be obtained in terms of χf and β respectively:

(59) $$C_{OH^-} = \frac{\chi f}{E_{(x)} F U_{H_2O}}$$

(60) $$C_{Cl^-} = \frac{\beta}{E_{(x)} F U_{HCl}} = \frac{C_{OH^-}}{\chi f U_{HCl}}$$

The final form of equation 60 was obtained by using equation 59 to eliminate E(x)F.

The hydrogen ion concentration is now given by:

(61) $$C_{H^+} = C_{OH^-} + C_{Cl^-} = C_{OH^-}\left[1 + \frac{\beta U_{NaOH}}{\chi f U_{HCl}}\right]$$

The dissociation constant now takes the form:

(62) $$K = C_{OH^-}^2\left[1 + \frac{\beta U_{NaOH}}{\chi f U_{HCl}}\right] = \left[\frac{\chi f}{E_{(x)} F U_{NaOH}}\right]^2\left[1 + \frac{\beta U_{NaOH}}{\chi f U_{HCl}}\right]$$

From equation 50 a final form relating F(b) to the empirical parameters is obtained:

(63) $$F(b) E_{(x)}^2 = \frac{\chi^2 f^2 + rf\beta\chi}{K_o F^2 U_{NaOH}^2} = Mf^2 + Nf$$

where r is the ratio

(64) $$r = \frac{U_{non}}{U_{ac}}$$

The values of U^2_{non} and r at different temperatures were obtained from the diffusion coefficients and activation energy given by Longsworth[35]. Equation 37 was used to convert diffusion to mobility. The water dissociation constants for the temperatures of interest were obtained from the Handbook of Chemistry and Physics[38]. The values are given in tables 6a and 6b.

It was thought that a better picture of the temperature behavior of $F(b)E(x)^2$ would be obtained if the values of χ and β were made to conform to the relations $\partial \ln \chi / \partial \gamma_T$ = constant and $\partial \ln \beta / \partial \frac{1}{T}$ = constant. The values that deviated from this relation were made to conform to the above equation by using the plots in figures 28 and 29. The experimental and corrected values of these empirical constants are given in table 5. The effect of these corrections on equation 41 is shown in figure 30.

Using these corrections the values of the coefficient M and N in equation 63 were calculated and recorded in table 6b. The values of $F(b)E(x)^2$ corresponding to different values of f are recorded in table 7. The plots of $F(b)E(x)^2$ vs. $E(x)$ and $F(b)$ vs. $E(x)$ are shown in figures 31 and 32 respectively.

Figure 29. Plot of $\log\beta$ vs. $\frac{1}{T}$

○ 0.050M HCl, MC3235

⊖ 0.025M HCl, MC3235

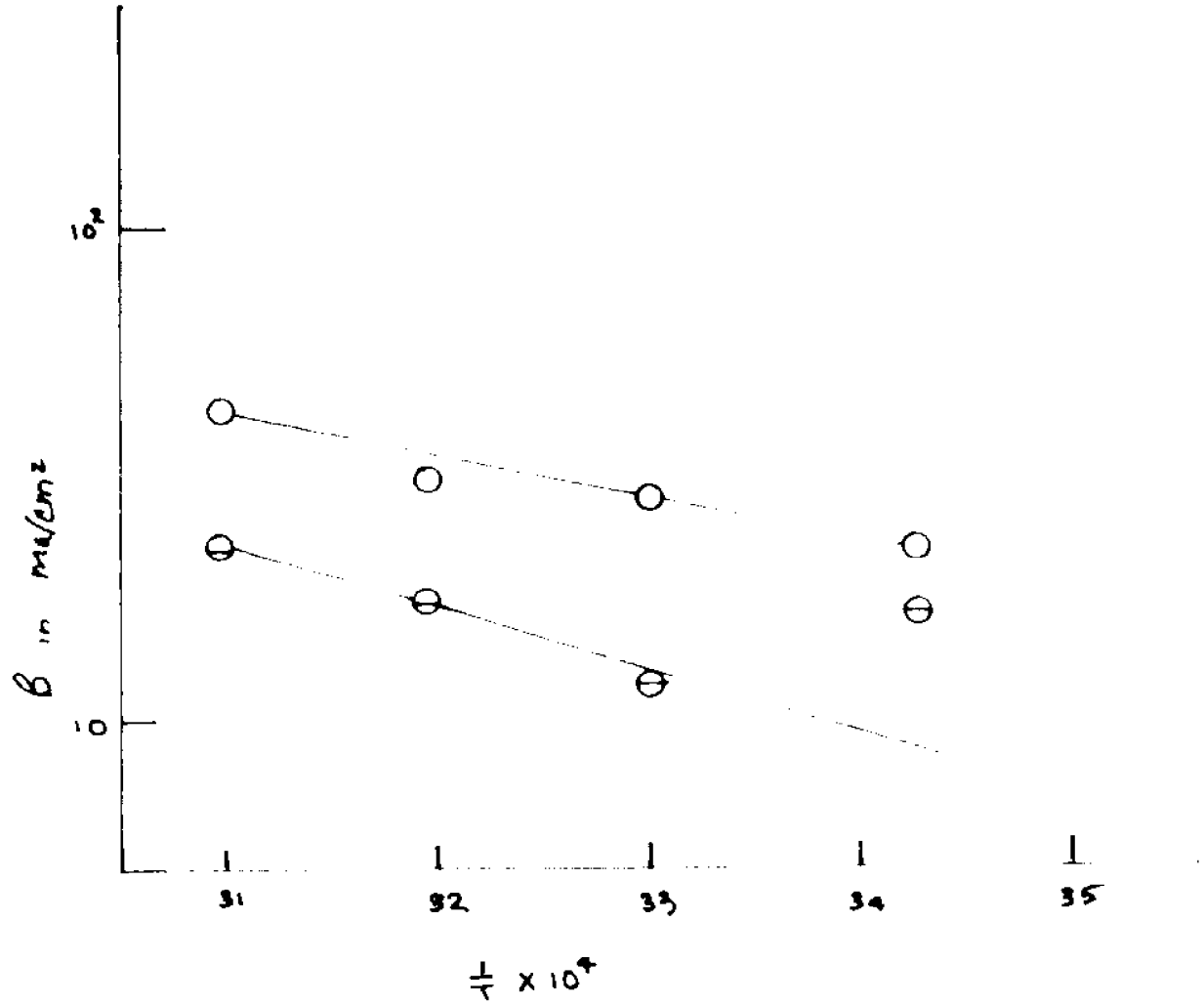

Figure 28. Plot of log k vs. $\frac{1}{T}$

⊖ 0.050M HCl, MC3235

○ 0.025M HCl, MC3235

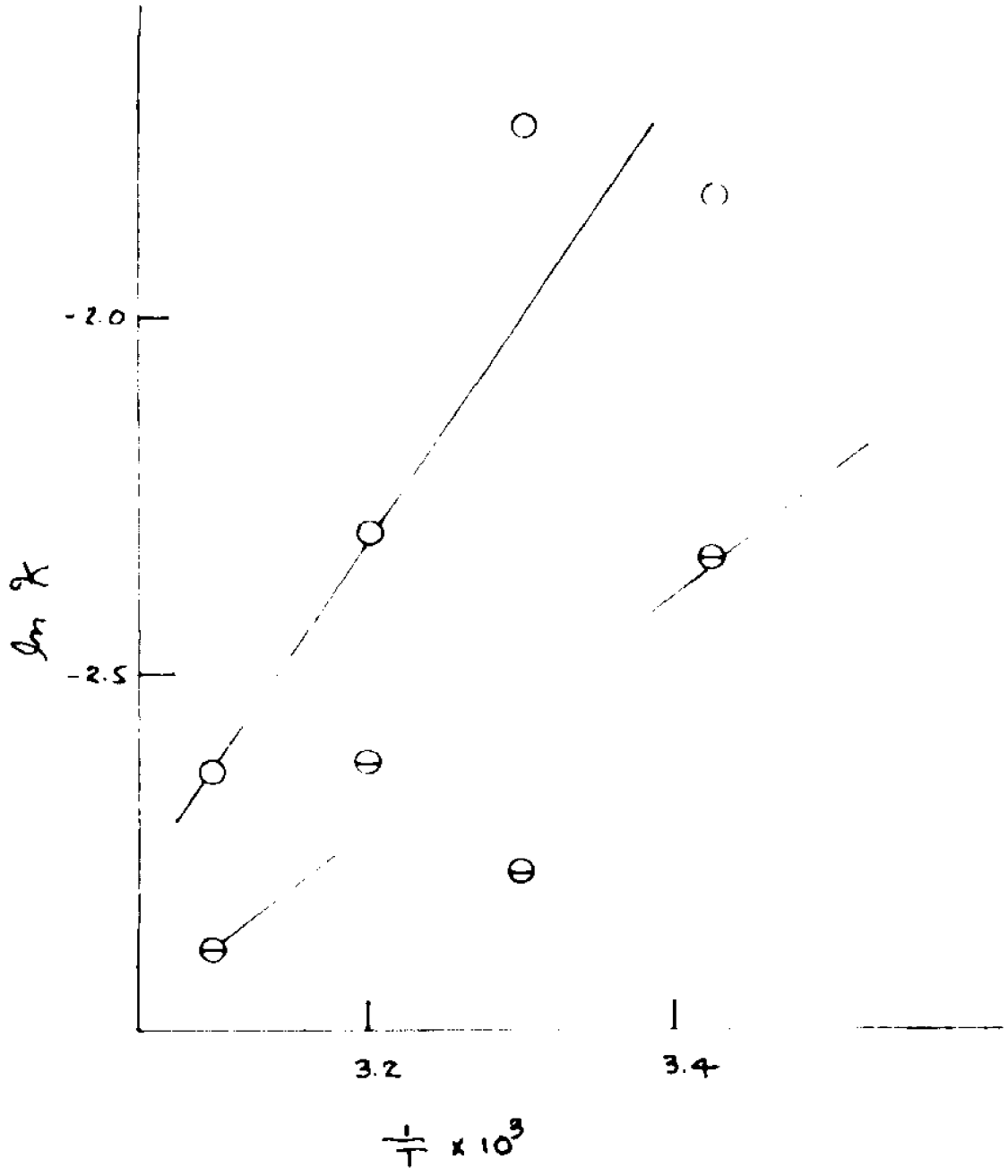

Figure 30

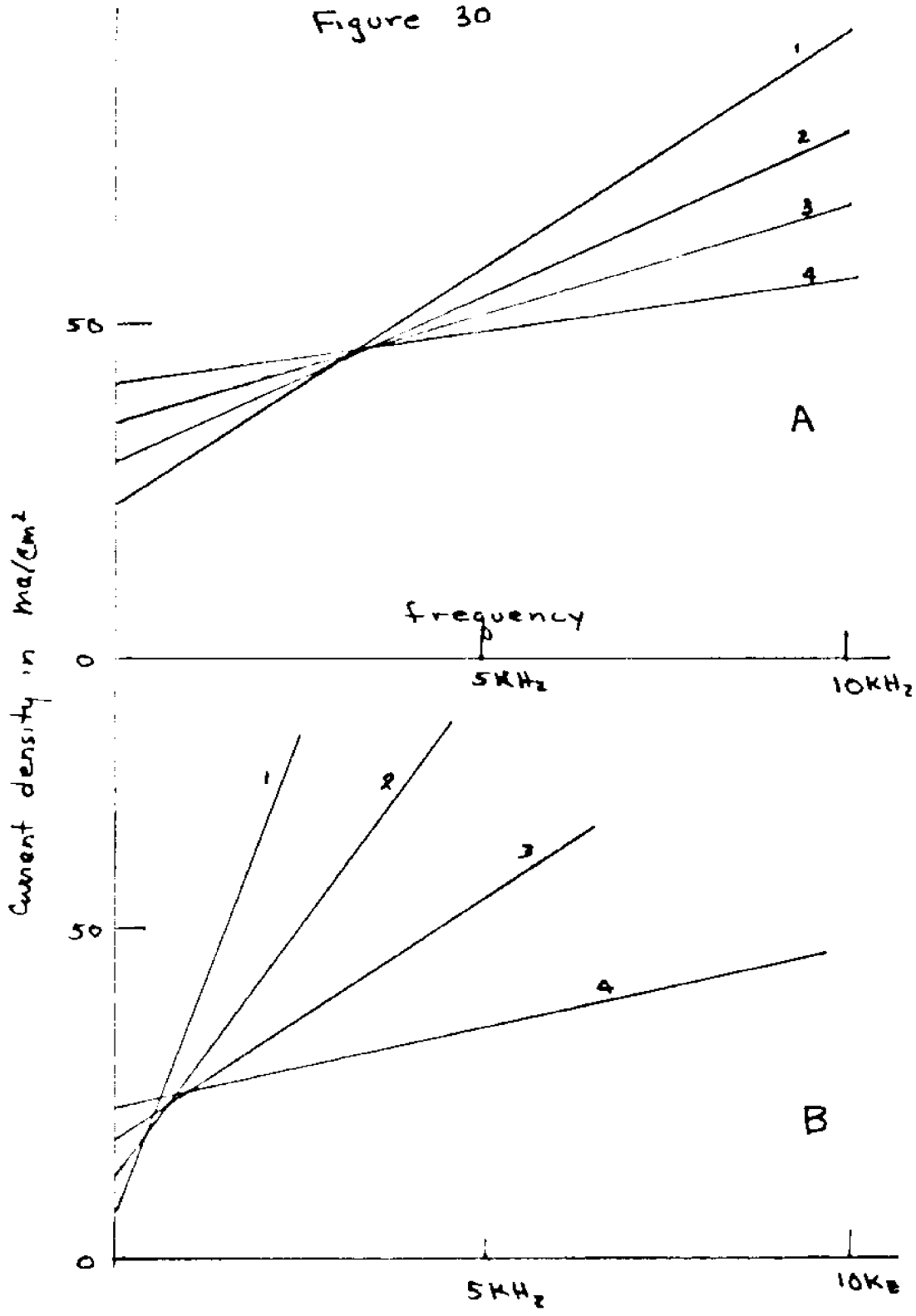
1
2
3
4
50
A
Frequency
0
5KH₂
10KH₂
Current density in ma/cm²
1
2
3
4
50
B
0
5KH₂
10KH₂

Figure 30. Corrected curves for: $\bar{J} = \kappa\phi + B$

A. 0.050M HCl

B. 0.025M HCl

1. 19°C, 2. 30°C, 3. 40°C, 4. 49°C.

The values used are given in Tables 8a - 8h. From Figure 31 and from equation 63, the relation of f to E(x) were obtained. The results can be seen in Figures 33a and 33b and in Table 8. Experimentally, the relaxation times are observed in the frequency range of 200Hz to 10KHz (Figure 24). In this range the field changes by about a factor of three from 10^7 volts/meter to 10^8 volts/meter (Figure 34). The water dissociation constant changes by a factor of up to 100 (Figure 32).

The frequency f can be converted to a rate term by equating f to k, a rate constant.

(65) $$\tau = \frac{1}{2\pi f} = \frac{1}{2\pi k}$$

By using values of f at constant field strength the change in logf with 1/T can be obtained from Figure 34. By this manner the contribution from the electrical free energy (Eq 31) can be eliminated. A plot of logf vs. 1/T should give the activation energy of the reaction. Values of 15.4 Kcal/mole and 17.5 Kcal/mole were obtained from Figure 34 for 0.050M and 0.025M solutions respectively.

The mean activation energy for the two concentrations of 16.5±1 Kcal/mole is too large for a diffusion controlled reaction. An electrostatic barrier of this height at the membrane surface is unlikely since the high electric field

Figure 31A. Plot of $F(b)\bar{E}(x)^2$ vs. $E(x)$. From 1 to 4: 49°C, 40°C, 30°C, 19°C, 0.050M HCl.

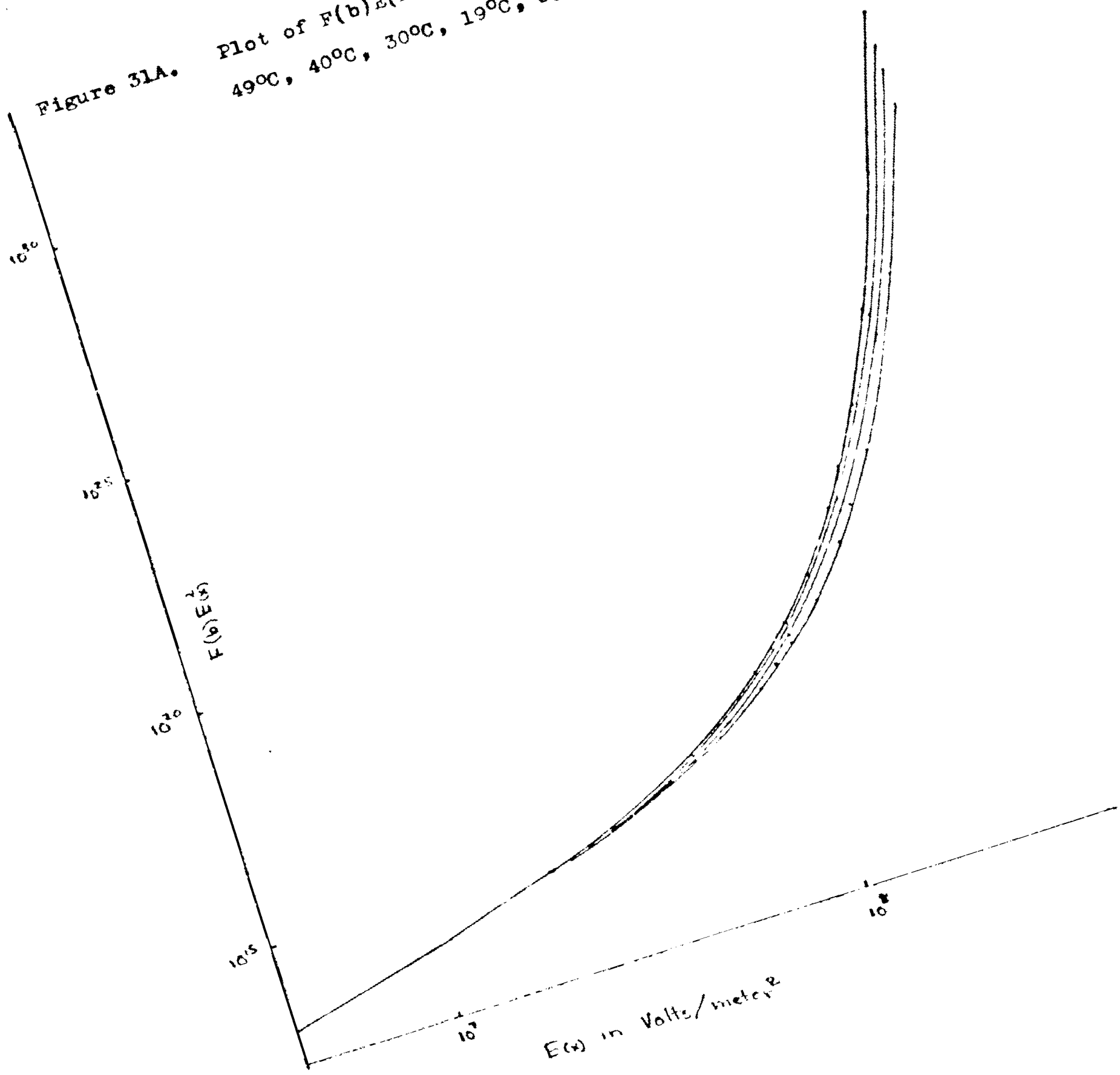

Figure 31B. Plot of $F(b)E(x)^2$ vs. $E(x)$ for 0.025M HCl. From 1 to 4: 49°C, 40°C, 30°C, 19°C.

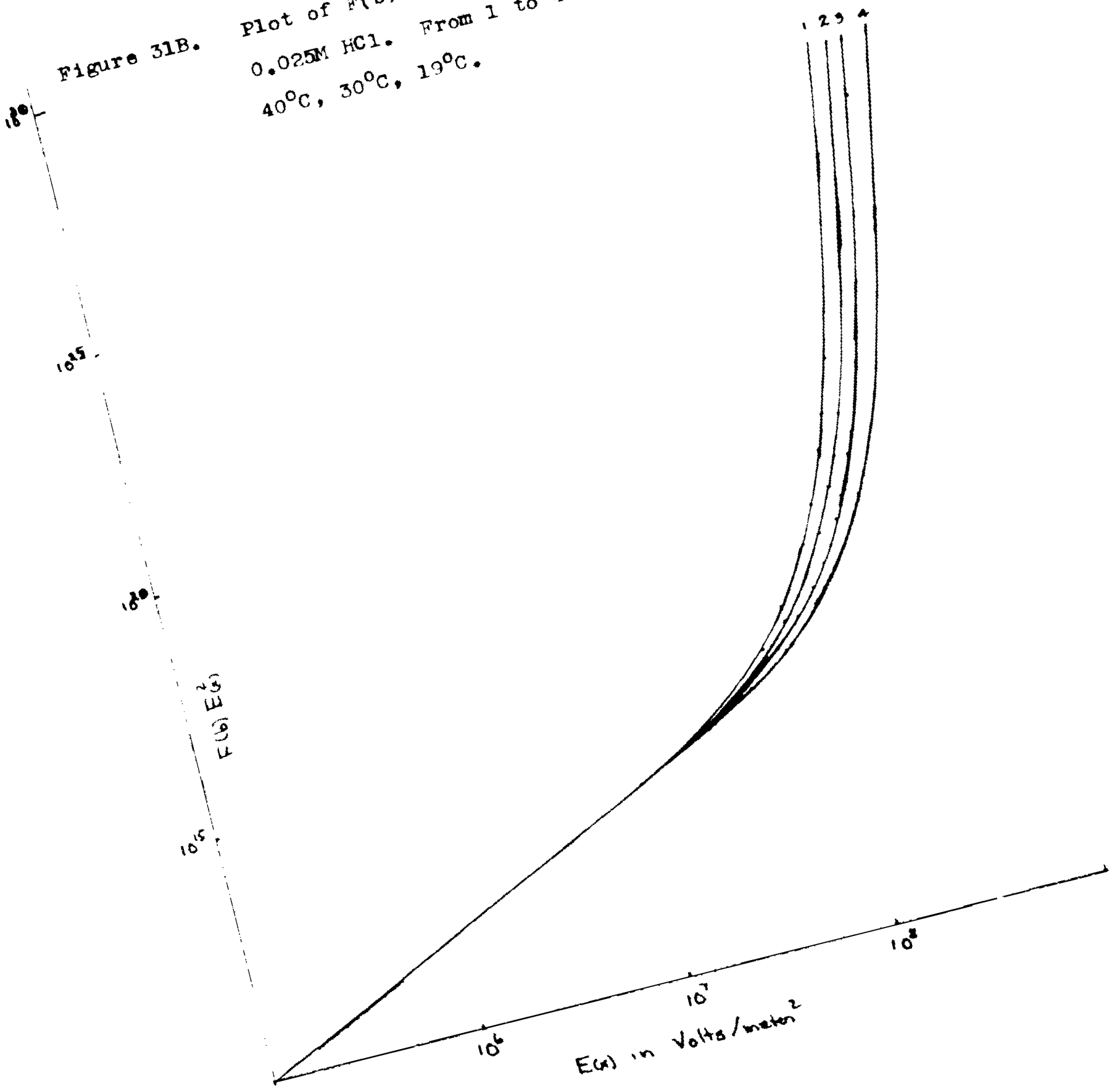

Figure 32A. Plot of F(b) vs. E(x) for 0.050M HCl. From 1 to 4: 49°C, 40°C, 30°C, 19°C.

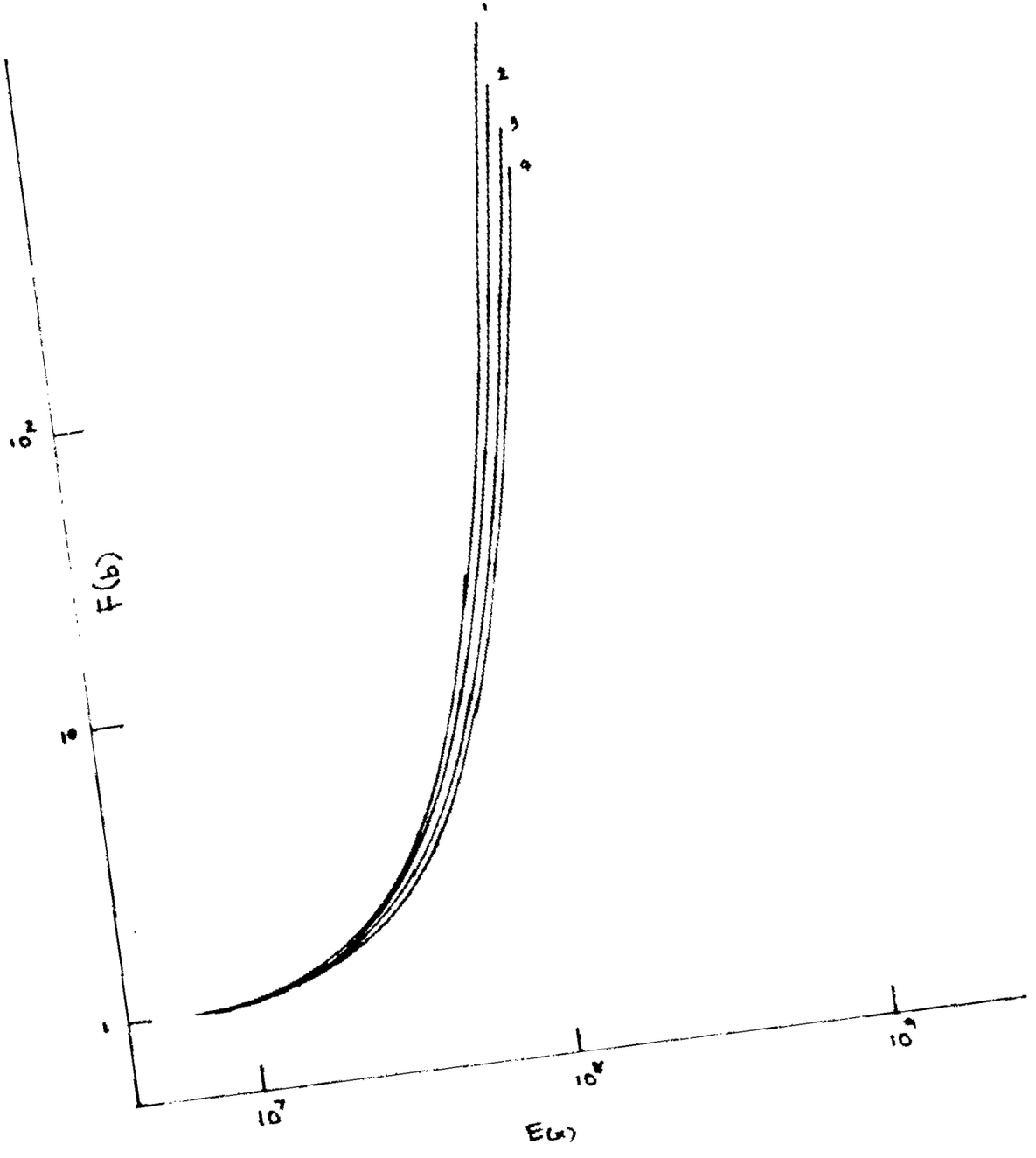

Figure 32B. Plot of F(b) vs. E(x) for 0.025M HCl. From 1 to 4: 49°C, 40°C, 30°C, 19°C.

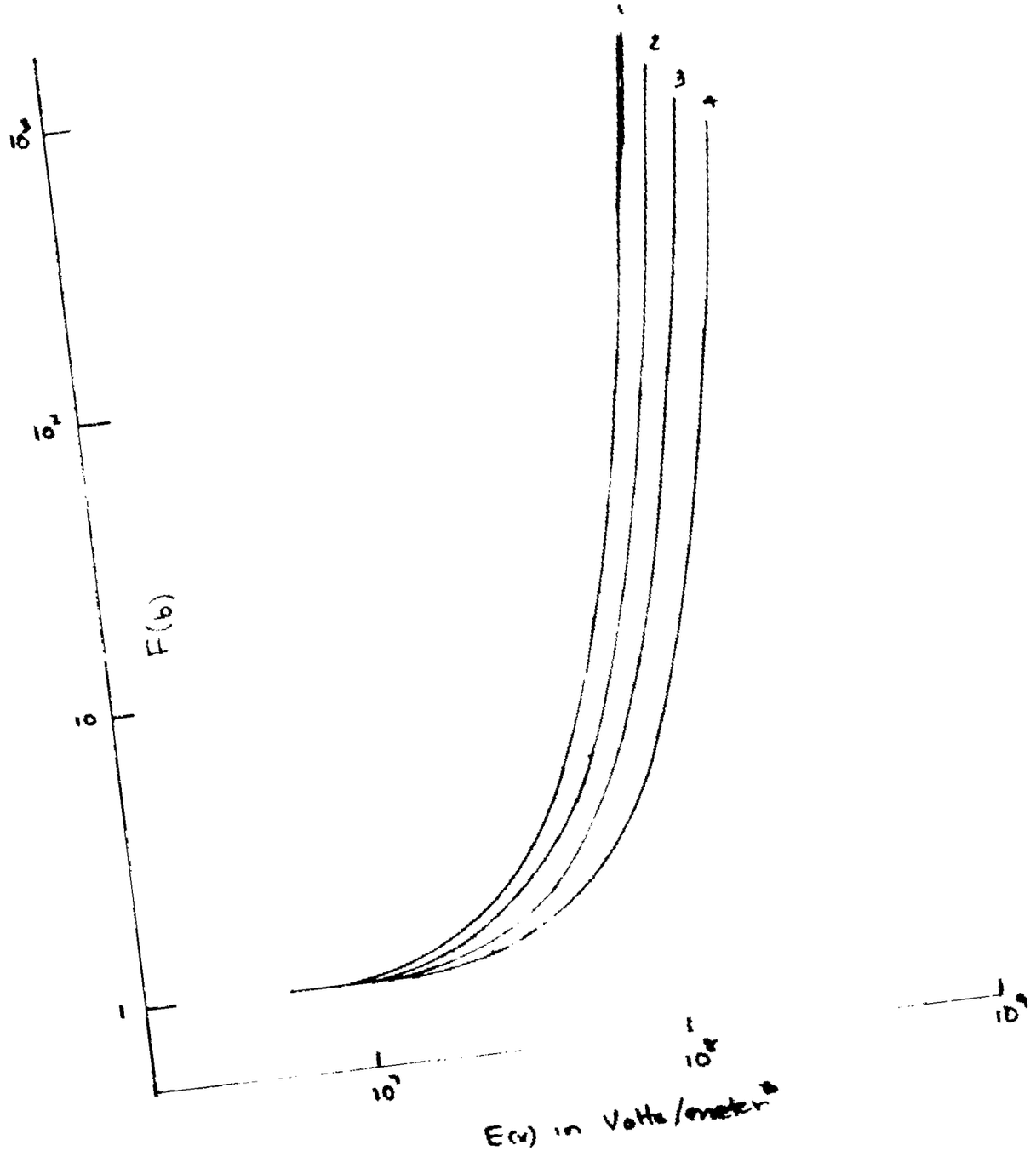

Figure 33 A. $f = \frac{1}{2\pi\tau}$ vs. E(x) for 0.05M HCl. From 1 to 4: 49°C, 40°C, 30°C, 19°C.

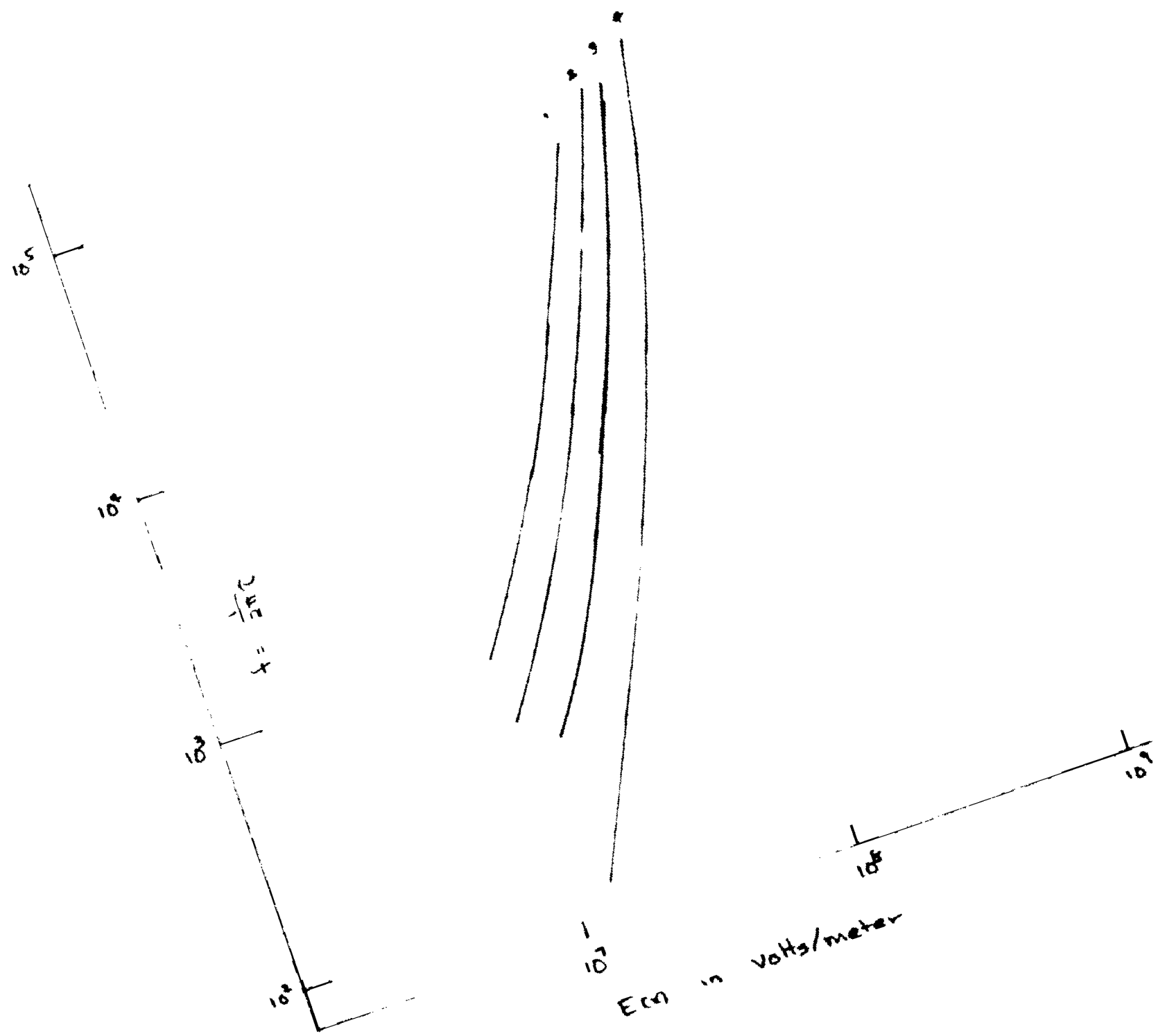

Figure 33B. $f = \frac{1}{2\pi\tau}$ vs. E(x) for 0.025M HCl. From 1 to 4: 49°C, 40°C, 30°C, 19°C.

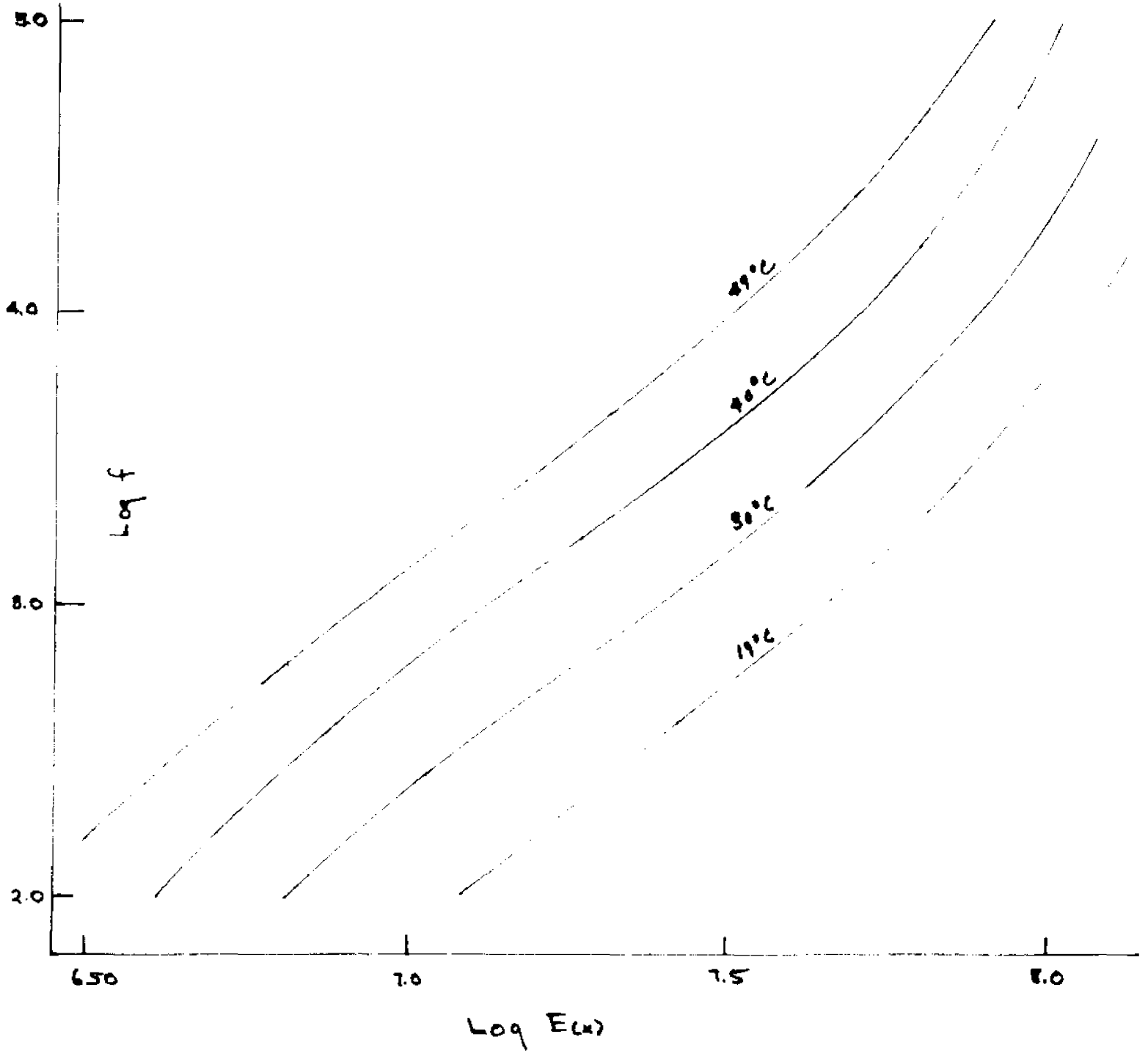

in the depletion layer and the electrical double layer at the membrane surface would oppose such a barrier. The most obvious reaction in an aqueous solution with an activation energy of this magnitude is the dissociation of water. The activation energy of this process is expected to be equal to or greater than the molar heat of neutralization of a strong acid with a strong base which is of the order of 14 Kcal/mole. This means that the space charge relaxation is primarily dependent on water dissociation. In solutions as dilute as that found in the depleted layer outside the membrane this is not unreasonable.

A self consistency check of these derivations can be made by using equations 35, 44 and 48. The flux is due to residual HCl given by:

(56) $J_{HCl} = \sigma_{HCl} E_{(x)} = F C_{HCl} U_{HCl} E_{(x)}$

The value of C_{HCl} obtained from 56 can be used to obtain the value of C_{OH^-}.

(66) $C_{OH^-} = \frac{K}{C_{H^+}} = \frac{K_0 F(b)}{C_{OH^-} + \frac{\beta}{F U_{HCl} E_{(x)}}} = -\frac{\beta}{2F U_{HCl} E_{(x)_a}} + \sqrt{\frac{\beta^2}{4F^2 U_{HCl}^2 E_{(x)_a}^2} + K_0 F(b)}$

Where J_{HCl} has been replaced by the empirical constant β and C_{H^+} is equal to $C_{OH^-} + C_{Cl^-}$ by the electroneutrality condition. The value of J_{HCl}, obtained in this manner can be compared with the experimental value 7Kf.

(67)

From equation 67, values for $J_{d.c.}$ for 0.50M HCl at 19° gave values of 94 amp/meter^2, 376 amp/meter2 and 950 amp/meter^2 for 10^3H_2, $4x10^3H_2$ and 10^4H_3 respectively. The experimental values given by Kf are 93, 372 and 930 respectively.

X. CONJECTURES CONCERNING THE EXCESS FACTOR OF 2 IN THE POWER SPECTRUM

The utility of noise measurements in evaluating the transport processes of ions in the environment of the membrane has been demonstrated by the previous discussion when the break in the slopes of the HCl spectrum was interpreted to result from a relaxation phenomenom. Such an interpretation was made in the absence of knowledge of any other mechanism that could produce such a break. Then the cause of the excess factor of two in the slopes must be explained.

At present sufficient information is not available for a conclusive answer. Meanwhile, some speculative models may prove useful in providing clues for further investigation. A simple model can incorporate all the data gathered up to the present. This model requires an equivalent low pass filter modifying a Lorentsian relaxation spectrum resulting

from water dissociation. The resulting filtered and non-filtered noise is shown in figure 36.

The first argument against this model is the result obtained from the external current source noise input test. Presumably the low pass filter proposed should affect external inputs as well. In effect the external noise was transmitted through the input unmodified (figure 41). An explanation for this behavior is proposed in figure 35 based on the proposed resistance vs. distance profile of figure 40. The proposed noise cell circuit is made up of a capacitance C and R_1 forming a low pass filter in series with R_2 and R_3. The noise source from water dissociation is ⓦ. The resistance R_1 is located in the depleted region where water dissociation occurs and the noise is generated. R_2 is the resistance across the concentration gradient where diffusion occurs, and R_3 is the sum of all the other resistances found in the rest of the circuit. If R_2 is sufficiently larger than R_1 the effect of the RC filter on the external input noise will be negligible since most of the IR drop will occur across R_2. The effect of the filter on the internally generated noise represented by ⓦ however, will be that of a low pass filter to give the filtered noise of figure 36. The specific resistivity of R_1 is greater than R_2 (figure 40). However the thickness of the depletion

Figure 35. Equivalent circuit for filtered noise.

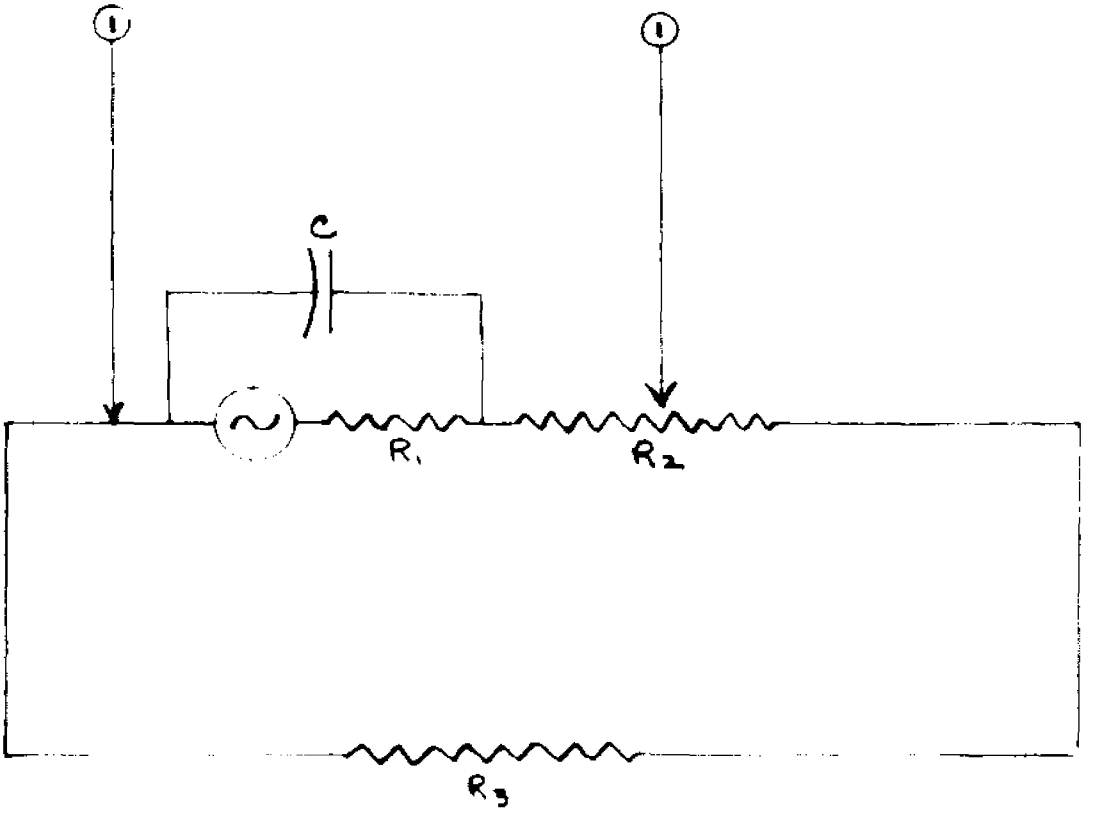

Figure 34. Log f vs. $\frac{1}{T}$ at E(x) = 3.16×10^7 volts/meter.

△ 0.050M HCl Ea. = 15.4 Kcal

○ 0.025M HCl Ea. = 17.5 Kcal

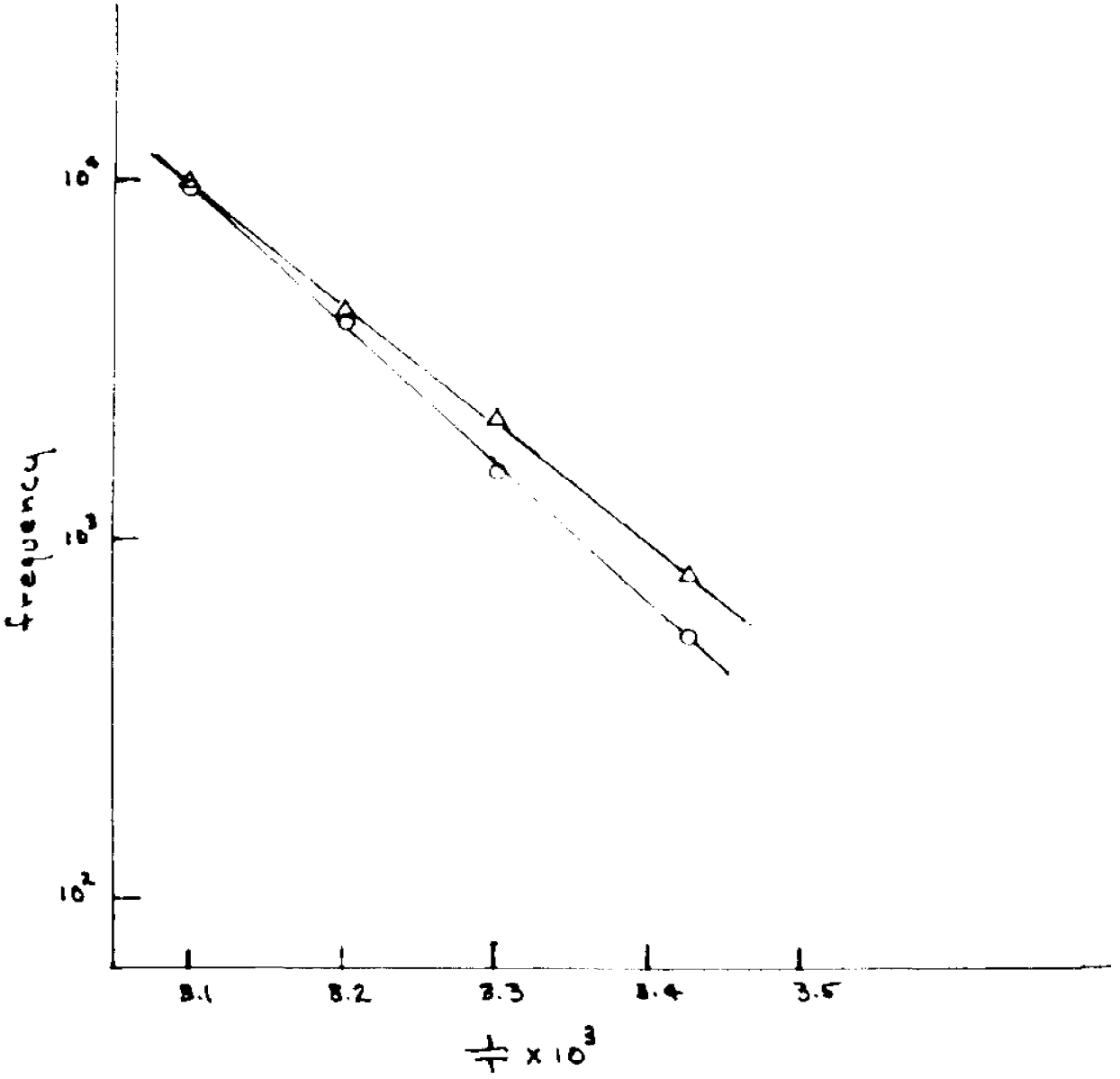

Figure 36. Power spectrum with a relaxation time of 10^{-3} seconds unfiltered (1) and filtered through a low-pass filter (2).

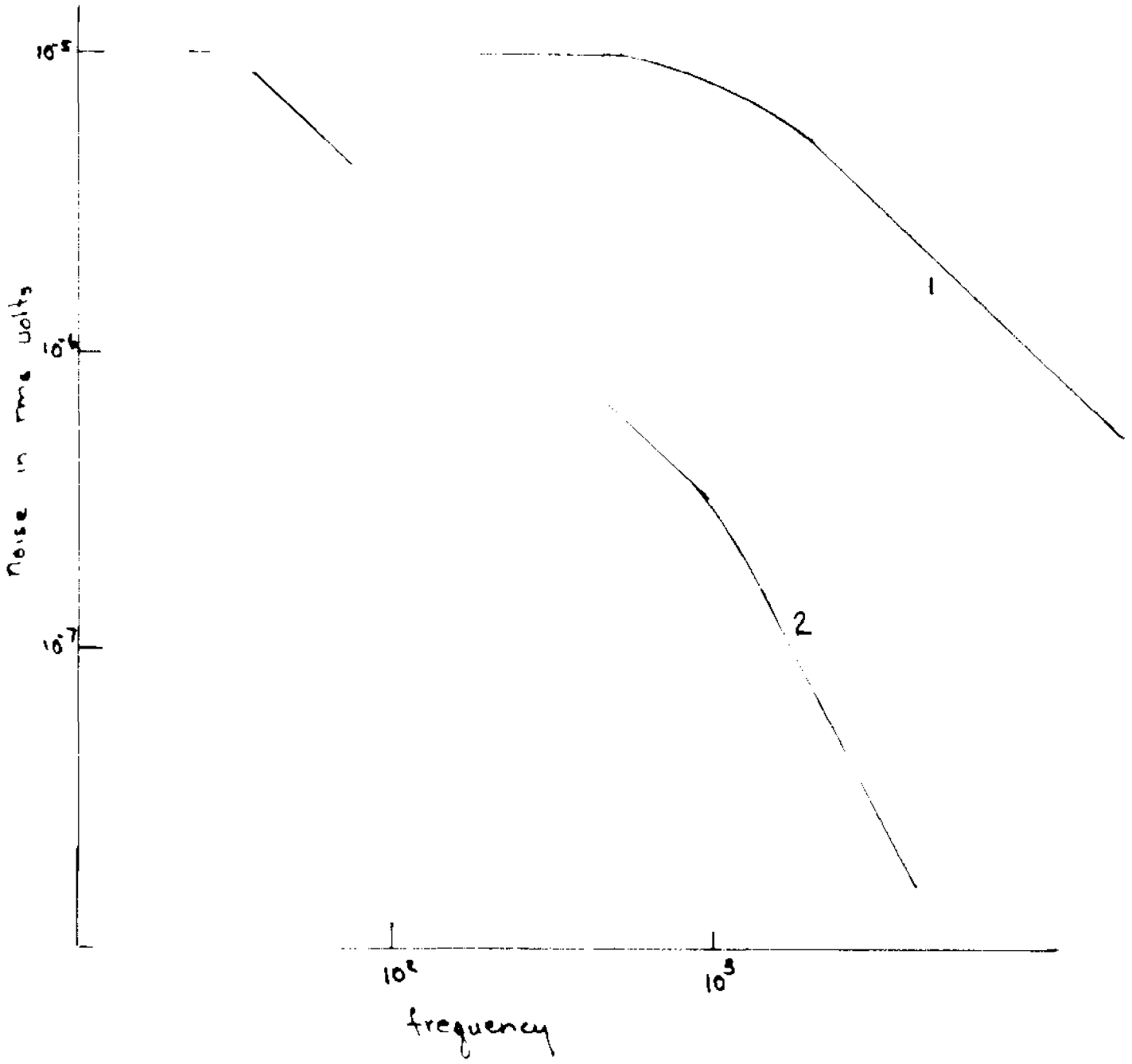

Figure 37. Proposed qualitative concentration profiles at various time intervals after current is applied. Co = Bulk concentration, O = Membrane surface, Ci = residual concentration in depletion layer, tss = time for the formation of a steady state concentration profile.

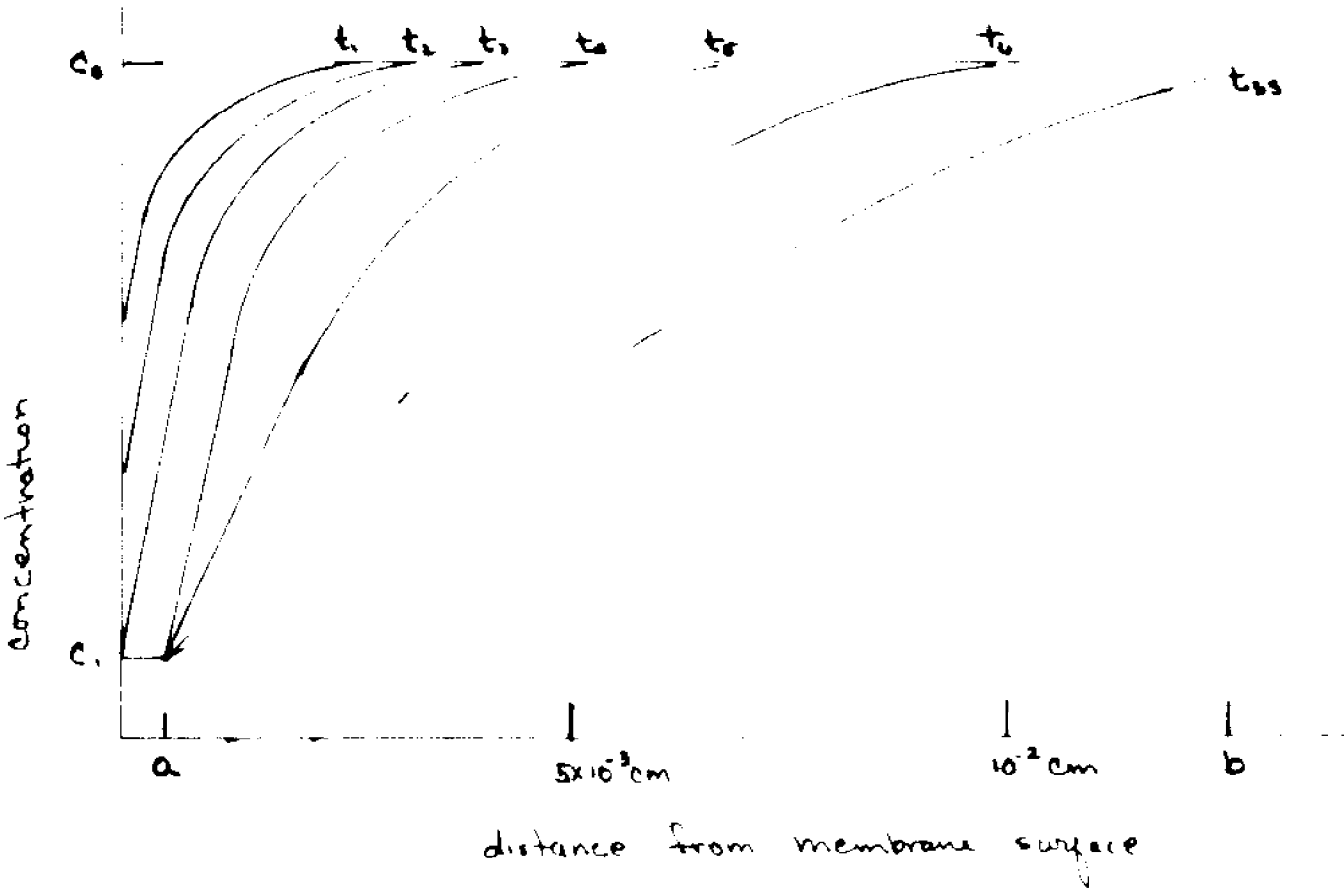

Figure 38. The super-position of f^{-2} noise source with a noise source with a relaxation time of 10^{-4} seconds.

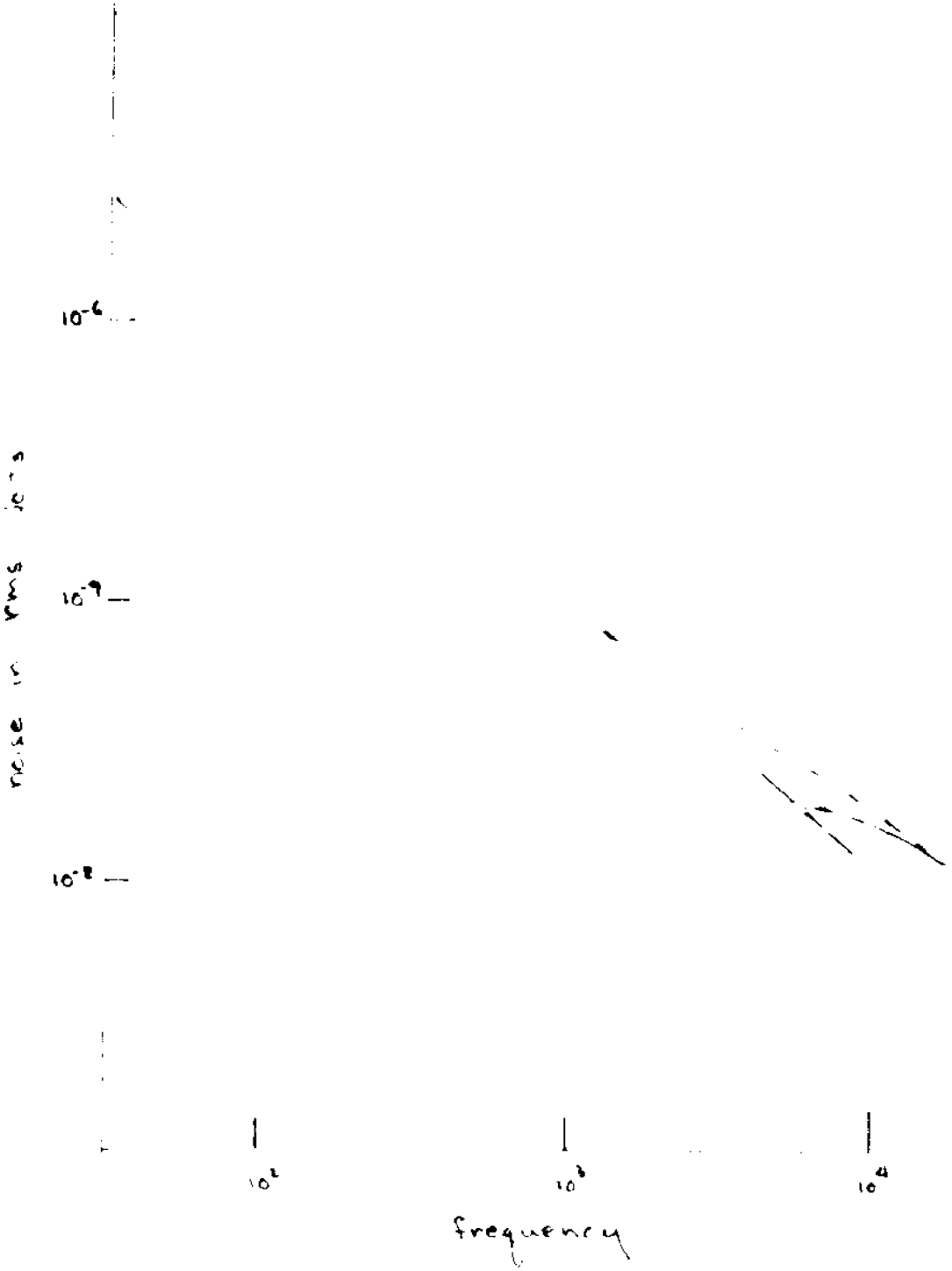

Figure 39. Comparison of power spectra of NaCl and Na_2HPO_4 with MC3235 at 43 ma/cm^2.

1. 0.056M Na_2HPO_4
2. 0.10M NaCl.

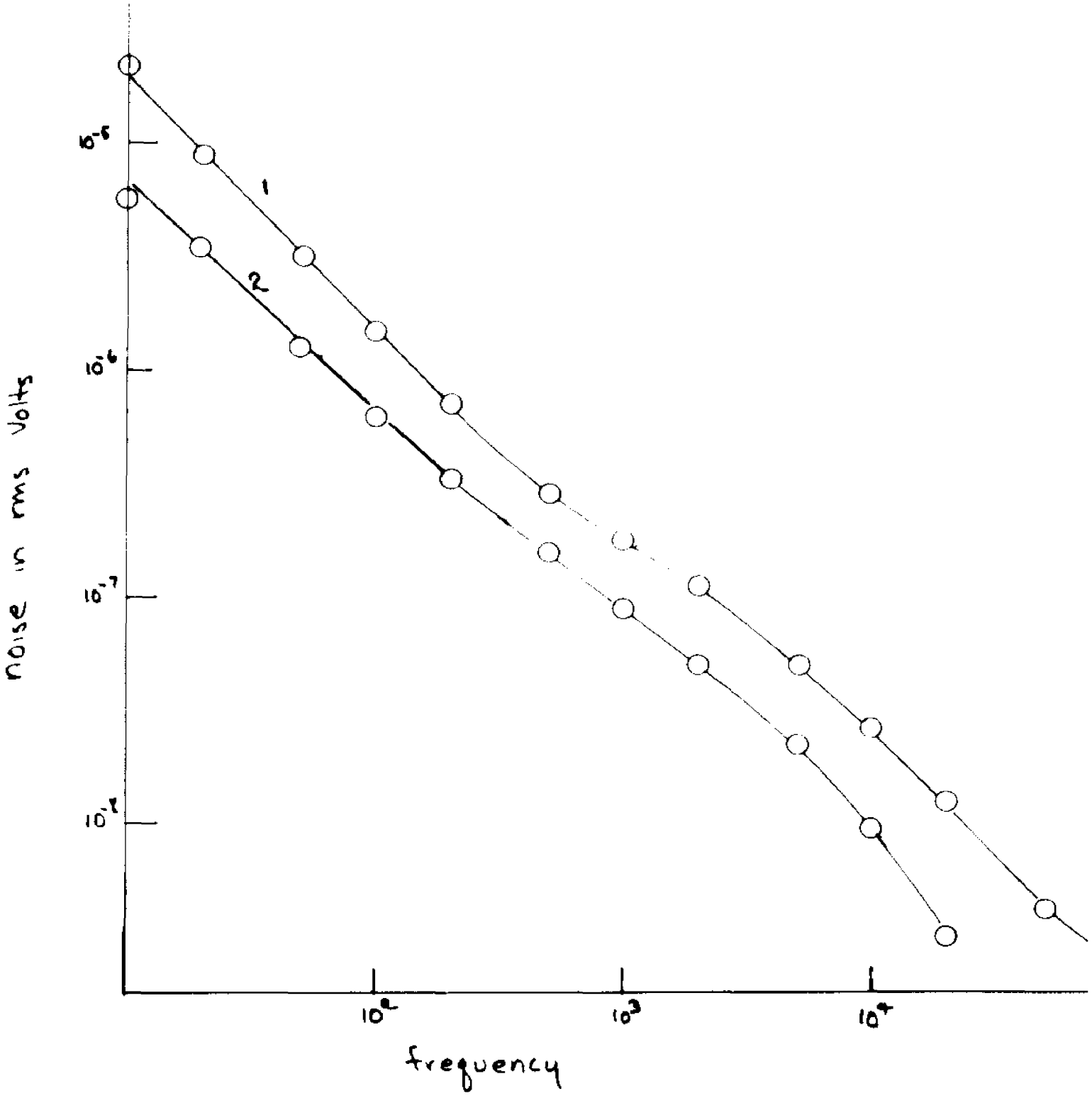

Figure 40. Proposed qualitative profile of specific resistance with distance from membrane.

Rd = Specific resistance of region of thickness, a, where water dissociation occurs.

Ro = Specific resistance of the bulk solution.

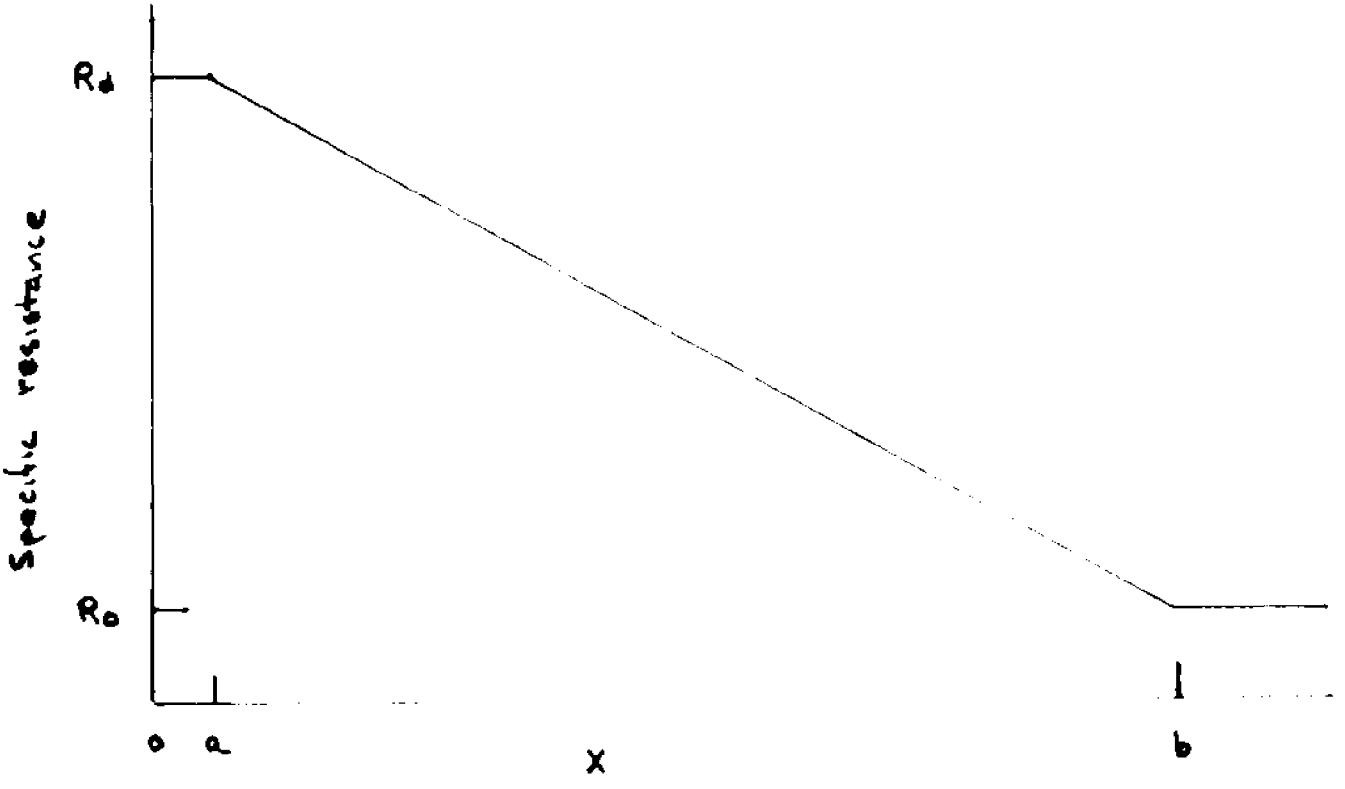

Figure 41. Current source noise with HCl spectra to show unmodified white noise. Broken line represents the external white noise level supplied by the 1390-B random noise generator. The initial slope is a HCl spectrum at 31 ma/cm^2 with MC3235.

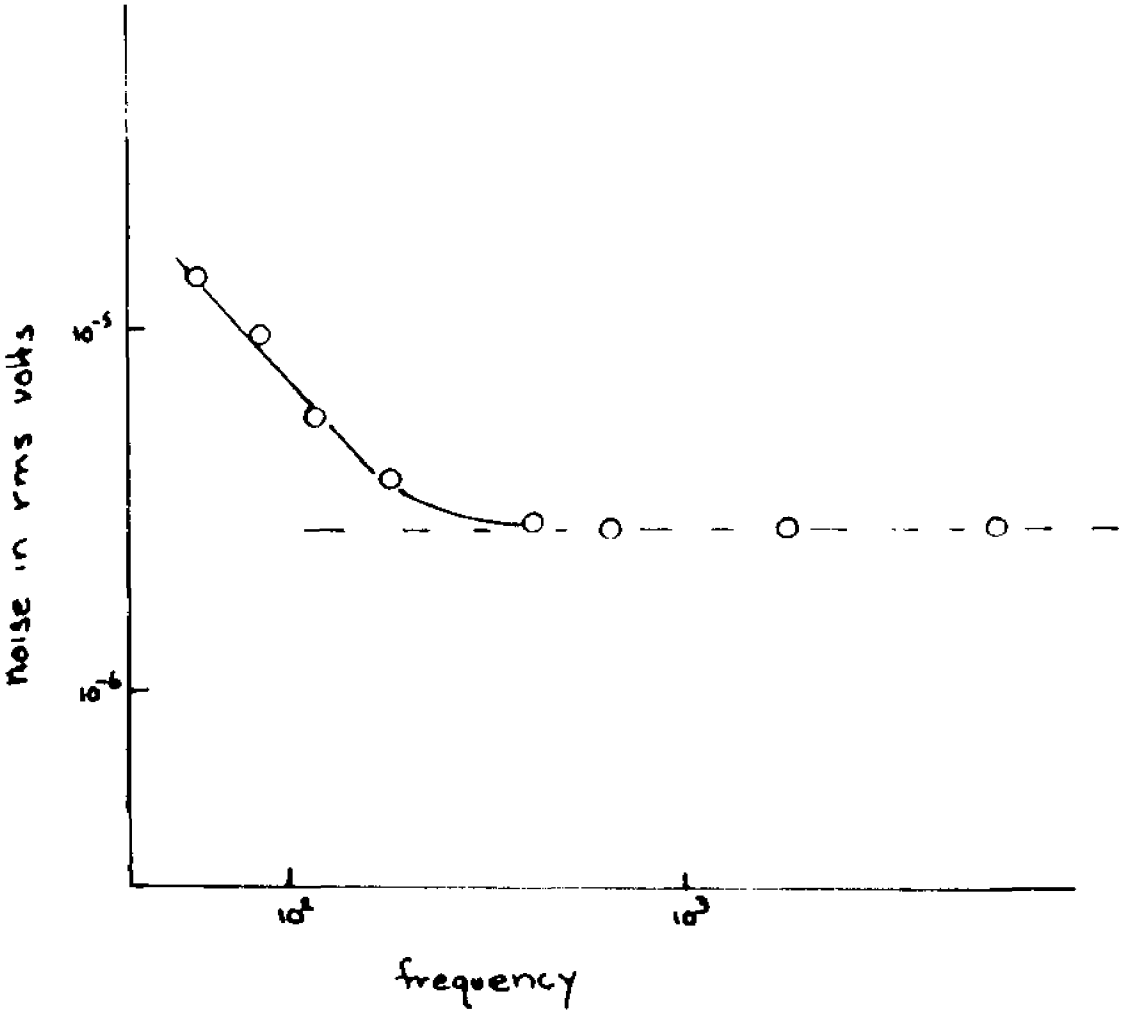

layer where water dissociation occurs is very small (10^{-9} to 10^{-8} meters) whereas the concentration gradient in the region of R_2 is spread out over 10^{-5} to 10^{-4} meters.[39] Therefore R_2 can be expected to exceed R_1 by a sufficient amount.

The second requirement for this model which is difficult to fulfill is a capacitance of the proper magnitude. An electrical double layer is known to exist on membrane and metal surfaces.[40] The capacitance of such a double layer can be evaluated by using the equation for a parallel plate capacitance:

$$C = \frac{\epsilon A}{X} \qquad (68)$$

Where C is the capacitance, ϵ the permittivity of the medium, water, A the area and X the distance between the plates. The capacitance required for the required time constant of .1sec or greater can be evaluated by: $C = \frac{1}{2\pi R f}$ where R is the resistance and f is the turnover frequency. R can be estimated from figure 10 using Ohm's law $V = IR$. V is 0.2 volts and I is 4 ma. R is then 50 ohm. The area of the hole is 0.09 Cm^2. For a cutoff frequency of 10Hz a capacitance of 300 microfarads is necessary. If the distance X is taken as 10A°, a capacitance of this magnitude requires a dielectric constant of the medium of the order of 4×10^3 compared to 70 for water, assuming that the membrane surface area is the same

as the area of the hole on the tape. This requirement apparently is too severe to justify the equivalent circuit proposed in figure 35. Nevertheless it should not be prematurely discarded until evidence is available.

There is the possibility that the observed slope results from the nonlinearity introduced into the rate constant due to a fluctuating voltage.

(69) $$k = k' e^{\frac{F(V+\Delta V)}{RT}}$$

Here, V is the voltage and ΔV the fluctuation in the voltage. The pre-exponential termand the energy of activation is combined in k'. This method is being explored by others at present.

Bibliography

1. Katz, B., Nerve, Muscles and Synapse, McGraw Hill, New York (1966).

2. Lakshminarayanaiah, N., Chem. Rev., 65, 491 (1965).

3. Prigogine, I., Introduction to the Thermodynamics of Irreversible Processes, 3rd. ed., Interscience Publishers, New York (1967).

   de Groot, S. R. Mazur, P., Non-Equilibrium Thermodynamics, North Holland Publishing Co., (1962).

4. Lax, Melvin, Rev. Mod. Phys., 32, 755 (1960).

5. Donnan, F. G., Z. Electrochem., 17, 572 (1911).

6. Helferich, F., Ion exchange, McGraw Hill, New York, 134 (1962).

7. Vetter, K., Electrochemical Kinetics, Theoretical and Experimental Aspects, Academic Press, New York, 58 (1967).

8. Onsager, L., Phys. Rev. 37, 405, (1931); 38, 2265 (1931).

9. Peers, A. M., Discussion Faraday Soc., 21, 124 (1956).

10. Gregor, H. P., Miller, I. F., J. Amer. Chem. Soc. 86, 5689 (1964).

11. Callen, H. B., Welton, T. A., Phys. Rev., 83, 34 (1951).

12. Kittel, C., Elementary Statistical Physics, John Wiley & Sons, Inc., New York (1958).

13. Rice, S. O., Selected Papers on Noise and Stochastic Processes, N. Wax, Ed., Dover Publications, Inc., New York (1954).

14. Greene, R. F., Callen, H. B., Phys. Rev., 83, 1231 (1951).

15. van Vliet, K. M., Fassett, J., Fluctuation Phenomena in Solid, R. Burgess, Ed., Academic Press, New York, 267 (1965).

16. Manes, M., J. Chem. Phys., 21, 1791 (1953).

17. Eigen, M., de Maeyer, L., Physical Method in Organic Chemistry, Vol. III - II, A. Weissberger, Ed., Interscience Publ. Co., New York, 895 (1963).

18. Morse, P. M., Feshbach, H., Methods of Theoretical Physics, Chapter 7, McGraw Hill, New York, (1953).

19. Green, M. E., M. Yafuso, J. Phys. Chem. 72 4072 (1968), correction: J. Phys. Chem., 73, 1629 (1969).

20. Lax, M., Mengert, P., J. Phys. Chem. Solids, 14, 248 (1960).

21. Derksen, H. E., Verveen, A. A., Science, 151, 1388 (1965).

22. McWhorter, A. L., Semiconductor Surface Physics, R. H. Kingston, Ed., University of Penn. Press, Phila., Pa., 207 (1957).

23. Kingston, R. H., McWhorter, A. L., Phys. Rev., 103, 534 (1956).

24. Rice, S., Nagasawa, M., Polyelectrolyte Solutions, Academic Press, New York (1969), Chapter 9.

25. Kittel, C., Introduction to Solid State Physics, 3rd. Ed., John Wiley and Sons, Inc. (1967), Chapter 9.

26. Oldom, K. B., Topal, L. E., J. Phys. Chem., 71, 3007 (1967).

Oldom, K. B., Topal, L. E., J. Phys. Chem., 72, 1455 (1968).

Oldom, K. B., Topal, L. E., J. Phys. Chem., 73, 1462 (1969).

27. Ives, D. J., Janz, G. J., Reference Electrodes, Academic Press, New York (1961).

28. Petritz, R. L., Proc. Inst. Radio Engrs., 40, 1940 (1952).

29. van der Ziel, A., Noise, Prentice Hall, New York (1954).

30. Firle, T. E., Winston, H., J. Appl. Phys., 26, 716 (1955).

Rollin, B. V., Templeton, I. M., Proc. Phys. Soc. (London), B66, 259 (1953).

31. Templeton, I. M., McDonald, D. K. C., Proc. Phys. Soc. (London), B66, 680 (1953).

32. Maple, T. G., Bess, L., Gebbie, H. A., J. Appl. Phys., 26, 490 (1955).

33. Spiegler, K., Private communications with M. E. M. Green.

34. Conway, B. E., Theory & Principles of Electrode Process, The Ronald Press Co., New York 93 (1965).

35. Longsworth, L. G., Electrochemistry in Biology and Medicine, T. Shedlovsky, Ed., John Wiley & Sons, Inc., New York, 225 (1955).

36. Marion, J. B., Classical Electromagnetic Radiation, Academic Press, New York, 105 (1965).

37. Onsager, L., J. Phys. Chem., 2, 599 (1934).

38. Handbook of Chemistry & Physics, 41st. Ed., Chemical Rubber Publishing Co., Cleveland, Ohio, 1743 (1959).

39. Peterson, M. A., Gregor, H. P., J. Phys. Chem., 68, 2201 (1964).

40. Segal, J. R., J. Theoret. Biol., 14, 11 (1967).

Coster, H. G. L., George, E. P., Simons, R., Biophys. J., 9, 666 (1969).

TABLE 1 CRITICAL CURRENT DENSITIES

MEMBRANE	CONC	SALT	CCD(ma/cm^2)	CURRENT AT WHICH NOISE APPEARED	TEMP.
MC3142	0.030	HCl	33	33	r.t.
	0.060	"	54	54	r.t.
	0.033	CsCl	16	11	r.t.
	0.10	"	38	38	r.t.
	0.033	NaCl	9	11	r.t.
	0.086	"	19	-	r.t.
	0.10	"	17	17	r.t.
	0.056	Na_2HPO_4	-	22	r.t.
	0.33	NH_4Cl	9	-	r.t.
	0.10	NH_4Cl	22	20	r.t.
	0.033	$CaCl_2$	-	8	r.t.
	0.05	"	10	10	r.t.
	0.10	"	19	-	r.t.
	0.05/0.05	NaCl/CsCl	30	27	r.t.
	0.03/0.05	NCl/NaCl	49	49	r.t.
MC3235	0.02	HCl	11	-	r.t.
	0.05	"	17	-	40°
	0.06	"	44	-	r.t.
	0.033	NaCl	7	-	r.t.
	0.10	"	16	15	r.t.
	0.056	Na_2HPO_4	22	21	r.t.
	0.28	"	-	44	r.t.
	0.10	NH_4Cl	21	22	r.t.
	0.05	$CaCl_2$	9	9	r.t.
	0.10	"	-	11	r.t.
	0.10	$CuSO_4$	18	18	r.t.
	0.10	Me_4NCl	8	8	r.t.
MA3148	0.056	Na_2HPO_4	-	1.1	r.t.
	0.033	NaCl	-	.5	r.t.
	0.10	"	5.4	2.7	r.t.
	0.50	KHPhth	2.7	0	r.t.
MA3236	0.10	NaCl	14	5.4	r.t.
	0.056	Na_2HPO_4	4.3	1.1	r.t.
	0.10	Na_2SO_4	55	1.1	r.t.

TABLE 2: Slopes of Power Spectra. The first number is the slope up to the frequency in KHz given by the second number. Slopes were constant where frequency is not recorded.

Salt	Conc. mol/l.	Current density mA/cm^{-2}	dlogP/dlogf MC3142	MC3235	MA3148	MA3236
Na_2HPO_4	0.056	43	2.4,1	2.4,.2	1.4	1.8
		22	1.6,1	1.3,.2	1.4	1.4
		11				1.1
NaCl	0.86	27			1.0	
	0.43	27			1.0	
	0.10	43	2.8,.5	2.6,.5	1.4	1.2
		33	3.0,.2			
		22	1.8,.5	2.6,.05	1.2	1.0
NH_4Cl	0.10	43	2.0,.1	2.0,1		1.4,.1
		22	1.8	1.8		1.4
$CuSO_4$	0.10	54	2.0,.2	2.0,1		
		43	2.0,.2			
		33	1.5,.1	2.0,.2		
	0.05	22	1.6,.1			
		16		2.0		
$CaCl_2$	0.10	43		3.0,.1		
		22		2.6		
Na_2SO_4	0.10	43			1.2,.5	
		22			1.4,.5	1.2

TABLE 3

Slopes of the HCl spectra in terms of $\frac{d(\log \text{power})}{d(\log f)}$.

X_1 = negative of the first slope.

X_2 = negative of the second slope.

CONC	TEMP(^{o}K)	J(ma/cm^2)	X_1	X_2
0.050M	292	22	2.7	5.1
"	"	28	2.3	4.7
"	"	41	2.4	4.3
"	"	50	2.2	4.5
"	"	67	2.3	3.6
"	"	74	2.2	3.4
"	303	31	2.5	5.0
"	"	35	2.0	5.0
"	"	44	2.4	4.2
"	"	50	2.6	4.5
"	"	57	2.6	4.5
"	"	67	2.5	3.8
"	"	75	2.4	3.7
"	313	33	2.0	4.7
"	"	42	2.2	4.5
"	"	50	2.6	4.0
"	"	60	2.5	4.0
"	"	75	2.3	3.6
"	322	34	2.4	4.7
"	"	50	2.0	3.9
"	"	62	2.5	4.2
"	"	75	2.5	4.2
0.025M	322	31	2.2	4.0
"	"	31	2.2	4.0
"	"	29	1.9	4.3
"	"	33	2.8	4.5
"	"	40	2.6	4.5
"	"	52	2.6	4.5
"	"	62	2.5	4.1
"	"	75	2.4	3.8
"	313	18	1.9	4.0
"	"	25	1.9	4.5
"	"	30	1.9	4.7
"	"	35	2.1	4.7
"	"	47	2.3	4.6
"	"	59	2.4	3.8
"	"	75	2.4	3.8

TABLE 3 cont'd.

CONC	TEMP(^{O}K)	J(ma/cm^2)	X_1	X_2
0.025	292	17		
"	"	20	2.7	4.6
"	"	23	2.9	4.6
"	"	28	2.9	4.1
"	"	33	2.8	4.7
"	"	42	2.9	4.6
"	"	50	2.8	4.7
"	"	59	2.4	5.0
"	"	67	2.2	4.8
"	"	84	2.5	4.4
"	303	16	2.2	4.7
"	"	18	1.9	5.0
"	"	23	2.5	5.0
"	"	28	2.2	5.0
"	"	33	2.2	4.7
"	"	42	2.1	4.5
"	"	50	2.1	4.3
"	"	59	2.2	4.5
"	"	67	2.4	5.0
"	"	84	2.4	4.7

Table 4 $f = f(n); f(v)$

TEMP °C	CONC(mole/l.)	f(v)	f(n)
19	0.025	$13.2V^{3.34}$	$36N^{1.43}$
30	"	$4.5V^{3.85}$	$29.2N^{1.37}$
40	"	$21.5V^{3.2}$	$55N^{1.16}$
50	"	$198\ V^{2.1}$	$93.5N^{1.26}$
20	0.50	$38.7V^{2.6}$	$163\ N^{0.95}$
30	"	$9.6V^{3.91}$	$156\ N^{1.057}$
30,40,50	"	$18.3V^{3.5}$	$225N^{0.946}$

The value f is $\frac{1}{2\pi\tau}$, where τ is the relaxation time, V is the IR drop across the probe electrodes, and N is the total noise in rms volts.

TABLE 5

CONC	TEMP	K	$K_{corr.}$	β	$\beta_{corr.}$
0.050M	298	0.096	0.093	230	220
0.050M	303	0.069	0.076	290	290
0.050M	313	0.093	0.063	31	350
0.050M	323	0.054	0.055	430	430
0.025M	298	0.153	0.149	169	160
0.025M	303	0.177	0.137	118	110
0.025M	313	0.099	0.097	170	170
0.025M	323	0.072	0.071	207	207

TABLE 6A

Mobilities calculated from diffusion activation energies cited in reference 35 in m^2/volt·sec.

$D = D_o \exp(-E_a/RT)$

$D_o(H^+) = 22.17 \times 10^{-7}$ m²/sec $E_a(H^+) = 3.30$ kcal

$D_o(OH^-) = 23.02 \times 10^{-7}$ m²/sec $E_a(OH^-) = 3.01$ kcal

$D_o(Cl^-) = 25.40 \times 10^{-7}$ m²/sec $E_a(Cl^-) = 4.21$ kcal

Temp	$u(H^+)(\times 10^{+8})$	$\mu_{OH^-} \times 10^{+8}$	$\mu_{Cl^-} \times 10^{+8}$	$\mu^2_{H_2O} \times 10^{13}$	κ
[illegible]	[illegible]	18.17	[illegible]	[illegible]	[illegible]
[illegible]	[illegible]	.33	[illegible]	[illegible]	[illegible]
313	[illegible].53	[illegible]6.1[illegible]	1[illegible].[illegible]1	.144	1.[illegible]78
323	51.[illegible]4	30.40	1[illegible].[illegible]	[illegible].[illegible]3	1.[illegible]75

TABLE 6.3

Values of K_o, K and N at different temperatures.

CONC	TEMP	K(l^{-1})	N(l^{-1})	Ko($mol^2/m^3 x l^{-8}$)
[illegible]	[illegible]	[illegible]	[illegible]	[illegible]
[illegible]	[illegible]	[illegible]	[illegible]	[illegible]
[illegible]	[illegible]	[illegible]	[illegible]	[illegible]
[illegible]	[illegible]	[illegible]	[illegible]	[illegible]
[illegible]	[illegible]	[illegible]	[illegible]	
[illegible]	[illegible]	[illegible]	[illegible]	
[illegible]	[illegible]	[illegible]	[illegible]	
[illegible]	[illegible]	[illegible]	[illegible]	

TABLE 7

Values of F(b)F(x)^2 at Different Value of f, Temperature and Concentration

	Log F(b)F(x)^2							
	0.050M HCl				0.025M HCl			
f	19°C	30°C	40°C	49°C	19°C	30°C	40°C	49°C
2.0	14.06	13.76			14.18	13.63	13.21	13.79
2.2	14.46				14.32	13.85	13.40	13.0
2.4	14.68	14.15	13.69	13.76	14.86	14.08	13.64	13.90
2.6	14.97	14.36	13.90	13.69	14.95	14.29	13.86	13.82
2.8	15.12	14.59	14.12	13.78	15.24	14.47	14.1[illegible]	14.[illegible]4
3.0	15.37	14.81	14.34	14.[illegible]	15.[illegible]6	1[illegible].98	14.7[illegible]	13.87
3.2	15.63	15.05	1[illegible].[illegible]7	14.[illegible]	1[illegible].90	1[illegible].18	14.[illegible]	14.1[illegible]
3.4	1[illegible].91	1[illegible].71	14.80	14.45	1[illegible]	1[illegible].51	14.91	14.[illegible]
3.6	16.21	1[illegible].[illegible]9	1[illegible].[illegible]9	14.90	1[illegible]	1[illegible].86	1[illegible]	14.[illegible]8
3.8	16.54	1[illegible].90	1[illegible].38	14.97	1[illegible]	1[illegible]	1[illegible]	1[illegible].[illegible]9
4.0	1[illegible].[illegible]8	1[illegible]	1[illegible].[illegible]8	1[illegible]	17.4	1[illegible]	1[illegible]	[illegible]
4.2	[illegible]	1[illegible]	1[illegible].[illegible]7	1[illegible]	[illegible]	1[illegible]	[illegible]	1[illegible]
4.4	1[illegible]	1[illegible].[illegible]3	1[illegible]	[illegible]	1[illegible].1	1[illegible]	1[illegible]	1[illegible]
4.6	1[illegible]	1[illegible].71	1[illegible].7[illegible]	1[illegible]	[illegible]	1[illegible].[illegible]5	1[illegible].[illegible]3	1[illegible]
4.8	1[illegible].77	1[illegible]	1[illegible].1[illegible]	1[illegible]	1[illegible].[illegible]7	[illegible]	1[illegible].[illegible]7	[illegible]
5.0	1[illegible]	1[illegible]	1[illegible].[illegible]1	1[illegible]	[illegible].37	1[illegible]	1[illegible]	1[illegible].1[illegible]

TABLE 2a

Values of F(b) and F(b)(x)^2 for Various

Values of (x)

0.[illegible]M HCl, 10°C., κ = [illegible].192

$$b = \frac{[illegible].758\times10^{-1[illegible]}(x)^2}{\kappa T^2} = 7.[illegible]73\times10^{-16}\,(x)^2$$

Log (x)	(x)(x10^{-7})	b	F(b)	F(b)(x)^2 (10^{-14})
[illegible]	[illegible].7082	[illegible].0052	1.005	0.1[illegible]32
[illegible].70	0.5013	.0082	1.[illegible]8	[illegible]
[illegible].80	[illegible].712	[illegible].017[illegible]	1.017	[illegible]
[illegible]	[illegible]	[illegible]	1.[illegible]1	[illegible].6[illegible]
[illegible]	1.[illegible]	[illegible]	1.[illegible]7	[illegible]
[illegible].1[illegible]	[illegible]	[illegible]1[illegible]	[illegible]	[illegible]
[illegible]	1.[illegible]	.0[illegible]	[illegible]	[illegible]
[illegible]	[illegible]	[illegible].17[illegible]4	[illegible].17[illegible]	4.[illegible]
[illegible].40	[illegible]	[illegible]	[illegible]1	[illegible].[illegible]07
[illegible]	[illegible].1[illegible]	[illegible]	[illegible]	1[illegible]
[illegible]	[illegible]	.1[illegible]	[illegible].17	[illegible]
[illegible]	[illegible]17	[illegible]	[illegible].0[illegible]1	.[illegible]1
[illegible]	[illegible]	[illegible]4	[illegible]	1[illegible]
[illegible]	[illegible]	[illegible]	[illegible]	[illegible]
[illegible]	1[illegible]	[illegible].077	1[illegible]	[illegible]
[illegible].1[illegible]	1[illegible]	.1[illegible]	[illegible]	[illegible]
[illegible]	1[illegible]	[illegible]	1[illegible]	[illegible]
[illegible].70	1[illegible]	1[illegible].04	[illegible]	[illegible]

[illegible] 8b

Values of [illegible] for Various

Values of [illegible]

[illegible] °C., [illegible]

$$[illegible] = \frac{[illegible]}{\kappa T^2} = [illegible]$$

Log (x)	[illegible]	[illegible]	[illegible]	[illegible]
[illegible]	[illegible]	[illegible]	[illegible]	[illegible]
6.70	[illegible]	[illegible]	[illegible]	[illegible]
[illegible]	[illegible]	[illegible]	[illegible]	[illegible]
[illegible]	[illegible]	[illegible]	[illegible]	[illegible]
[illegible]	[illegible]	[illegible]	[illegible]	[illegible]
[illegible]	[illegible]	[illegible]	[illegible]	[illegible]
[illegible]	[illegible]	[illegible]	[illegible]	[illegible]
[illegible]	[illegible]	[illegible]	[illegible]	[illegible]
[illegible]	[illegible]	[illegible]	[illegible]	[illegible]
[illegible]	[illegible]	[illegible]	[illegible]	[illegible]
[illegible]	[illegible]	[illegible]	[illegible]	[illegible]
[illegible]	[illegible]	[illegible]	[illegible]	[illegible]
[illegible]	[illegible]	[illegible]	[illegible]	[illegible]
[illegible]	[illegible]	[illegible]	[illegible]	[illegible]
[illegible]	[illegible]	[illegible]	[illegible]	[illegible]
[illegible]	[illegible]	[illegible]	[illegible]	[illegible]
[illegible]	[illegible]	[illegible]	[illegible]	[illegible]

TA[illegible] 8c

[illegible] (b) and ( ) (x) for [illegible]

[illegible] (x)

[illegible] X= [illegible]

[illegible] XT2

[illegible] (x)	(x)([illegible])	[illegible]	(b)	( ) (x) (1 [illegible])
[illegible]	[illegible]	[illegible]	[illegible]	[illegible]
[illegible]	[illegible]	[illegible]	[illegible]	[illegible]
[illegible]	[illegible]	[illegible]	[illegible]	[illegible]
[illegible]	[illegible]	[illegible]	[illegible]	[illegible]
[illegible]	[illegible]	[illegible]	[illegible]	[illegible]
[illegible]	[illegible]	[illegible]	[illegible]	[illegible]
[illegible]	[illegible]	[illegible]	[illegible]	[illegible]
[illegible]	[illegible]	[illegible]	[illegible]	[illegible]
[illegible]	[illegible]	[illegible]	[illegible]	[illegible]
[illegible]	[illegible]	[illegible]	[illegible]	17.37
[illegible]	[illegible]	[illegible]	[illegible]	6.7
[illegible]	[illegible]	[illegible]	[illegible]	[illegible]
[illegible]	[illegible]	[illegible]	[illegible]	[illegible]
[illegible]	[illegible]	[illegible]	[illegible]	[illegible]
[illegible]	[illegible]	[illegible]	[illegible]	[illegible]

TABLE 8d

Values of [illegible] and [illegible] for Various

Values of [illegible](x)

[illegible] Cl, 49°C., κ = [illegible]14

[illegible] = [illegible] = [illegible]

[illegible] (x)	[illegible]	[illegible]	[illegible]	[illegible]
[illegible]	[illegible]	[illegible]	[illegible]	[illegible]
[illegible]	[illegible]	[illegible]	[illegible]	[illegible]
[illegible]	[illegible]	[illegible]	[illegible]	[illegible]
[illegible]	[illegible]	[illegible]	[illegible]	[illegible]
[illegible]	[illegible]	[illegible]	[illegible]	1.[illegible]
[illegible]	[illegible]	[illegible]	[illegible]	[illegible]
[illegible]	[illegible]	[illegible]	[illegible]	[illegible]
[illegible]	[illegible]	[illegible]	[illegible]	[illegible]
[illegible]	[illegible]	[illegible]	[illegible]	[illegible]
[illegible]	[illegible]	[illegible]	[illegible]	[illegible]
[illegible]	[illegible]	[illegible]	[illegible]	[illegible]
[illegible]	[illegible]	[illegible]	[illegible]	[illegible]
[illegible]	[illegible]	[illegible]	[illegible]	[illegible]
[illegible]	[illegible].94[illegible]	[illegible]	[illegible]	[illegible]
[illegible]	10.0	[illegible]	[illegible]	[illegible]

[illegible] 8e

[illegible] of [illegible] and [illegible] for [illegible]

[illegible]

[illegible], $K =$ [illegible]

$$= \frac{[\text{illegible}]}{KT^2}$$

[illegible]	[illegible]	[illegible]	[illegible]	[illegible]
[illegible]	[illegible]	[illegible]	[illegible]	[illegible]
[illegible]	[illegible]	[illegible]	[illegible]	[illegible]
[illegible]	[illegible]	[illegible]	[illegible]	[illegible]
[illegible]	[illegible]	[illegible]	[illegible]	[illegible]
[illegible]	[illegible]	[illegible]	[illegible]	[illegible]
[illegible]	[illegible]	[illegible]	[illegible]	[illegible]
[illegible]	[illegible]	[illegible]	[illegible]	[illegible]
[illegible]	[illegible]	[illegible]	[illegible]	[illegible]
[illegible]	[illegible]	[illegible]	[illegible]	[illegible]
[illegible]	[illegible]	[illegible]	[illegible]	[illegible]
[illegible]	[illegible]	[illegible]	[illegible]	[illegible]
[illegible]	[illegible]	[illegible]	[illegible]	[illegible]
[illegible]	[illegible]	[illegible]	[illegible]	[illegible]
[illegible]	[illegible]	[illegible]	[illegible]	[illegible]
[illegible]	[illegible]	[illegible]	[illegible]	[illegible]

TABLE 8c

Values of [illegible] and [illegible] (x) for Various Values

of [illegible](x)

[illegible] HCl, [illegible], κ = [illegible]

[illegible] = [illegible] $\frac{[illegible]}{\kappa T^2}$ [illegible]

[illegible] (x)	[illegible] (x)([illegible])	[illegible]	[illegible]	[illegible]
[illegible]	[illegible]	[illegible]	1.[illegible]	[illegible]
[illegible]	[illegible]	[illegible]	1.[illegible]	1.[illegible]
[illegible]	1.[illegible]	[illegible]	1.[illegible]1	[illegible]
[illegible]	[illegible]	[illegible]	1.[illegible]	[illegible]
[illegible]	[illegible]	1.[illegible]	[illegible]	[illegible]
[illegible]	[illegible]	[illegible]	[illegible]	[illegible]
[illegible]	1[illegible]	[illegible]	[illegible]	[illegible]
[illegible]	1[illegible]	1[illegible]	[illegible]	[illegible]
[illegible]	[illegible]	48.	[illegible].98x10^6	[illegible]

TABL. 8q

Values of F(t) and F(t)N(x)^2 for Various

Values of N(x)

0.050M HCl, 40°C., κ = [illegible].065

= $\frac{8.[illegible]x10^{-16}}{\kappa T^2}$ (x)^2

Log (x)	(x)(10$^{[illegible]}$)	[illegible]	F(t)	F(t) N(x) (10^{-14})
6.80	[illegible]	0.077	1.[illegible]	0.419
7.[illegible]	1.[illegible]	[illegible].08	[illegible]	1.[illegible]8
7.20	1.59	[illegible].91	1.[illegible]	7.1[illegible]
7.40	[illegible]	[illegible].[illegible]7	[illegible]	1[illegible].70
7.[illegible]	[illegible]	1.[illegible]	[illegible]	[illegible]
7.[illegible]	[illegible].70	[illegible].33	1[illegible]	[illegible]
[illegible]	1[illegible].[illegible]	.7[illegible]	11	1.[illegible]
[illegible]	1[illegible].9	[illegible]1	[illegible].[illegible]7x10$^{[illegible]}$	[illegible].84x10$^{[illegible]}$
[illegible]	[illegible]	[illegible]	[illegible]	[illegible]
[illegible].[illegible]0	[illegible].[illegible]	1[illegible]	[illegible]x10$^{[illegible]1}$	[illegible].07x10^{14}
[illegible].8[illegible]	[illegible]	[illegible]	[illegible].[illegible]4x10^{19}	[illegible]x10^{27}

TABLE 8h

Values of [illegible](b) and [illegible](b) [illegible](x)[illegible] for Various

Values of [illegible](x)

[illegible].05[illegible] [illegible]Cl, 40°C., χ = [illegible].0[illegible]5

[illegible] = $\frac{[illegible].144\times10^{-16}}{\chi T^2}$ [illegible](x)[illegible]

Log [illegible]	[illegible]	[illegible]	[illegible]	[illegible] (10^{-14})
[illegible]	1.[illegible]	[illegible].[illegible]91	1.[illegible]94	[illegible]
[illegible].30	[illegible]	[illegible].366	1.41	[illegible]
[illegible].477	[illegible]	[illegible]	[illegible].1[illegible]	1[illegible]
7.7[illegible]	5.00	[illegible]	[illegible]	24[illegible]
[illegible]	[illegible]	[illegible]	[illegible]	[illegible]
[illegible]	[illegible]	[illegible]	[illegible]	[illegible]
[illegible]	[illegible]	[illegible]	[illegible]	[illegible]
[illegible]	[illegible]	[illegible].41	[illegible].4	[illegible]x10[illegible]
[illegible]	[illegible]	[illegible].1[illegible]	1[illegible]	[illegible]x10[illegible]
[illegible]	[illegible]	[illegible]	[illegible]	[illegible]
[illegible]	[illegible]	[illegible]	[illegible]	[illegible]
[illegible]	[illegible]	[illegible]	[illegible]	[illegible]
[illegible]	[illegible]	[illegible]	[illegible]x10[illegible]	1.1[illegible]x10[illegible]

TABLE 9

Values of log E(x) corresponding to log f.

Log E(x)

Log f	0.050N HCl 19°C	30°C	40°C	49°C	0.025N HCl 19°C	30°C	40°C	49°C
[illegible]	7.12	[illegible]	[illegible]	[illegible]	7.08	[illegible]	[illegible]	
[illegible]	[illegible]	[illegible]	[illegible]	[illegible]	[illegible]	[illegible]	[illegible]	[illegible]
[illegible]	[illegible]	[illegible]	[illegible]	[illegible]	7.31	[illegible]	[illegible]	[illegible]
[illegible]	[illegible]	[illegible]	[illegible]	[illegible]	[illegible]	[illegible]	[illegible]	[illegible]
[illegible]	[illegible]	[illegible]	[illegible]	[illegible]	[illegible]	[illegible]	[illegible]	[illegible]
[illegible]	[illegible]	[illegible]	[illegible]	[illegible]	[illegible]	[illegible]	[illegible]	[illegible]
[illegible]	[illegible]	[illegible]	[illegible]	[illegible]	[illegible]	[illegible]	[illegible]	[illegible]
[illegible]	[illegible]	[illegible]	7.36	7.20	[illegible]	7.59	[illegible]	[illegible]
[illegible]	7.74	[illegible]	7.43	[illegible]	7.91	[illegible]	[illegible]	[illegible]
[illegible]	[illegible]	[illegible]	[illegible]	7.41	[illegible]	[illegible]	[illegible]	[illegible]
[illegible]	[illegible]	[illegible]	[illegible]	[illegible]	[illegible]	[illegible]	7.74	[illegible]
[illegible]	[illegible]	[illegible]	[illegible]	[illegible]	[illegible]	[illegible]	[illegible]	[illegible]
[illegible]	[illegible]	[illegible]	[illegible]	[illegible]		[illegible]	[illegible]	[illegible]
[illegible]	[illegible]	[illegible]	[illegible]	[illegible]		[illegible]	[illegible]	[illegible]
[illegible]							7.98	[illegible]
[illegible]							[illegible]	[illegible]

AUTOBIOGRAPHICAL SKETCH

Name: Masao Yafuso

Born: May 28, 1933 (Hakalau, Hawaii)

Education: B.S. Polytechnic Institute of Brooklyn (June 1964)

Professional: Lecturer, Cehmistry Department, The City College of New York, February 1966 to date

Research Chemist, U.O.P. Chemical Company, E. Rutherford, New Jersey, 1962-1966

Research Chemist, Orbis Products, Elizabeth, New Jersey, 1960-1962

Lab Technician, U.S. Atomic Energy Commission, 476 Hudson St., N.Y.C., 1960-1960

Publications: M.E. Green and M. Yafuso, "A Study of Noise Generated by Ion Transport across a Membrane." J. Phys. Chem., 73, 1629 (1969).

M. Dunkel and M. Yafuso, "Method for Color Improving of 5,6,7,8,9,9-Hexahalo-1,2,3,4,4a,5,8,8a-Octahydro-5,8-Methano-2,3,Naphthalene Dicarboxylic Anhydride with a monohydride alkyl alcohol." U.S. Pat. 4,446,822. May 28, 1969.

Honors: Recipient, Louis J. Curtman Award, Chemistry Department, The City College of New York, 1968.

Professional Societies: American Association for the Advancement of Science, Member

Military Service: U.S. Army, June 1956 - May 1958, Honorable Discharge